VB diagrams and chemical reactivity

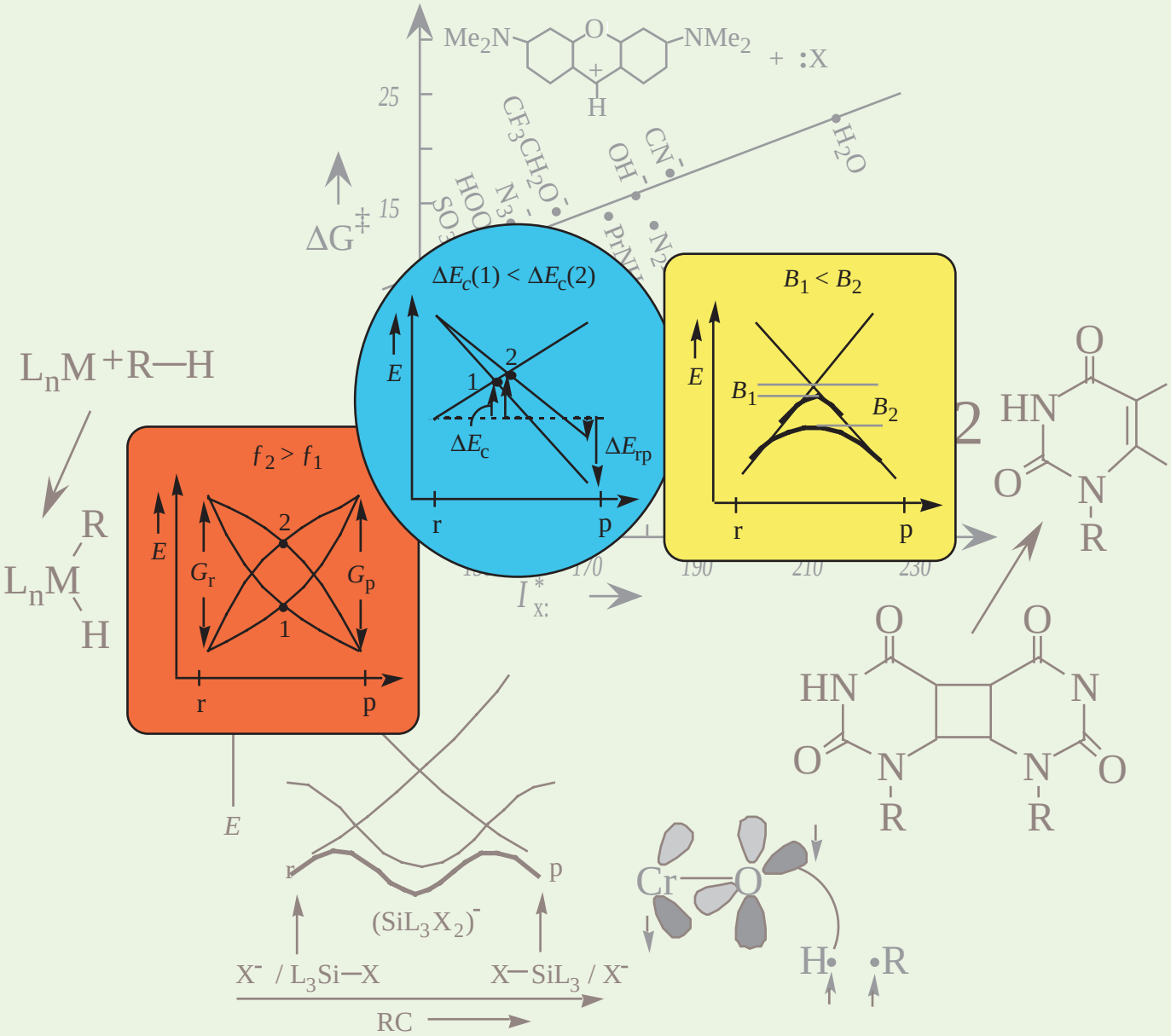

$$\Delta E^{\ddagger} = f_{av} G_r + F(\Delta E_{rp}) - B$$

ANGEWANDTE CHEMIE

Valence Bond Diagrams and Chemical Reactivity

Sason Shaik* and Avital Shurki

Dedicated to Roald Hoffmann on the occasion of his 60th birthday

Eighteen years after the first publication, valence bond (VB) diagrams have developed into a unified system of thought on fundamentals of chemical reactivity: barriers and reaction mechanisms. In this review the reader is led into the model, in a manner which enables to build know-how, through a gamut of applications from the elementary problem of bond breaking to more complex mechanisms where barriers and intermediates are involved in stepwise processes. How does a bond undergo heterolysis, and what is electrostatic catalysis by metal ions? What is the rate-enhancing factor in the in situ DNA repair mechanism? When do "forbidden" reactions become facile, and why do some "allowed" and highly exothermic reactions possess very large barriers? What is the mechanism of C–H activation by CrO_2Cl_2? How do lanthanide cations and other metal cations activate C–F bonds? How can we derive stereoselection rules for reaction mechanism and transition state stereochemistry, or stereoselection and mechanistic selection rules for the reactivity of ion radicals and for radical reactions? What are the electronic mechanisms by which complex molecules find low-energy pathways for otherwise high-barrier transformations? What is the difference between nucleophilic substitutions on silicon and carbon, or between concerted, nucleophilic and electron transfer pathways in polar cycloaddition? What are the origins of the novel $S_{RN}2$ and $S_{RN}2^c$ reaction mechanisms? What are the origins of reactivity reversals and reactivity zigzags? And what are entangled mechanisms? These are part of the problems which are addressed by use of VB diagrams.

Keywords: avoided crossing · reaction mechanisms · selection rules · transition states · valence bond diagrams

1. Introduction

What are the origins of the barrier to a reaction and the factors which control reaction mechanisms? These are fundamental questions in chemical reactivity. At the threshold of the 21st century such questions are expected to be tackled by applying quantum-chemical approaches which overcome the mathematical complexity of the problem and produce effective and chemically lucid models. Once a quantum-chemical mechanism of barrier formation is formulated, understanding of reactivity patterns is likely to follow, and conceptual means will become available for the generation and solution of new chemical problems.

"What Happens to Molecules as They React? A Valence Bond Approach to Reactivity" was a title of a 1981 paper[1] which utilized the connection between molecular orbital (MO) and valence bond (VB) wave functions to derive a general mechanism for barrier formation which could serve as a unified paradigm for chemical reactivity. This was a timely paradigm in some respects. Because on the one hand MO theory, which was the main conceptual matrix, could not offer a mechanism of barrier formation (with the exception of "forbidden" reactions where the principle of orbital-symmetry conservation led to a lucid explanation of the origins of the barrier)[2] and on the other hand VB theory, which was able to arrive at such a mechanism,[3] was considered passé and its knowledge restricted to a handful of experts who were more inclined at the time to develop the computational know-how of the theory. Thus, the MO – VB relationship was essential to create bridges, and at the same time to generate a reactivity paradigm which enjoyed the qualitative insights of both theories; these are the locality of the bond reorganization—best described by VB structures—and the orbital symmetry and nodal features—best described by MO theory.

It took time for the ideas to ripen through applications to a variety of reactions[4] and through ab initio VB computations of diagrams,[5] which showed that the qualitative formulations have rigorous computational analogues. The centerpiece of

[*] Prof. Dr. S. Shaik, A. Shurki
Department of Organic Chemistry
and
The Lise Meitner-Minerva Center For
Computational Quantum Chemistry
The Hebrew University
91904 Jerusalem (Israel)
Fax: (+972) 26585345
E-mail: sason@yfaat.ch.huji.ac.il

  1433-7851/99/3805-0587 $ 17.50+.50/0

the model is the VB correlation diagram, which traces the energy of VB states or configurations along the reaction coordinate and, by mixing of the configurations, projects the root cause of the barrier, the nature of the transition state, and the origins and make-up of reaction intermediates. This gamut of reactivity phenomena requires merely two generic diagrams, which are depicted schematically in Figure 1 and which

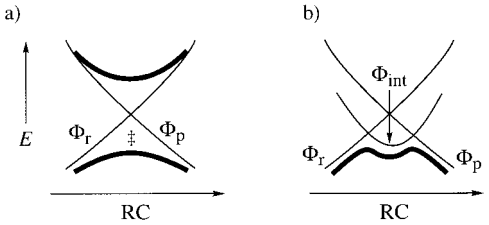

Figure 1. Generic VB diagrams: a) VBSCD, b) VBCMD. Curves of states after VB mixing are shown in the bold. RC = reaction coordinate, Φ_r = wave function of the reactant, Φ_p = wave function of the product, Φ_{int} = wave function of the intermediate state.

enable a unified systematic view of chemical reactivity. The first is a diagram of two interacting states, called a VB state correlation diagram (VBSCD), which describes the formation of a barrier in a single chemical step due to avoided crossing or resonance mixing of the VB states. The second is a three-curve diagram, called a VB configuration mixing diagram (VBCMD), which describes a stepwise mechanism in agreement with the avoided crossing and VB mixing of the three curves.

A review of these VB diagrams in chemical reactivity is deemed timely in view of the surge of interest in these VB concepts by experimentalists, and in the face of the renaissance which VB theory seems to enjoy in recent years.[6] Thus, a natural need emerges to create elements of know-how which can serve experimental chemists to apply VB ideas to reactivity.

There is a vast literature on the topic of avoided crossing,[1–3] and there have been a great many applications to chemical reactions. Even though a few of these applications are mentioned here (e.g., references [3b, 16, 24, 33, 117]), basically the review focuses on VBSCDs and VBCMDs, which as stated above incorporate insights from both VB and MO theories.[4, 7] Earlier reviews by Shaik,[4a–e, 7] Pross,[4e–i] and Hiberty[4d, 5a–e, 7c] have discussed theoretical aspects of the VB diagrams, and their applications to model reactions as well as to classical physical-organic mechanisms. With an eye toward synthesis of a uniform picture of chemical reactivity, the present review focuses on merging new developments with more classical applications of the model. Thus, we present here a selection of these new applications—such as to bond activation by inorganic and organometallic species,[8] new mechanisms like $S_{RN}2$ and $S_{RN}2^c$,[9] ion radical chemistry, the in situ DNA repair mechanism, reactions induced by metal ions (e.g. C–H and C–F activation), electrostatic catalysis, stereoselection rules, and Zipper reactions—blended into classical problems such as S_N2 and cycloaddition.

Since the review aims at a wide audience of experimentalists working in areas of chemical reactivity, its central role is to develop a didactic and yet effective scheme which will enable application by nonexperts. As such, while the article deviates from the formal structure of a review, it covers many applications of VB theory which are integrated in a problem-solving routine intended to build-up and gradually strengthen the know-how.

The review starts with key elements, the VB configurations which describe a two-electron bond, and shows how to think about various mixing patterns of these configurations and

S. Shaik

A. Shurki

Sason Shaik started his chemistry studies in Bar-Ilan University, where he obtained his M.Sc. under the supervision of M. Albeck. His M.Sc. studies involved experimental investigations of electrophilic mechanisms of organotellurium reagents. In 1974 he went to the U.S., where he completed his Ph.D. in quantum chemistry under the supervision of Professor N. D. Epiotis. In 1978 Shaik started his postdoctoral studies with Professor R. Hoffmann at Cornell University. In 1980 he began his first academic position as a Lecturer at Ben-Gurion University, where he became Professor in 1988. In 1992 he moved to the Hebrew University, where he teaches and does research now. He has held visiting appointments in Orsay, Kingston, Basel, Lund, Fribourg, Goteborg, Huntsville, Rochester, and the Technische Universität Berlin. He was a Fulbright scholar in the U.S. from 1974 to 1979, and has been awarded the Isreal Chemistry Society Prize for the Young Chemist in 1987, the Bergman Prize in 1996, and the Lise Meitner–Alexander von Humboldt Senior Award in 1995. His research interests are in the use of quantum chemistry to develop paradigms which can lead to the generation and solution of new chemical problems.

Avital Shurki began studying chemistry in 1990 at the Hebrew University, where she finished summa cum laude and was on the Dean's and Rector's Lists. In 1995 she received the Sara Wolf Prize for graduate students. In 1994 she joined the group of S. Shaik and is currently doing her Ph.D. in quantum chemistry. Her research involves applications of VB ideas and calculations to chemical reactivity and bonding.

their relationships to reactivity. Then the discussion turns to more complex situations of VB configurations and construction of VBSCDs and VBCMDs, which allow some generalizations and a variety of applications to chemical reactions.

2. Behavior of Valence Bond Configurations in Chemical Reactions

It is worthwhile to review some elementary features of VB configurations in the context of chemical reactivity. The description of VB configurations will rely on cartoon representations, from which we shall try to extract essential characteristics without resort to explicit expressions of wave functions and energetics. Readers who are interested in technical details of VB theory may consult a review[7a] which teaches an approximate VB theory (see also the appendix of reference [10]) and a monograph which includes a systematic treatise of VB theory.[11]

2.1. One-Bond Reactions

2.1.1. Valence Bond Configurations of Polar Covalent Bonds

Let us consider the VB configurations in Scheme 1, which mix to form a typical polar C–X bond in a R–X molecule, where R is an alkyl group and X is an electronegative atom or

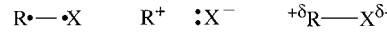

1, Φ_{HL} **2**, Φ_I **3**, Φ_L

Scheme 1. VB configurations (**1**, **2**) which mix to form a polar covalent bond (**3**).

group. Structure **1** is the covalent VB configuration in which the two electrons, occupying the hybrid orbitals on R and X, are paired into a singlet. The pairing is denoted by the line connecting the two dots, which in turn symbolize electrons. For historical reason this structure is called the HL structure (Φ_{HL}) after Heitler and London,[12] who first used this kind of wave function for the H_2 molecule. The second structure, **2**, is ionic (Φ_I), which by mixing with the covalent structure gives the bond its polarity. A third structure of inverse ionicity exists, but for most qualitative purposes its contribution may be neglected due to its high energy. The bond wave function following the VB mixing results in the Lewis structure **3** (Φ_L).

The HL and ionic structures have some general features which typify most bonds, albeit important exceptions are well recognized.[13] The HL structure is generally characterized by a covalent bonding energy which is associated with the spin pairing illustrated in Figure 2a. Thus, to create a singlet-paired HL structure we mix one form which has a spin up–spin down pattern with the one having the opposite pattern (see rule 8 in Section 8.1.4). This mixing contributes the covalent binding energy, which is a resonance energy stabilization and proportional to the product of the resonance integral β and overlap integral S of the bond hybrid orbitals.[7a]

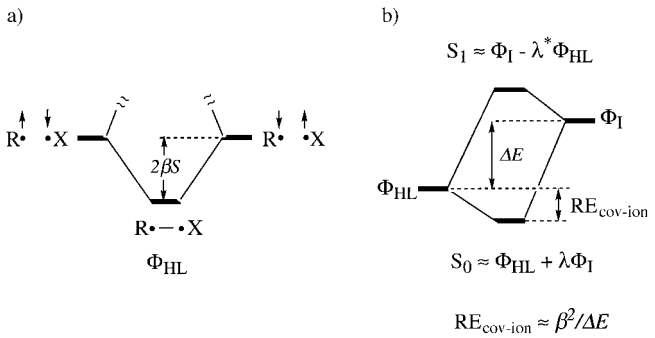

Figure 2. a) The covalent energy stabilization ($2\beta S$) of the HL configuration due to mixing of the spin up-spin down and spin down-spin up forms. b) VB interaction diagram of the mixing of the ionic (Φ_I) and covalent structures (Φ_{HL}).

The ionic structure enjoys electrostatic stabilization, which for alkyl groups is in the range of 90–130 kcal mol^{-1}.[14] The mixing between the covalent and ionic structures can be represented by the VB interaction diagram[7a] in Figure 2b, which follows the usual rules of perturbation theory; that is, the mixing results in resonance energy stabilization which is proportional to the resonance integral and inversely proportional to the energy gap between the configurations. This resonance energy due to the mixing of the covalent and ionic structures is significant for R–X bonds; for example, it is of the order of 40 kcal mol^{-1} for H_3C–Cl.[14a] Even though the ionic–covalent resonance energy is large, the principal VB structure of polar covalent bonds is still the HL structure, while the ionic structure remains secondary.

This compact picture contains the essence of bonding, as might be deduced from recent VB ab initio studies.[13, 14] Figure 3 shows the ab initio VB curves for the isolated CH_3Cl molecule along the C–Cl bond stretching coordinate. The HL structure is the lowest and exhibits a minimum at short distances, while the ionic curve lies higher and exhibits a minimum at longer distance. The mixing between the two structures follows the VB interaction diagram of Figure 2b at each point along the "reaction coordinate" (i.e., for every

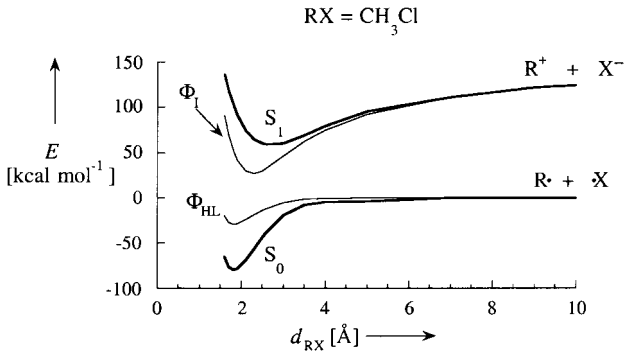

Figure 3. VB correlation diagram for cleavage of the C–Cl bond. Here and in all subsequent figures, VB configurations (here Φ_{HL} and Φ_I) are traced in regular lines, while states (here S_o and S_1) after VB mixing are the bold curves.

R–X distance), and leads to bonding and antibonding state curves for the ground (S_0) and excited states (S_1) of the C–Cl bond. In accord with rules of mixing, the ground state is described mainly by the HL structure, while the excited state mainly by the ionic structure. The covalent-ionic resonance energy, which is proportional to β and hence to the overlap between the bond hybrid orbitals, diminishes gradually and becomes zero at infinite R–X distance; at this point, the ground state becomes a purely covalent radical pair, while the excited state purely ionic. Figure 3, which is typical for polar covalent bonds, shows that in the gas phase the profile for bond cleavage is homolytic and proceeds without a transition state separating the R–X "reactants" and the R$^{\bullet}$ + $^{\bullet}$X "products".

2.1.2. Valence Bond Configurations of Ionic Bonds

An ionic bond like in NaCl can be described by the same two structures Φ_{HL} and Φ_I. However, the low ionization energy of Na generates a weak covalent bonding interaction in Φ_{HL}, and, at the same time, this lowers significantly the energy of the ionic structure. The consequences are seen in Figure 4, which exhibits an ionic–covalent curve crossing

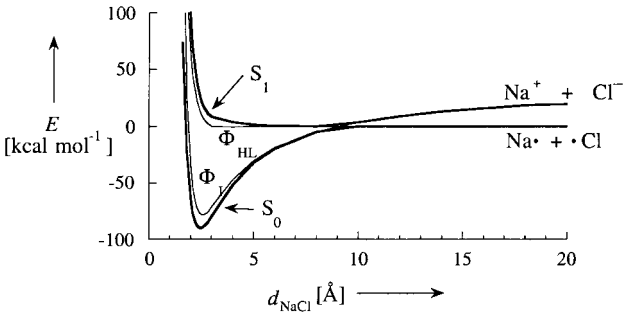

Figure 4. VB diagram for a cleavage of the Na^+Cl^- bond. The curve crossing is avoided by resonance mixing (avoided crossing) of the ionic and covalent configurations.

along the bond stretching coordinate. Now the ground state is primarily ionic, and the excited state is primarily covalent. At the crossing point, the VB mixing generates a pair of bonding and antibonding states, which leads to avoidance of the crossing. It is seen that avoided crossing results from resonance interaction of the VB structures at their point of crossing. Thus, unlike the situation in a covalent bond, here there is a resonating ionic–covalent state en route from the molecule Na^+Cl^- toward the product Na$^{\bullet}$ + $^{\bullet}$Cl radical pair. Since at infinite distance the energy gap between the curves is small, the crossing occurs at a long distance between Na and Cl, and the resonance interaction is very tiny. Consequently, the resonating state feature becomes a bottle-neck responsible for the slow dynamics of Na^+Cl^- formation from its atomic constituents.[15]

2.1.3. Heterolysis of Polar Covalent Bonds in Solution

Let us turn now to an R–X bond cleavage in solution by appeal to Figure 5a. For large alkyl groups like *tert*-butyl, or for R groups with sufficiently low ionization energy ($\leq$7 eV), the gap between the ionic and covalent curves is less than

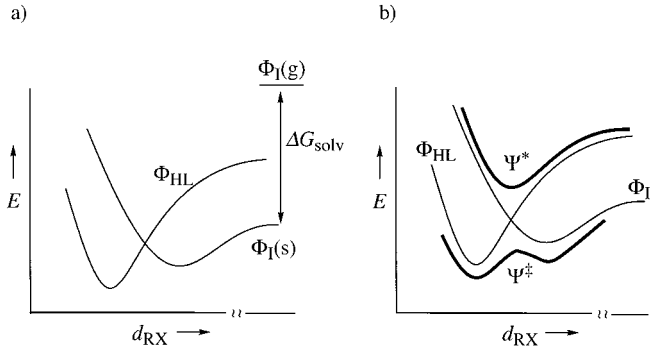

Figure 5. Heterolysis of an R–X bond in solution. ΔG_{solv} = free energy of solvation. a) Solvent-assisted VB curve crossing ((g) and (s) indicate gas phase and solution phase, respectively). b) Resonance mixing and generation of the transition state $\Psi^{\ddagger}$ and its twin excited state Ψ^*.

about 100 kcal mol^{-1}, while the solvation energy of the two ions exceeds 100 kcal mol^{-1}. Consequently the ionic structure will be much more stable than the covalent structure at long R–X distances.[3b, 4e, f, 16–18] At shorter distances the solvation decreases, and the ionic curve returns to its position above the HL structure. Consequently, in solution there is a solvent-assisted crossing of the ionic and covalent VB curves along the C–X bond stretching coordinate.

Much the same as in the ionic bond, here too the crossing will be avoided by resonance mixing of the two configurations (Figure 5b). The major difference is that the crossing occurs at a relatively short distance between R and X (ca. 2.2–2.5 Å), where overlap is significant and the resonance interaction is therefore large (ca. $\geq$10 kcal mol^{-1}). The resonance mixing will generate two twin states which are the bonding and antibonding combinations of the covalent and ionic structures [Eqs. (1a) and (1b)].[17] It is seen in Figure 5b that the

$$\Psi^{\ddagger} = (2)^{-1/2}\,[(R^{\bullet}\!-\!^{\bullet}X) + (R^{+}\,{:}X^{-})] \quad (1a)$$

$$\Psi^{*} = (2)^{-1/2}\,[(R^{\bullet}\!-\!^{\bullet}X) - (R^{+}\,{:}X^{-})] \quad (1b)$$

bonding combination occupies the top of the barrier on the ground-state profile, and may be associated with the transition state which separates the R–X molecule and the solvated R^+ and X^- ions. This general picture has been recently treated qualitatively by Pross and Shaik,[4e, 17] and quantitatively by Warshel and Weiss[3b] and by Kim and Hynes,[18] who used empirical VB calculations including solvation models.

The utility of the avoided-crossing mechanism for conceptualizing reactivity patterns may be illustrated by considering the barrier for ion recombination in solution (Figure 6).[17]

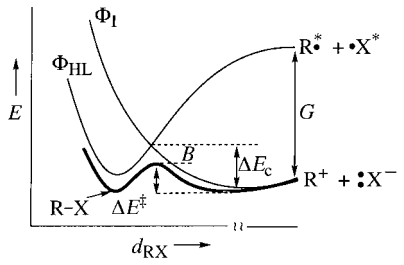

Figure 6. VB diagram showing the origins of the barrier for the ion-recombination process, and the key quantities which control its height.

The barrier is seen to be the balance between the height of the crossing point (ΔE_c) and the resonance energy stabilization B as expressed in Equation (2). The height of the crossing point

$$\Delta E^{+} = \Delta E_c - B \tag{2}$$

is the destabilization energy of the ions, which is required in order to bring them into resonance with the radicals at the crossing point; resonance mixing establishes a transition state for the reaction.

To apply Equation (2), one may use some typical mathematical curves to obtain a quantitative expression for ΔE_c. However, a much simpler approach is to relate this quantity to the energy gap G separating the two curves at their onset (that is, at infinite R–X distance). This is a vertical gap where both states have a common geometry and solvent orientations, specified by the ground-state ions. A rigorous expression, albeit obvious, is Equation (3a), which shows that the quantity ΔE_c is a fraction f of the gap G. In turn, G is the vertical charge transfer energy, given by Equation (3b) as the difference between the vertical ionization energy ($I^*_{X:^-}$) of $X:^-$ and the electron attachment energy ($A^*_{R^+}$) of the carbocation. This leads to the final expression for the barrier in Equation (3c).

$$\Delta E_c = fG \tag{3a}$$

$$G = I^*_{X:^-} - A^*_{R^+} \tag{3b}$$

$$\Delta E^{+} = f(I^*_{X:^-} - A^*_{R^+}) - B \tag{3c}$$

In solution, the vertical charge transfer energy refers to the process in which the radicals retain the same solvation shells and internal geometries as the ions.[17] These vertical states of the radicals are denoted in turn by the asterisks [Eqs. (4a) and (4b)], and the associated vertical ionization and attachment

$$X:^- \rightarrow X^{\cdot *} + e^- \quad \Delta E = I^*_{X:^-} \tag{4a}$$

$$R^+ + e^- \rightarrow R^{\cdot *} \quad \Delta E = -A^*_{R^+} \tag{4b}$$

energies are nonequilibrium quantities, which include also the role of solvent reorganization. These quantities are either available from photoelectron emission spectra and studies of charge transfer to solvent,[19] or can be readily estimated.[4a, b, 17, 20] In cases when the ion pair is sufficiently stable, the vertical charge transfer transition energy may be obtained from spectroscopy of the ion pair. To illustrate the use of the covalent-ionic resonance mixing model, consider the ion-recombination reaction described in Equation (5), where the

$$Y\text{–}P^+ + X:^- \rightarrow Y\text{–}P\text{–}X \tag{5}$$

carbocation Y-pyronin (Y–P$^+$) reacts with a series of nucleophiles in aqueous solution, as studied by Ritchie.[21]

Since the carbocation does not vary in the series, the charge transfer energy gap G is given by the vertical ionization energy of the nucleophile $X:^-$ minus a constant quantity, which is the vertical attachment energy of the Y-pyronin cation. As can be seen from Figure 7, the free energy barriers for all the nucleophiles correlate linearly with the vertical ionization energy of the nucleophile. While the correlation

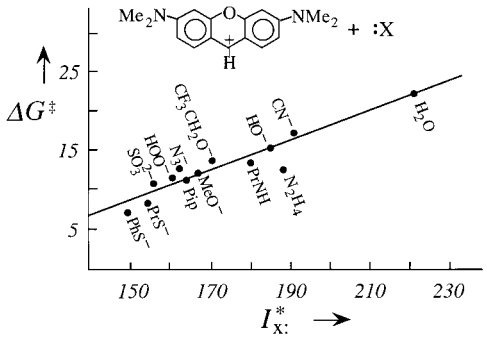

Figure 7. Free energy barriers[21] for recombination of the pyronin cation with nucleophiles in aqueous solution, plotted against the vertical ionization energy of the nucleophile (adapted from ref. [17]). Energies in kcal mol^{-1}.

coefficient is far from being excellent ($r = 0.94 - 0.96$), it is nevertheless impressive for such a variety of nucleophiles. It shows that nucleophilicity can oftentimes be related to a single fundamental property of the nucleophile. This correlation highlights the role of the vertical charge transfer energy gap G as an organizing quantity of the reactivity in the series, and lends support to the mechanism of activation associated with the covalent-ionic resonance in Figure 6. Furthermore, as discussed before,[17] the correlation provides a basis for the N^+ nucleophilicity scale of Ritchie, but shows also its inherent limitations noted recently by Mayr and Patz.[22]

2.1.4. Heterolysis of Polar Covalent Bonds Catalyzed by Metal Ions or External Charges

Bond cleavage can occur also in the presence of an "external" positively charged metal ion or charge $z+$. Let us consider this process with focus on the electrostatic effects exerted on the principal configurations. The electrostatic energy of mono-charged ions like K^+ and Cl^- at their equilibrium distance, given by the sum of ionic radii, is of the order of 130 kcal mol^{-1}, while for a di-positive ion like Zn^{2+}, Ca^{2+}, and Mg^{2+} with Cl^- or F^-, this interaction energy exceeds 260 kcal mol^{-1}. It is apparent therefore that the ionic VB structures of a polar bond will be highly affected by interaction with a positively charged metal ion or external charge. Figure 8 shows the energy levels of the VB configurations for the isolated molecular species, and in the

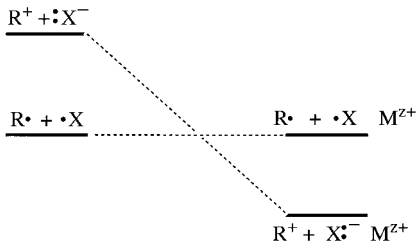

Figure 8. Energy ordering of the ionic and HL configurations at the dissociation limit in the gas phase (left) and in the presence of a metal cation or an external charge (right).

presence of the external charge. It is seen that, while for the isolated molecule the HL configuration is the lowest in energy, in the presence of M^{z+} it is the ionic structure which is

more stable. Thus, a positively charged metal ion promotes a covalent-ionic curve crossing along the bond stretching coordinate, and will heterolyze the bond much like a solvent.

Actually, because electrostatic energies in the case of localized charges exceed solvation energies, it is expected that such metal ions will catalyze bond heterolysis more efficiently. A schematic representation of the effect is illustrated in Figure 9, which shows that the stabilization of the ionic VB

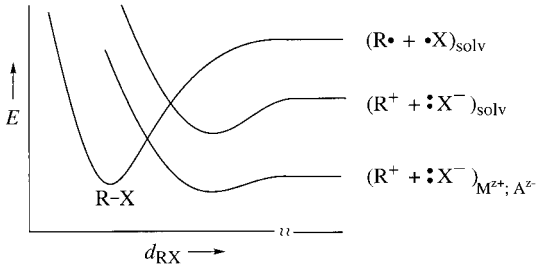

Figure 9. Covalent and ionic VB curves for a polar bond R–X in a solvent and in the field of two immobilized ions.

structure by a pair of external ions (charges) pulls down the ionic curve and lowers the height of the crossing point and hence of the respective barrier. This can be termed "electrostatic catalysis".

An ideal setup for electrostatic catalysis would be a bond heterolysis that is effected between two external ions M^{z+} and A^{z-}, which are immobilized in a cavity so that their own interaction is constant throughout the bond heterolysis. In such a case, the stabilization of the ionic structure $R^+:X^-$ will be very large, and the electrostatic catalysis will result in a small heterolysis barrier, if any. The catalytic tetrads of metalloenzymes (e.g., Zn^{2+} proteinases[23]) have charge setups which may introduce electrostatic catalysis into their native processes. Warshel[3b, 24] has treated heterolysis of the glycosidic bond of disaccharides in enzymes like lysozyme, and has shown that the electrostatic interactions between the ionized groups in the enzyme's active site and the ionic fragments of the glycosidic bond can account for the rate enhancement of bond heterolysis relative to the same reaction in a solvent.

Other effects associated with the stabilization of the ionic VB component of a bond, and which enable thereby bond heterolysis, may be analyzed in a similar manner. Examples are effects of protonation or interaction with a Lewis acid.

2.2. Valence Bond Structures for Two- and Multi-Bond Reactions

To remain consistent in our approach, we shall focus on the principal configurations of the bonds which participate in the process, and only subsequently will we worry about the secondary structures. In so doing there will emerge a general VB correlation diagram based on the principal VB structures (Section 3).

2.2.1. Is There Wisdom in Valence Bond Cartoons? Valence Bond Structures of Many-Center Species

Let us consider first a few features of VB structures which will serve us in subsequent discussions. Structures **4a–c** in

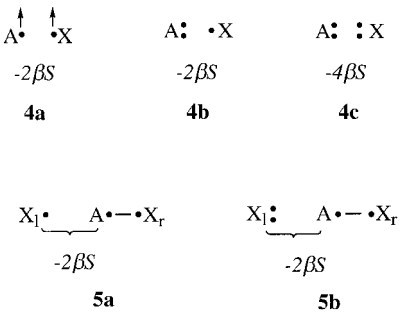

Scheme 2. Archetypal repulsive VB interactions (top) and their use in describing the VB structures of bond exchange reactions in a simple way (bottom).

Scheme 2 depict the archetypal repulsive VB interactions which arise from the combination of the overlap between the bond hybrid orbitals and the Pauli exclusion principle; hence overlap repulsions or Pauli repulsions. Structure **4a** describes the basic quantity of overlap repulsion due to a triplet pair of electrons in two overlapping orbitals. This quantity is proportional to the product of the resonance and overlap integrals between the two orbitals ($\beta < 0$, and hence $-2\beta S > 0$). In **4b** two of the electrons must possess the same spin, and therefore the overlap repulsion equals the basic quantity $-2\beta S$. Similarly, in **4c** there exist two pairs of electrons with identical spins, and the overlap repulsion is twice the basic quantity.

Based on these archetypal interactions, we shall use the cartoon representation of VB structures as a source of information on the wave function. This is illustrated for **5a** and **5b**, which are key structures in bond-exchange reactions. Both structures are seen to involve a HL bond pair and nonbonding electrons which maintain some interaction with the bonding electrons. In VB theory, nonbonding interactions which arise from overlap are repulsive;[7a] for example, in **5a** the unpaired electron maintains principally a triplet relationship with each one of the bond-pair electrons. It follows that as X_l approaches A, the triplet relationship will develop into a triplet state of the X_l–A linkage, and the energy of the VB structure will duly rise. Similarly, in **5b** the three-electron interaction between the electron pair on X_l and each of the bond-pair electrons will develop into overlap repulsion as the X_l–A distance decreases. Consequently, the VB structure will rise in energy and become a charge transfer excited structure (for the VB ground state in which X_l and A are bonded and X_r is the seat of the electron pair).

The triplet and charge transfer states are the two fundamental states which will appear time and again as excited states in VB correlation diagrams. The reasoning presented in Scheme 2 will be helpful in identifying these excited situations and constructing thereby VB correlation diagrams.

3. Valence Bond Correlation Diagrams for Two-Bond Processes of Covalent Bonds

The essential features of VB diagrams for the exchange of covalent bonds derive from the behavior of the HL structures, which are the principal configurations of covalent bonds. The following sections describe VB correlations for generic processes.

3.1. Radical Exchange Reactions

Figure 10 describes the VB correlation diagram for an identity process which involves bond cleavage by a radical. The two HL structures **6** and **7** evolve along the reaction

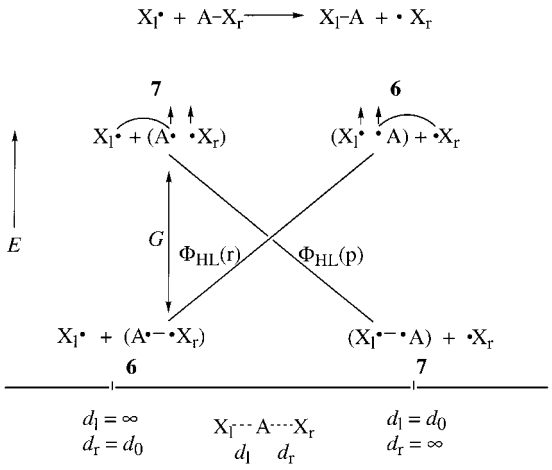

$$G = \Delta E_{ST}(A\text{–}X)$$

Figure 10. VB correlation diagram of the HL structures of reactants, $\Phi_{HL}(r)$, and products, $\Phi_{HL}(p)$, for a radical exchange process. G = promotion energy, $\Delta E_{ST}(A\text{–}X)$ = singlet – triplet excitation of the A–X bond. The pairing mode of each structure (**6** or **7**) is conserved throughout the respective curve.

coordinate into two intersecting VB curves. Initially, when the left hand side distance (d_l) is infinite and the right hand one (d_r) is short, the ground state is **6**. The structure rises in energy along the reaction coordinate, because the HL bond A–X_r is homolyzed and the X_l–A interaction develops into a triplet pair. At the extreme of the reaction coordinate, where the d_l linkage is short and d_r infinite, **6** becomes an excited state. The ground state at this geometry is **7**, which in turn becomes an excited state along the reverse direction of the reaction coordinate. The energy gap between the two curves at the reactant and product extremes is given approximately by the singlet – triplet excitation energy of the A–X bond which is exchanged during the reactions. A useful way of understanding this gap is as a promotion energy, required in order to enable the A–X_r bond to be broken and be replaced by another bond, X_l–A.

3.2. Nucleophilic Exchange Reactions

Figure 11 illustrates the formation of the VB correlation diagram from the HL structures **8** and **9**, corresponding to a reaction between a nucleophile and a molecule. The ground state at the reactant geometry is **8**, which gets gradually destabilized as the A–X_r bond is homolyzed and the three-electron overlap repulsion builds up across the X_l–A linkage. Structure **9** behaves in the same manner along the reverse of the reaction coordinate. The result is that the two HL structures interchange along the reaction coordinate, and define two ground and two excited states for the VB diagram.

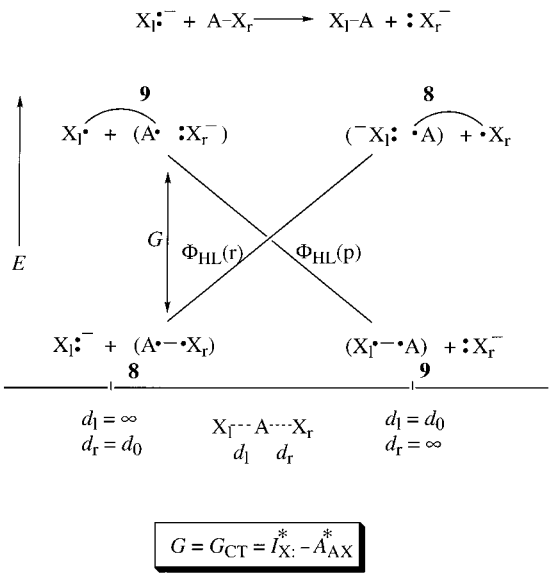

$$G = G_{CT} = I^*_{X:^-} - A^*_{AX}$$

Figure 11. VB correlation diagram of the HL structures of reactants and products for a nucleophilic exchange process. G_{CT} = vertical charge transfer promotion energy. I^* = vertical ionization energy, A^* = vertical attachment energy (electron affinity).

It is seen that in each extreme of the diagram, the excited state is obtained from the ground state by one-electron transfer from the anion $X{:}^-$ to the molecule A–X. Thus, the excited states in the diagram will correspond to charge transfer states, and the promotion energy of the reaction will be given by the vertical charge transfer energy.

3.3. Electrophilic Exchange Reactions

Figure 12 shows the behavior of the HL structures **10** and **11** along the same reaction coordinate as in preceding Figures. It is seen that the HL curves interchange along the reaction coordinate, and define two ground and two excited states for

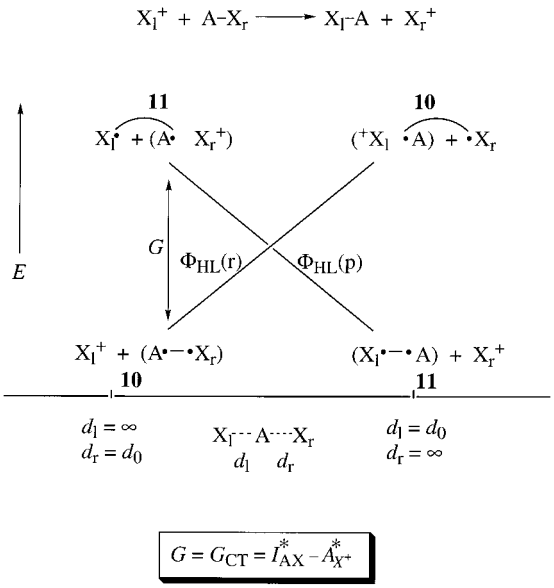

$$G = G_{CT} = I^*_{AX} - A^*_{X^+}$$

Figure 12. VB correlation diagram of the HL structures of reactants and products for an electrophilic exchange process.

the VB diagram. The excited states are related to the ground states by transfer of an electron from the bond into the empty orbital of the electrophile. As such, the promotion gap in the diagram is the vertical charge transfer energy.

3.4. Examples for Radical, Nucleophilic, and Electrophilic Attacks on Polar Covalent Bonds

To illustrate the relationship between the generic VB diagrams and to exercise their application, we show in Figure 13 three types of processes using an olefin as a common substrate. The three processes correspond to fundamental mechanisms of additions to a double bond by radicals,[25] nucleophiles,[26] and carbocations.[22] Following our discussions above, it is concluded that a common feature for all the mechanisms is the intersection of the HL structures along the reaction coordinate. The resulting VB correlation diagram is anchored in two ground states and two excited states. The two ground states possess the HL bonds for the reactants and products, while the two excited states are obtained from the ground states by electronic promotions which prepare the reacting moieties for the bond and electron reorganization. The promotion energies involve triplet excitation of the π bond in the radical process, and vertical charge transfer energies for the nucleophilic and electrophilic processes.

4. Valence Bond Correlation Diagrams for Two-Bond Processes of Ionic Bonds

Whenever ionic bonds are involved in the exchange process, the respective ionic configurations will dominate the VB diagram. Since the HL structure of an ionic bond possesses a weak covalent bonding energy, the respective HL structure will be secondary and serve to dress the VB diagram, but will not change its essence. To illustrate these VB correlation diagrams we use two specific processes of bond activation by a metallic species. These two processes are then contrasted with one in which the bond interchange can be described by a single ionic structure.

4.1. Bond Cleavage by Metallic Species

The bond activation which may initiate the Wurtz coupling is described by the VB correlation diagram in Figure 14. A quantitative VB correlation diagram was computed by Sevin et al.[27] for an analogous process. The R–Cl bond is covalent (**12**), while NaCl is ionic (**13**). The VB curves for **12** and **13** cross along the reaction coordinate. The promotion gaps in the two extremes of the diagram involve the vertical charge transfer energy at the product side, and the singlet–triplet excitation of the NaCl bond at the product side.

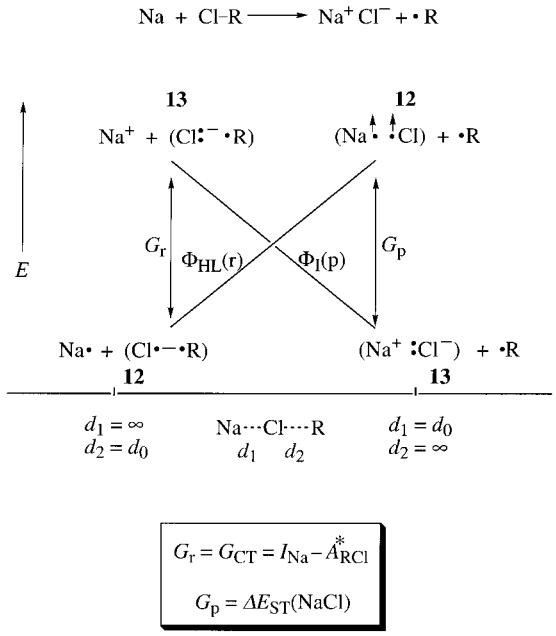

Figure 14. VB correlation diagram consisting of one HL (**12**) and one ionic VB structure (**13**) for C–Cl activation by Na.

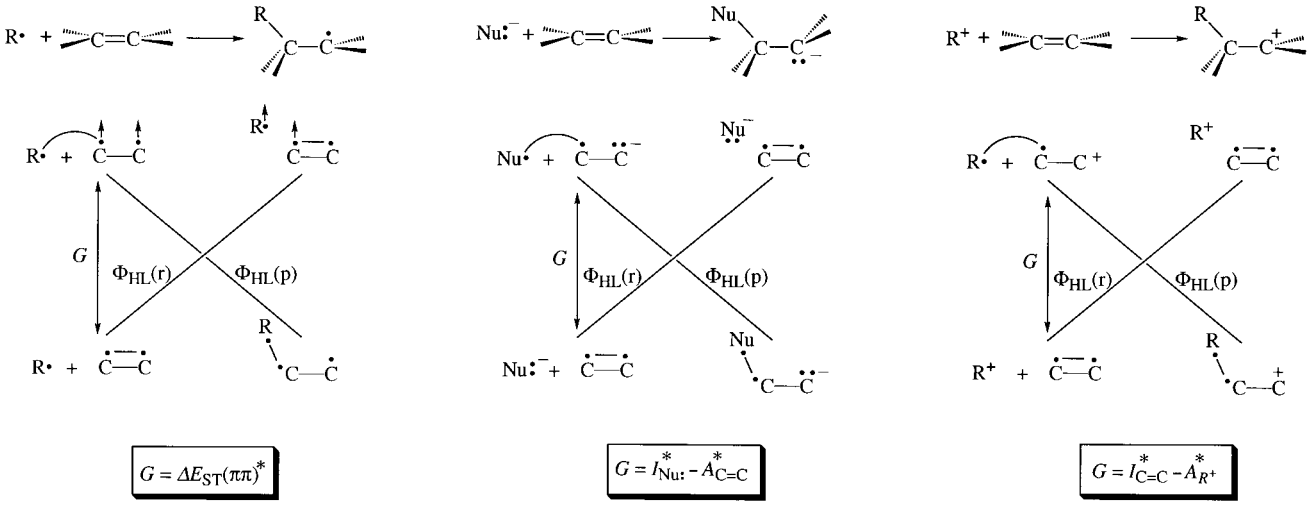

Figure 13. VB correlation diagrams for three elementary addition processes to an olefin. The corresponding promotion energies are specified in the boxes below the diagrams.

Figure 15 depicts the VB correlation diagram for a C–F bond activation by a lanthanide cation (Ln^+).[28] The C–F bond in an isolated molecule is 45% ionic,[14b, c] and its

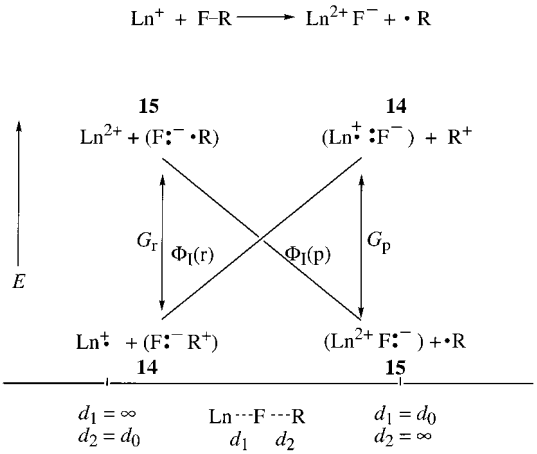

$$G_r = G_{CT} = I_{Ln^+} - A^*_{RF}$$

$$G_p = G_{CT} = I^*_{R\bullet} - A^*_{LnF^+}$$

Figure 15. VB correlation diagram consisting of the ionic VB structures **14** and **15** for C–F activation by a lanthanide cation (Ln^+).

covalent structure has a weak covalent energy.[13, 14] In the presence of Ln^+, the contribution of the ionic structure will increase, and we may consider the ionic structure **14** as the principal structure of the reactants. The LnF^+ bond is mostly ionic, and hence the product's principal structure is **15**. These curves for these two ionic structures intersect along the exchange coordinate, and as such, the excited states of the VB diagram are vertical charge transfer states; the corresponding charge transfer energies are the promotion gaps.

4.2. Ionic Bond Exchange Reactions Which Do Not Involve Valence Bond Crossing

The reactions discussed in Section 4.1 involved formal redox processes in which the metallic species loses an electron during the reaction. As such, the principal structures of reactants and products differ by a single electron shift, and their curves intersect along the reaction coordinate. Exchange of ionic bonds not accompanied by a formal redox will not feature VB crossing. Scheme 3 shows a putative process of ionic bond exchange between a Na^+ ion and a Na^+Cl^- molecule. It is seen that the principal VB structures **16a** and **16 b** are one and the same, and are drawn in the different geometries of reactants and products. Thus, the entire process is described in terms of a single VB structure. The same will be true for reactions which involve exchange of many ionic bonds, as illustrated schematically in **16c**. Thus, in exchange reactions of ionic bonds which do not involve a formal redox, the barrier will not arise from the promotion energy which separates the VB structures, but rather from fluctuations in the Coulomb energy along the reaction coordinate.

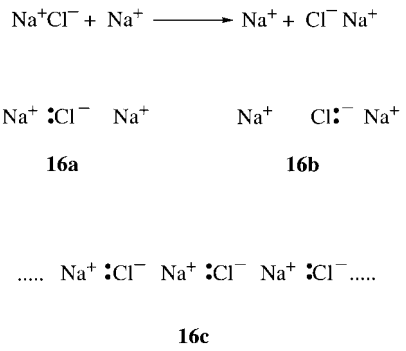

Scheme 3. Examples of bond exchange reactions without crossing of VB curves.

5. Valence Bond Correlation Diagrams for Multi-Bond Processes Involving Polar Covalent Bonds

The term multi-bond process refers to those which involve exchange of more than two bonds or electron pairs. For these processes, the promotion energies as well as the promoted states are more complex than in the case of two-bond processes. Nevertheless, the construction of the VB correlation diagram is still straightforward if one adheres to tips based on Scheme 2, and uses the principal structures which are required to describe the interchanging bonds and electron pairs. Four reaction types are selected to illustrate the construction process of the VB correlation diagram.

Figure 16 depicts the VB correlation diagram for a deprotonation reaction of a carbocation by a base. Scheme 4 shows the reactant's HL structure **17** and the VB structure **18**, which

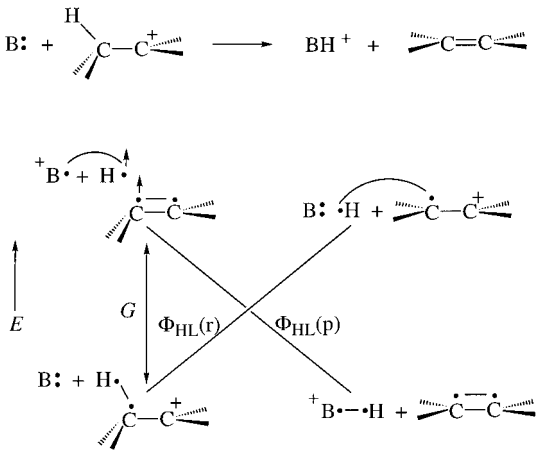

$$G = I^*_{B:} - A^*_{C^+} + \Delta E_{ST}(H\text{–}C) - D_\pi(C{=}C)$$

Figure 16. VB correlation diagram of the HL structures for deprotonation of a carbocation by a base (B:). Note the doubly excited promoted state at the reactant onset. D_π is the π bond energy.

would have been obtained from **17** by mere deprotonation of the C–H bond with no additional reorganization. The resulting olefin moiety in **18** is ionic, and hence **18** corresponds to an excited state of the $\pi\pi^*$ type, and not to the product

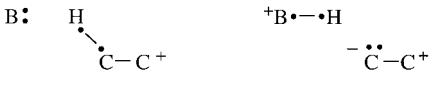

17 **18**

Scheme 4. VB structures of reactants (**17**) and hypothetical products (**18**) of the deprotonation reaction. For the correct VB description of the products, see Figure 16.

state.[7a] Thus, the deprotonation of a carbocation is not a simple bond exchange reaction, and this is revealed in Figure 16 by the intersection of the curves for the HL structures along the reaction coordinate. It is seen that the electronic promotion at the reactant side involves triplet unpairing of the C–H bond along with a single electron shift from the base to the carbocationic center. Note, however, that upon renewed pairing of the electrons in the excited state, two of the electrons are paired into a π bond in the C–C moiety, and therefore part of the excitation energy is paid back, as shown in the expression for *G* in Figure 16.

Figure 17 shows the VB correlation diagram for the Diels–Alder reaction. The excited states in the diagram are seen to involve triplet excitations of all the bonds that are broken

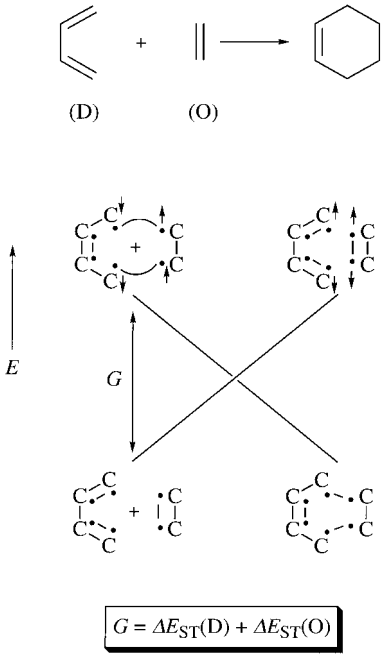

$G = \Delta E_{ST}(D) + \Delta E_{ST}(O)$

Figure 17. VB correlation diagram of the HL structures for a Diels–Alder reaction.

during the reaction, while pairing of the electrons anew takes place across the new linkages. Thus, the excited state on the reactant side involves a triplet diene that possesses a double bond in the central C–C linkage, and its two unpaired electrons on the termini are coupled into two singlet pairs with the triplet ethylene moiety.

To emphasize the unity of the VB correlation diagram we show in Figure 18 the VB correlation diagram for a cycloaddition of two olefins. Much the same as in the Diels–Alder reaction, here too the curves of the HL structures cross along the reaction coordinate and define two ground states and two excited states. It is seen that, in accord with the bond count in

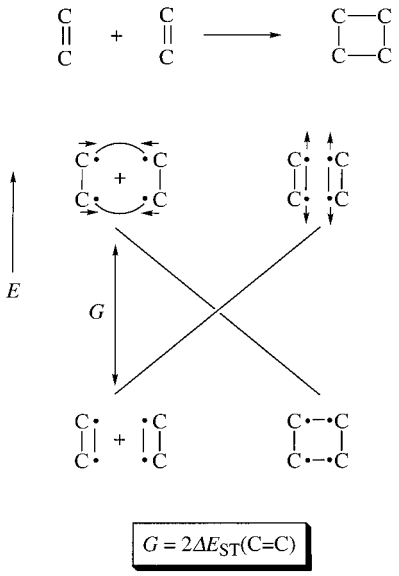

$G = 2\Delta E_{ST}(C{=}C)$

Figure 18. VB correlation diagram of the HL structures for a cycloaddition of two olefins.

the reaction, the promotion energy involves the sum of triplet excitations of the reacting π bonds. Note that unlike the VB crossing in Figure 18, which has a molecular orbital (MO) analogue,[2] the VB crossing in Figure 17 is masked in the MO approach. Much the same holds true for the other processes discussed so far. Thus, with the exception of "forbidden" reactions, where orbital crossing is apparent, in all other cases the origins of the barrier in MO theory are masked, whereas VB theory provides a lucid and unified mechanism for the barrier formation in terms of the crossing of the curves of the principal VB structures associated with the active bonds and electron pairs which participate in the reaction.

Figure 19 shows an application of the VB diagram to an oxidative addition of an organometallic species L_nM into an R–H bond. The organometallic species which are considered

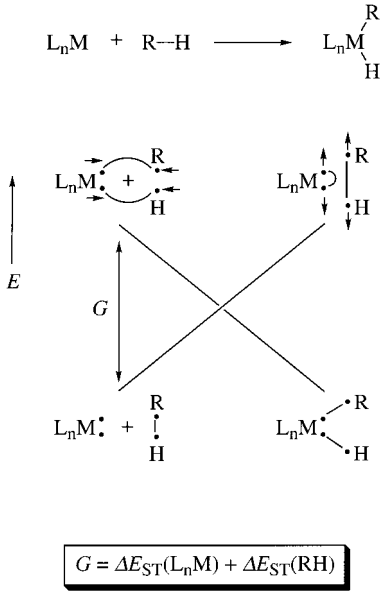

$G = \Delta E_{ST}(L_nM) + \Delta E_{ST}(RH)$

Figure 19. VB correlation diagram of the HL structures for an oxidative addition of a coordinatively unsaturated L_nM fragment across an R–H bond.

possess a filled orbital and a low-lying empty orbital, and are as such isolobal[29] with singlet carbene. Examples are $[Pt(PR_3)_2]$, which is a d^{10} L_2M species, or $[Ru(CO)_4]$ or $[Os(CO)_4]$, which are typical d^8 L_4M species. Once again, the HL structures form a VB correlation diagram in which the promoted states involve excitation of the two moieties into triplet situations while pairing anew of the unpaired electrons across the intermolecular linkages takes place. Of course, insertion of singlet carbene itself and other main group element analogues into a covalent bond will exhibit precisely the same VB correlation diagram.

Before proceeding to generalize, we draw attention to an important aspect which emerges from Figures 16–19, but which is common to all other VB correlation diagrams. The VB correlations themselves are reflections of the electronic properties of the reactants and products. As such, the VB crossing is independent of either the trajectory of the reaction, or of the assignment of the reaction as either formally "allowed" or "forbidden" (e.g., in Figures 17 and 18). Thus, the pairing of the two new bonds in the promoted state in both Figures 17 and 18 can proceed either in a synchronous manner, as implied in the Figures, or one bond at a time along a stepwise trajectory. The difference in the barriers of the competing synchronous and stepwise processes will depend on other factors, such as the resonance energy for the transition state, as discussed later in the article.

6. Rules for Constructing Valence Bond Correlation Diagrams

The preceding applications project a general form of the VB correlation diagram, which may be summarized in rule 1.

***Rule 1**: In any reaction (with restriction of the exchange of ionic bonds unaccompanied by formal redox, as discussed in Section 4.2), the curves of the principal VB configurations intersect along the reaction coordinate. If the bonds which interchange during the reaction are covalent, the intersecting curves are made from the HL structures, whereas when the bonds are primarily ionic the curves will be made from the respective ionic structures.*

An important quantity of the VB correlation diagram is the promotion energy gap at the diagram extremes. The concept of promotion energy emerges naturally from the VB treatment, and inspection of Figures 10–19 shows that the promotion is the mechanism whereby the molecules can break old bonds or electron pairs and replace them by new ones. Since the promoted states are initially vertical states, the mechanism of bond reorganization takes place by VB crossing that interchanges the ground with its promoted state along the reaction coordinate. Eventually part of the promotion energy will enter the barrier of the reaction by the resonance mixing of the VB structures.

As demonstrated in Figures 10–19, the promotion gap is based on two elementary excitations: that of the vertical charge transfer and the singlet–triplet varieties. A simple way to deduce the promotion energy for a given reaction is by "electron bookkeeping" using the formal oxidation states of the reaction centers (groups or atoms) in the two principal VB structures. To illustrate the procedure, let us turn back to Figures 10 and 11. In Figure 10 the principal structures conserve the oxidation state of the reaction centers, and the only change is the interchange in the spin pairing between the two exchanging bonds. In this case, the promotion energy is the singlet–triplet excitation of the bond that interchanges during the reaction. In Figure 11, however, the principal structures involve a change in the formal oxidation state of the reaction centers, so that a single electron shifts from the anion $X:^-$ to the radical $^{\cdot}X$. In this case, the promotion involves a vertical charge transfer from the donor moiety to the acceptor moiety. The nature of the promotion energy can be summarized in rule 2 based on the elementary excitations which are involved in the principal VB configurations.

***Rule 2**: An interchange of spin pairing in the two principal configurations requires singlet–triplet excitation, while a change in the formal oxidation state requires charge transfer excitation. For reactions which involve no formal redox process at the reaction centers, the promoted states involve only singlet–triplet excitations, one for each bond which has to be broken in the transformation. For reactions which involve a formal redox process at the reaction centers in addition to bond exchanges, the promoted states involve one charge transfer excitation for each pair of centers which undergo formal redox reactions. The rest of the excitations will be of the singlet–triplet variety. In each case, the unpaired electrons are paired anew across the new linkages.*

7. State Correlation Diagrams—Origins of the Barrier and Reactivity Patterns in Chemical Reactions

As noted at the beginning of Section 2.2, in addition to the principal VB structures there exist secondary ones which mix with the principal structures. As such, there are two alternative approaches to conceptualize reactivity patterns: VB configuration mixing diagrams and state correlation diagrams (the past abbreviations[1, 4, 7] VBCM and SCD are changed here into VBCMD and VBSCD, respectively, for the sake of consistency). The VBCMD alternative, which is described later in this article, includes explicitly the additional VB structures in the diagram. This way has quite a few advantages (e.g., explicit account of bond ionicity in bond exchange reactions), but the simplicity of the two-curve diagram is lost. The VBSCD alternative, which we shall discuss now, conserves the two-curve format of the VB correlation diagram, by mixing the secondary structures into the principal curves and generating thereby two semi-delocalized state curves which are anchored in spectroscopic-like states, hence the name a state correlation diagram (VBSCD).[1, 4a, b, 7] An appealing feature of the VBSCD is the retention of simplicity of the two-curve VB correlation diagram, and the advent of a unified mechanism for the origins of the barrier.

To illustrate the relationship of the VBSCD to its VB correlation diagram precursor, we show the nucleophilic exchange process in Figure 20. Figure 20a recalls the VB

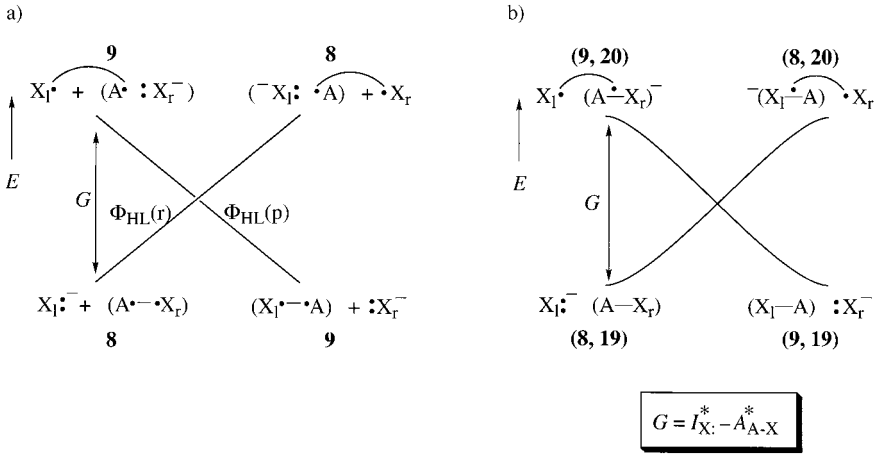

Figure 20. a) VB correlation diagram of the HL structures for a nucleophilic exchange process, b) corresponding VBSCD. See text for details.The contributing VB configurations to the ground and excited anchor states in the VBSCD are shown in parentheses (see also Scheme 5).

correlation diagram based on the HL structures (see Figure 11), while Figure 20b shows the VB state curves; the ground states are the Lewis structures of reactants and products, and the excited states are the corresponding charge transfer states. Scheme 5 shows the two secondary structures

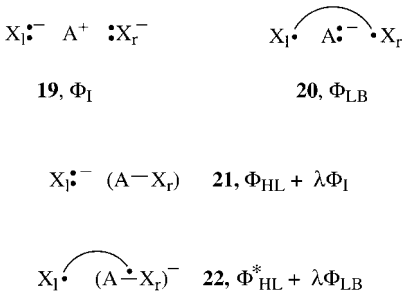

Scheme 5. Secondary VB structures and concrete examples for VB states that play a role in the attack of a nucleophile.

19 and **20**, which by mixing with the HL configurations transform the latter into VB states; a pair of ground and promoted states is depicted explicitly with **21** and **22**. Accordingly, **19** is an ionic structure, which by mixing with the reactant's HL structure (**8**) generates the Lewis ground state structure of the reactants, **21** (λ is the mixing coefficient). The product's Lewis structure is obtained by the mixing of **19** with the product's HL structure **9**. Similarly, **20** is a long-bond structure which possesses three electrons in both A–X linkages. By mixing with the excited HL structure **9**, **20** generates the charge transfer state **22**, where the radical anion moiety has three electrons delocalized over the A and X groups through the VB mixing. The other charge transfer state arises by mixing of **20** with the excited HL structure **8**. These mixing patterns account for the generation of the VB states in Figure 20b.

By comparison of Figure 20a and 20b, it becomes apparent that the VBSCD is anchored at the states which are obtained from the principal VB structures. This enables drawing of the VBSCD in a general form, as shown in Figure 21a, with two ground states and two promoted excited states which can be deduced from the principal VB structures (review rules 1 and 2 in Section 6) for any desired reaction. The promoted states are indicated with two subscripts, the first specifies the geometry and the second the electron-pairing pattern. For example, Ψ^*_{rp} is a vertical excited state at the geometry of the reactants (r) with the electron-pairing pattern of the products (p).

In a subsequent step, the two VBSCD curves are allowed to mix with each other, as shown in Figure 21b. As a result, the crossing of the two curves is avoided by their resonance mixing, which leads to a resonating transition state on the lower energy profile. The barrier for the forward reaction can be expressed as a balance between the destabilization

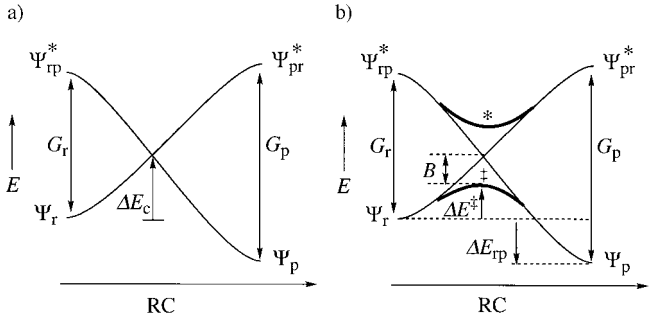

Figure 21. a) Generic VBSCD with two ground states and two promoted excited states, and b) the resulting states due to resonance mixing (avoided crossing). G = promotion energies, ΔE_c = energy of the crossing point relative to the reactant state, ΔE_{rp} = thermodynamic driving force of the reaction, $\Delta E^{\ddagger}$ = barrier, B = resonance energy of the transition state, Ψ_r = reactant state, Ψ_p = product state, Ψ^*_{rp} and Ψ^*_{pr} = promoted excited states.

energy ΔE_c needed to reach the crossing point and the resonance interaction energy B. The destabilization energy ΔE_c is a fraction f of the promotion gap G_r that enters under the crossing point. Consequently, the barrier will have the form of Equation (6), which describes a simple activation

$$\Delta E^{\ddagger} = fG_r - B \qquad (6)$$

mechanism which is in tune with the electronic reorganization required in order to break old bonds or electron pairs and replace them by new ones during the reaction.

The transition state is the situation where the ground state and the corresponding promoted state are in resonance. Since the two states are initially separated by the promotion energy, structural changes are required to destabilize the ground state (e.g., by means of bond deformations and nonbonding repulsions) and to simultaneously stabilize the promoted state (by bond formation and release of nonbonding repulsions). At some point along the reaction coordinate the promotion gap separating the states is closed and a resonating transition situation is achieved, enabling the bonding pattern to change from reactantlike to productlike.

7.1. Structure – Reactivity Relationships Dominated by the Reaction's Promotion Energy

While both Figure 21b and Equation (6) implicitly show that trends in the barrier will be determined by an interplay of factors, it is apparent that the factor that originates and gauges the barrier is the promotion energy gap which has to be overcome during the reaction. We might therefore anticipate that quite a few reactivity patterns will be dominated by the promotion gap. This restrictive outlook is didactically necessary in order to appreciate the impact of the promotion energy on reactivity. With this in mind we turn to discuss reactivity puzzles and their origins in the variation of the promotion gap. Relying on Figure 21, rule 2 (strictly correct for state curves), and Equation (6), most of the cases are discussed by showing the ground state and promoted state ($\Psi^*_{\rm rp}$) without constructing the entire VBSCD.

7.1.1. Barriers of Identity Reactions in Hydrogen Abstraction from Alkanes

Identity reactions proceed without a thermodynamic driving force, and project therefore the role of promotion energy as the origins of the barrier. Let us consider the identity process of hydrogen abstraction by an alkyl radical shown in Equation (7). The barriers for a series of radicals have been

$$R^{\cdot} + H{-}R \rightarrow R{-}H + {}^{\cdot}R \qquad (7)$$

computed by Yamataka and Nagase,[30] and were found to increase as the R–H bond energy D increases. Thus, for example, the relative barriers for $R = CH_3$ and $R = C(CH_3)_3$ (22.4 and 15.3 kcal mol^{-1}, respectively) were found to be in accord with the relative bond strengths in the two alkanes (104 and 94 kcal mol^{-1}, respectively). Since the effect of bond breaking and bond making is balanced in the symmetric transition state, one might wonder why should the barrier reflect only the strength of the bond which is broken during the reaction.

This trend has been interpreted by Pross et al.[31a] using the VBSCD model. Figure 22 depicts the ground states and the promoted state in the respective VBSCD (which follows from

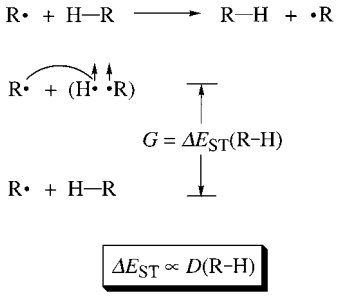

Figure 22. Ground state, promoted excited state, and promotion energy gap for an identity hydrogen atom transfer.

Figure 10 and rule 2). The promotion gap which originates the barrier involves singlet – triplet excitation of the R–H bond. With VB theory[7a] it is possible to show that the singlet – triplet excitation of a bond is proportional to the respective bond energy. Therefore, the correlation of the barrier with the bond strength is in fact a correlation with the promotion energy, and reflects the electronic reorganization which is required during the reaction.

A spectacular relationship between excitation energy and the barrier to reaction has been observed for $X_3^{\cdot}$ clusters, which occur en-route for the radical exchange process shown in Figure 23. Here, a very large triplet promotion energy for

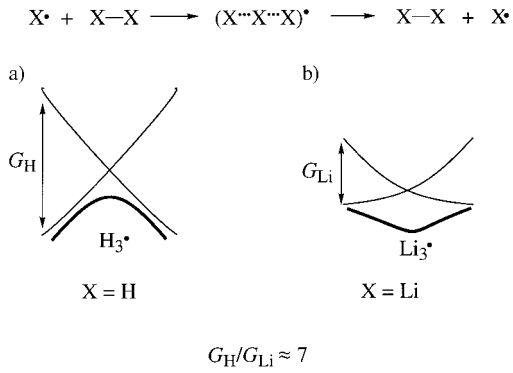

Figure 23. Schematic representations of VBSCDs computed[5a] with the ab initio VB method for a) H-atom transfer where the avoided crossing leads to a barrier, and b) Li-atom transfer where the avoided crossing leads to an intermediate cluster.

$X = H$ (250 kcal mol^{-1}) results in an $H_3^{\cdot}$ transition state, while the small promotion energy for $X = Li$ (32 kcal.mol^{-1}) results in a stable $Li_3^{\cdot}$ cluster. The VB computations by Maitre et al.[5a] show that, as the promotion gap drops drastically, the avoided crossing leads to a stable cluster as in the case of $Li_3^{\cdot}$ in Figure 23b.

Of course, effects of bond ionicity exist in general in radical reactions and can be discussed by considering the consequences of mixing the ionic structures on the state curves and on the resonating transition state.[31b]

7.1.2. One Electron Less, One Electron More: Why Are Cycloaddition Reactions of Ion Radicals So Fast?

It is well known that the cyclodimerization of olefins is a sluggish process which proceeds with a barrier greater than 40 kcal mol^{-1}. In contrast, as shown by the seminal work of Bauld et al.,[32] the corresponding reaction between an olefin and its cation radical is a very facile process. Figure 24 shows the promotion energies for the two processes along with barriers calculated by Bernardi et al.[33] and Jungwirth and Bally.[34] Based on Figure 18 and rule 2, the cyclodimerization of ethylene, which requires unpairing of the electrons of two bonds, has a promotion energy which is twice the singlet – triplet excitation of the π bonds. In contrast, in the attack of a radical cation on a neutral olefin the promotion energy is halved, because now only the neutral olefin needs to be unpaired.[35] While other factors certainly help (e.g., the reaction driving force and electrostatic interactions), the significant drop in the promotion energy (by about 100 kcal mol^{-1}) accelerates the reaction and accounts for a significant drop in its barrier.

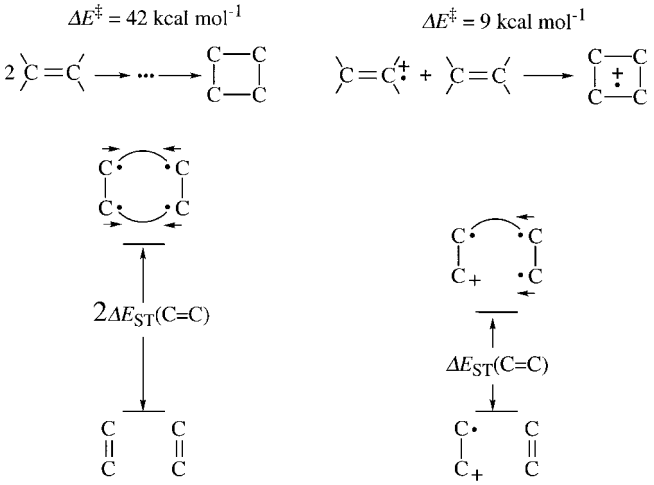

Figure 24. Ground states, promoted excited states, barriers, and promotion energy gaps for a cyclodimerization of two neutral ethylene molecules, and for a combination of an ethylene cation radical with a neutral ethylene molecule.

A related catalytic effect is found in the DNA repair mechanism.[36] One of the DNA damages initiated by sunlight is the dimerization of DNA bases to form cyclobutane photodimers such as the thymine photodimer in the top left of Figure 25. The in situ repair mechanism involves a photo-induced electron transfer from a reduced flavin and folate,

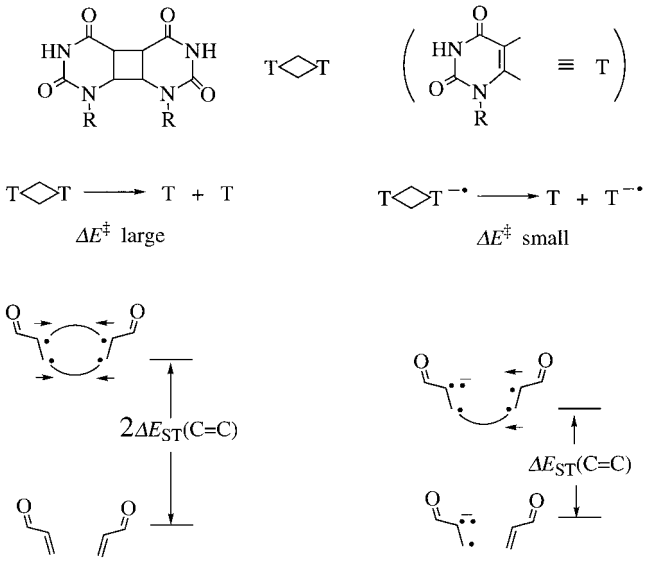

Figure 25. Comparison of the cleavage of the thymine photodimer (left) and the corresponding anion radical, which is responsible for the in situ repair mechanism of DNA (right). Ground states, promoted excited states, and promotion energy gaps are shown for the reverse processes using the enone moieties of thymine.

which are cofactors of the photolyase enzyme. The electron transfer process generates in turn the radical anion of the dimer, which undergoes facile cleavage to its constituents (Figure 25, middle right). This is contrasted with the neutral photodimer, which resists decomposition[36a] (Figure 25, middle left) even at temperatures above 200 °C and despite the fact that the reaction is exothermic (-27 kcal mol^{-1}).[36a] To appreciate the effect we show at the bottom of Figure 25 the VB states for the reverse process, where it is seen that dimerization of the neutral bases will require singlet–triplet excitation of the two reacting π bonds, in comparison with only half of this quantity for the cycloaddition of the anion radical and the neutral molecule. Thus, the DNA repair is catalyzed by the reduction in promotion energy for the reaction.

7.1.3. Why Do Some "Allowed" and Very Exothermic Reactions Possess High Barriers?

Scheme 6 depicts three cycloaddition processes taken from a recent study by Ioffe and Shaik.[37] All the reactions are formally allowed, but nevertheless the latter two have very

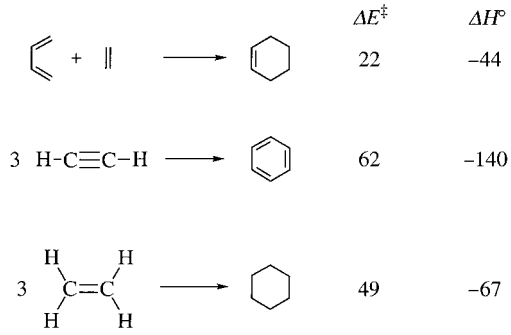

Scheme 6. "Allowed" cycloadditions with very different barriers. The energies are given in kcal mol^{-1}.

high barriers. Moreover, the reactions with the high barriers are extremely exothermic, while the least exothermic Diels–Alder reaction has the lowest barrier. Figure 26 compares the

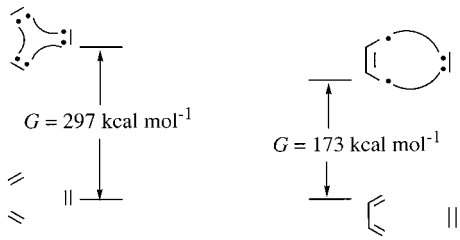

Figure 26. Ground states, promoted excited states, and promotion energy gaps for the trimerization of ethylene (left) in comparison with the Diels–Alder reaction (right).

promotion gaps of the Diels–Alder reaction (right) and the trimerization of ethylene (left), based on the discussion of Figure 18 and rule 2. In the trimerization reaction, the promoted state involves unpairing of the three π bonds into triplets, while pairing anew of the electrons across the infinitely long intermolecular linkages is of no energetic significance. The resulting promotion energy is high (297 kcal mol^{-1}), much larger than the corresponding quantity for the Diels–Alder process (173 kcal mol^{-1}).

The small promotion energy of the Diels–Alder process originates in the diene, for which the excitation energy is less than half of the corresponding energy for the promotion of two isolated π bonds. Thus, unpairing the double bonds of the ground-state diene to two triplets and pairing anew the four electrons creates a π bond in the central C–C linkage and

localizes two triplet electrons on the termini, thereby minimizing the triplet repulsion energy. These two effects together reduce the promotion energy of the diene to 79 kcal mol^{-1}, in comparison with almost 200 kcal mol^{-1} for two isolated double bonds. Thus, using a conjugated diene creates a huge intramolecular advantage in the promotion energy over the intermolecular situation and lowers the barrier significantly.

The very high barrier for the trimerization of acetylene (Scheme 6) can now be understood easily by simply considering the promotion gap (ca. 375 kcal mol^{-1}) corresponding to the triplet excitation of three acetylene molecules.

7.1.4. When Do "Forbidden" Reactions Become Facile?

Scheme 7 shows that the computed barrier for ethylene dimerization[33] is very large, as anticipated. However, the corresponding silaethylene and disilene dimerizations are

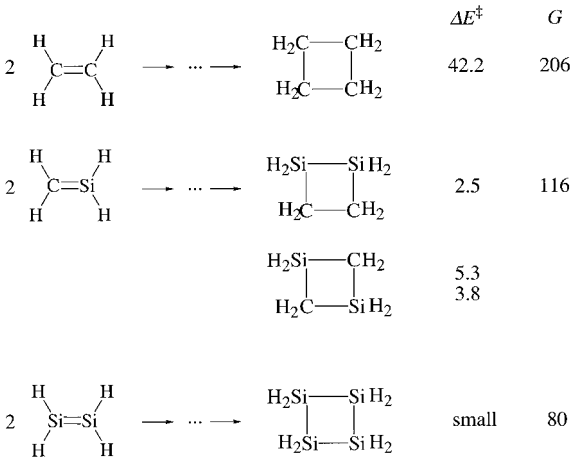

Scheme 7. Comparison of the barriers and excitation energies (in kcal mol^{-1}) for several "forbidden" cycloadditions.

seen to have negligible barriers, despite their formal "forbiddenness". While the computational studies differ in their mechanistic conclusions, regarding the question of whether or not the head-to-tail dimerization of silaethylene proceeds in a concerted fashion,[38] all calculations agree that the barriers are tiny irrespective of the precise mechanistic details.[33, 38] These computational trends model faithfully the experimental findings.[39]

It is true that the dimerizations of the silicon compounds are more exothermic than that of ethylene. However, as noted for the examples in Scheme 6, even extreme exothermicity is insufficient to produce a small barrier when the promotion energy is large. The promotion energy, which is the sum of singlet–triplet energies of the two reactants calculated by us[40] at the CASSCF/6-311G**//CASSCF/6-311G** level, is displayed in Scheme 7. It is seen that a substitution of carbon by one or two silicon atoms reduces the excitation by a sizeable amount of 100 kcal mol^{-1} and more, which accounts for a significant lowering of the barriers.

The reduction in the promotion energy in Scheme 7 is in accord with the trends of excitation energies in the periodic table. Thus, small triplet excitation energies generally occur among main group elements which are located in the lower rows and in the metallic block, and this is where formally forbidden reactions will possess low barriers. In fact, four-center clusters of alkali metals are more stable than their separated diatomic molecules.[41]

7.1.5. Zipper Reactions: When Are They Facile?

The impact of the promotion energy on reactivity may be appreciated by analyzing the feasibility of zipper reactions, in which many bonds would participate synchronously in an exchange or a cycloaddition process. A similar question was posed by Dewar quite a few years ago.[42] The answer to this question depends on whether the bonds which participate in the reaction are covalent or ionic.

In the case of covalent or polar covalent bonds the isomerization and structural reorganization require a promotion energy which increases with the number of participating bonds. As such, reactivity tends to be localized in a small number of bonds, and collective zipper reactivity is usually prohibitive. Exceptions may be encountered when the molecules involve either conjugated bonds, or when the bonds are fixed in proximity; in both these situations the reaction will benefit from lowering of the promotion energy by the "intramolecular advantage",[37] in analogy to the situation in Figure 26. This reduction of the promotion energy, by the intramolecular or proximity effects, will generally lower the barrier, and may thereby enable zipper reactivity of covalent bonds.

In the case of ionic bonds, such as Na^+Cl^-, isomerization and structural reorganization require no promotion energies, since the entire energy hypersurface of such a reaction will be described by a single VB configuration, that is, the ionic VB structure (**16c** in Scheme 3). Consequently, zipper reactions of ionic bonds are expected to be facile. Ionic exchange reactions have been considered by King and Herschbach,[43] who dubbed these processes as "no-electron reactions" to emphasize their exclusive ionic nature across the reaction path.

7.1.6. Why Does C–H Activation by CrO_2Cl_2 Exhibit a Radical-Like Selectivity Even Though the Reagent Is Diamagnetic?

The mode of spin pairing in the promoted states of a reaction may serve also as an indicator of mechanistic possibilities. Let us illustrate this feature by considering the intriguing mechanism suggested recently by Mayer and Cook[44] for C–H activation by CrO_2Cl_2 (Scheme 8a). The

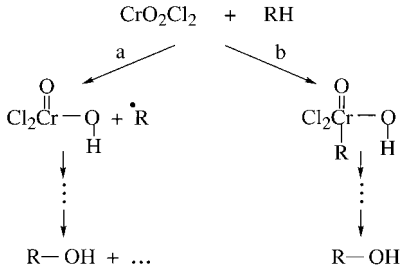

Scheme 8. Mechanistic alternatives of C–H activation by CrO_2Cl_2.

initial step is a hydrogen abstraction followed by trapping of the alkyl radical to form alcohol, among other products. As was pointed out by Cook and Mayer repeatedly,[44] CrO_2Cl_2 is a diamagnetic species and nevertheless the process transpires by a stepwise radical mechanism, and its structure–reactivity patterns exhibit a radical-like selectivity. To balance this view, Scheme 8b shows the mechanism discussed by Rappé and Goddard[45] based on their GVB calculations. Thus, in addition to a radical mechanism of the type found by Mayer and Cook, the calculations suggest that a concerted addition of the C–H bond to the Cr=O bond should also be considered. This last mechanism appears to be the main mechanism of C–H activation by metal oxide cations in the gas phase.[8, 46]

The electronic structure of the Cr=O bond was investigated by Rappé and Goddard,[45] and the main features are depicted in Figure 27a. Thus, in analogy with the C=O bond in ketones

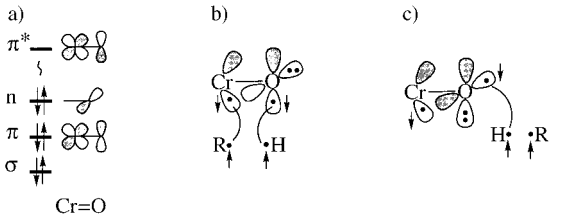

Figure 27. a) Schematic orbital diagram for the Cr=O bond in CrO_2Cl_2. b, c) Alternative promoted excited states for the reaction of CrO_2Cl_2 with R–H.

or aldehydes, the Cr=O moiety possesses a double bond and a lone pair on the oxygen, whose orbital is perpendicular to the plane of the π bond. By the same analogy to the carbonyl group, two promoted states of the Cr=O bond might be considered to affect the nature of the bond-activation step. The first state (Figure 27b) involves a ππ* triplet Cr=O coupled to a singlet with the promoted C–H bond moiety. This coupling mode may be associated with the concerted addition mechanism (Scheme 8b) which occur so often in metal oxide cations. The second promoted state (Figure 27c) involves an nπ*-promoted coupling of Cr=O to the promoted C–H moiety. This latter situation correlates nicely with the product state of the hydrogen abstraction (Scheme 8a). Based on spectroscopic and computational data,[47] these two promoted states are expected to be close in energy, and to originate thereby the two possible competing mechanisms. Thus, the modes of electron pairing in the promoted states have mechanistic significance.

7.1.7. What Is the Role of Charge Transfer Promotion in Reactions between Electrophiles and Nucleophiles?

Figure 28 shows a structure–reactivity correlation for the nucleophilic cleavage of an ester, based on the VBSCD analysis of the reaction by Buncel et al.[48] It is seen that the free energies of activation correlate with the vertical ionization energy of the nucleophiles in the reaction solvent. Furthermore, localized and delocalized nucleophiles appear to generate correlation lines of different slopes. Similar correlations were found for three other esters.[48] The rate-determining step of the mechanism had been shown by

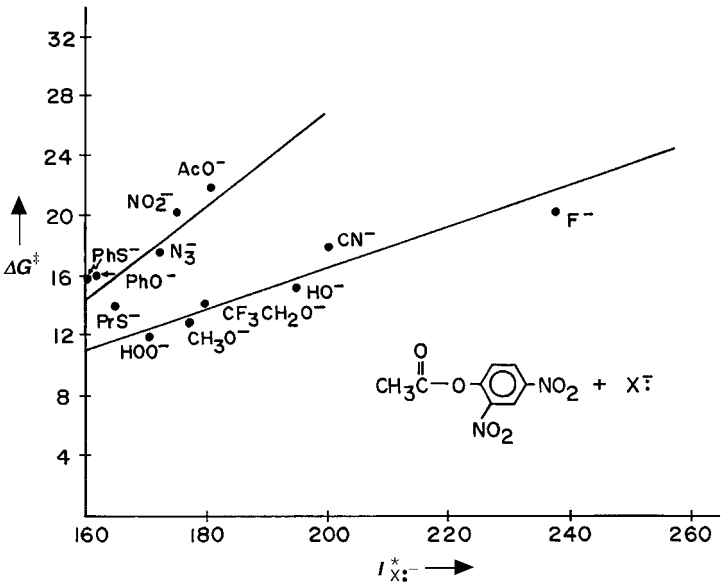

Figure 28. Correlation of free energy barriers with vertical ionization energy of nucleophiles for nucleophilic cleavage of an ester (adapted from ref. [48]). Energies in kcal mol^{-1}.

Schowen et al.[49] and Gold et al.[50] to involve the formation of the tetrahedral intermediate, as depicted in Figure 29.

Following the general VBSCD in Figure 21b and rule 2, we show in Figure 29 that the promoted state in the VBSCD for the formation of the tetrahedral intermediate is the vertical charge transfer state. The promotion energy is, accordingly,

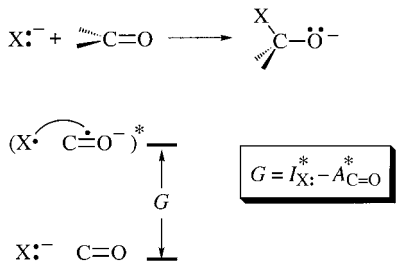

Figure 29. Ground state, promoted excited state, and promotion energy gap for the nucleophilic addition to a carbonyl group to form a tetrahedral intermediate.

the difference between the vertical ionization potential of the nucleophile and the electron attachment energy of the carbonyl group. The latter quantity is a constant for a given ester, and therefore the correlation of barriers with the promotion energy becomes a correlation with the vertical ionization energy of the nucleophiles.

The two correlation lines obtained for the experimental data in Figure 28 are readily understood based on Equation (6) as corresponding to different f values, where the localized nucleophiles possess the smaller f value and hence the smaller structure–reactivity slope in comparison with the delocalized nucleophiles. Thus, when the nucleophiles are delocalized a larger fraction f of the promotion gap enters under the crossing point, reflecting thereby the need to localize the transferred electron in order to form the X–C bond, and effects the correlation of the charge transfer state down to the tetrahedral intermediate product. This

emphasizes that the correlation of reactivity with the vertical charge transfer energy is a manifestation of the mechanism of activation, which consists of bringing the two states in Figure 29 into resonance mixing. It follows therefore that significant lowering of the charge transfer promotion energy will be expected to facilitate the process. The reduction of the charge transfer promotion gap may account in part for the catalysis of ester hydrolysis by proteolytic Zn^{2+} metalloenzymes (e.g., carbopeptidase A[23a]), where the coordination of the metal ion to the carbonyl group increases the electron attachment energy of the ester moiety.

Correlations of free energy barriers with the vertical charge transfer energies have been amply observed for classical "polar" reactions between electrophiles and nucleophiles by Kochi and co-workers in their seminal work on "charge transfer activation".[51] A variety of reactions between electrophiles such as bromine, chlorine, and mercury diacetate with π nucleophiles such as olefins and arenes have been found to follow the same charge transfer correlations. The studies were extended by Fukuzumi et al.[52] to other processes, including hydride transfers. The interpretation of this correlation type has been shrouded with controversy. For example, the recent *mise au point* by Baciocchi and Mandolini[53] confronts the applicability of this concept to electrophilic aromatic substitution, and concludes that it is "unsound" because the experimental data does not indicate that an electron transfer component plays a role in the reaction.

In our view, much of the controversy originates in a misconception that the correlation necessarily indicates some type of an electron transfer mechanism.[51] Because of the ubiquity of the correlation, it is important to outline the relationship between a polar and an electron transfer (ET) reaction which can transpire between a pair of closed-shell[4c, 54] nucleophiles and electrophiles. Figure 30 shows the VBSCDs of the two processes which are initiated from the same pair of states in the center of the diagram, and then proceed along two different reaction coordinates indicated by the bond order *n* between the reactants. In the polar process, the crossing between the ground and charge transfer states occurs along a reaction coordinate which exhibits a progressive increase of the Nu···El bond order. In this case, the resonance mixing between the two VB configurations is large, and the resonating transition state is typified by strong bonding, that is, a large resonance energy *B*. To the left, the same two states cross either along a coordinate which keeps a zero bond order throughout—that is, a weakly bonded outer-sphere ET mechanism—or along a path where the reactants initially approach one another to achieve significant bonding and then recoil to give the separated radicals—that is, a bonded ET mechanism.[54]

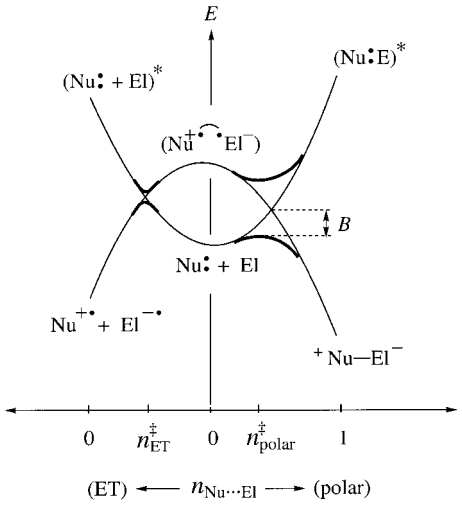

Figure 30. VBSCDs for competing polar and ET pathways available to a pair of closed-shell nucleophile and electrophile (Nu:+El). The ground state and promoted excited state of the reactants are common to the two mechanisms, and avoided crossing occurs along different reaction coordinates specified in terms of the bond order *n* between the two reactants.

Thus, the polar and ET mechanisms are related in the origins of their barriers by the avoided crossing of the same two states, and hence may exhibit similar free energy correlations with the vertical charge transfer energies. However, in all other aspects these are different mechanisms. This is the reason why we have suggested to call polar reactions "single electron shift processes" to link them to, and at the same time distinguish them from, single electron transfer mechanisms.[4a, e]

Aspects of this mechanistic dichotomy can be found in the various reviews and monographs.[4, 55] Recently, Verhoeven et al.[56a] have used the VBSCD model to explain the correlations found between the hydride transfer process and electron transfer energies. A similar treatment of hydride transfer between carbocations and silanes was later published by Apeloig et al.[56b] In any event, a simple test can be used to show that a polar reaction is not an ET reaction, as has been reported by Eberson,[55] Verhoeven et al.,[56a] and Mayr, Fukuzumi et al.[57] Thus, the controversy can be avoided and replaced by efforts to extract useful information about the origins of the barrier and the structure of the transition state from correlations[48] as those in Figure 28 and in Kochi's work.[51]

7.1.8. Origins of the Correlation between C–F Bond Activation Ability of Metal Cations and Their Ionization Energy

Recent studies by Cornehl et al.[28a] showed that lanthanide cations (Ln^+) are capable of activating C–F bonds quite selectively from aryl and alkyl fluorides, even though there exist weaker C–C and C–H bonds in the substrates. Furthermore, the reactivity patterns of the Ln^+ species did not follow the trends in the C–H/C–C bond activation mechanism,[58] which involves an initial insertion into the bond. Whereas the insertion efficiency into C–H/C–C bonds was found to correlate with the promotion energy of Ln^+ to a state which contains two non-f electrons capable of covalent bond formation, the C–F activation efficiency did not follow that trend. Instead, the efficiency of C–F activation was found to depend on the ionization energy of the Ln^+ (Figure 31). Similar trends have been noted by Harvey et al.[28b] for transition metal cations ($M^+ = Y^+$, Sc^+, Ti^+, V^+).

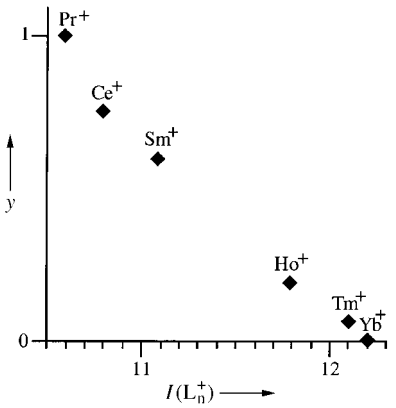

Figure 31. Correlation of relative efficiency y of C–F bond activation by lanthanide cations (Ln^+) with the ionization energy of Ln^+ (adapted from ref. [28a]).

While these trends are suggestive of an electron transfer or a "harpoon" mechanism, it is very clear that a long-distance electron transfer cannot occur due to unfavorable thermodynamics. Moreover, there are clear indications that the C–F activation mechanism involves bonding between the reaction partners and is not a simple electron transfer process. First, the transition state for the C–F bond activation by Ca^+ was computed by Harvey et al.,[28b] who found it to be structured, as depicted in Scheme 9. Second, for the same M^+ ionization energy, the activation capability was found to be largest for a transition metal ion, intermediate for Ca^+, and lowest for a Ln^+ ion, and thus reflecting the respective relative covalency of the essentially ionic M^{2+}–F^- bonds. These trends indicate that the correlation in Figure 31 exists for related ions, but its slope will differ for different families of ions, and will reflect thereby the relative covalent bonding in the transition states.

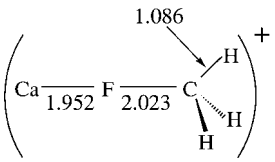

Scheme 9. Calculated transition state of C–F activation by Ca^+.

Figure 32 shows a schematic VBSCD for the C–F activation by metal ions. It is seen that the reaction involves an avoided crossing of ground with charge transfer states. The corresponding transition state arises by resonance mixing of the VB state curves, and will possess thereby considerable bonding. The promotion energy for the C–F bond activation is seen to depend on the ionization energy of the metal ion, and therefore in a family of related ions like Ln^+ one might anticipate that the promotion energy will dominate the reactivity trends. Thus, the experimental correlation in Figure 31 does not indicate an electron transfer mechanism, but is a reflection of the nature of the activation process which overcomes the charge transfer promotion energy and generates a resonating transition state. A similar conclusion was reached for electrophile/nucleophile reactivity (Section 7.1.7).

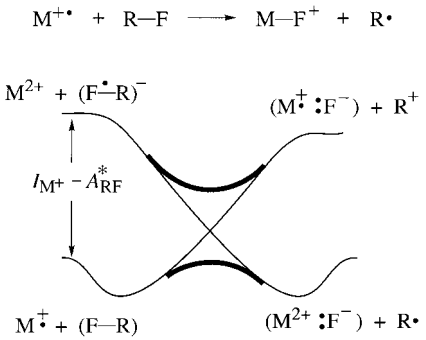

Figure 32. VBSCD for the C–F bond activation by a positive metal ion M^+ (based on the VB correlation in Figure 15).

7.1.9. Other Reactivity Trends Which Respond to the Promotion Energy Gap

There are plenty of other applications of the VBSCD which project the role of the promotion energy. Su[59] has discussed the reactivity of carbenes and their isolobal organometallic analogues in bond insertion reactions. A related work by Pross and Moss[60] has shown the role of promotion energies in carbene addition to olefins. Our own treatments of S_N2 reactivity,[4a-c] β-elimination of organometallic complexes,[61] nucleophilic cleavages of σ-cation radicals,[62] nucleophilic vinylic substitution reactions,[63] stability of clusters with $4n/(4n+2)$ electrons,[64] hyper coordinated radicals,[65] and so on[4, 7] all reflect the impact of promotion energies.

8. General Structure – Reactivity Patterns Based on the VBSCD Model

While the role of the promotion energy as the origin of the barrier is evident by now, the VBSCD model in Figure 21b contains other factors which scale the barrier for a given promotion energy. It is apparent that the height of the crossing point is a fraction f of the promotion gap, as expressed in Equation (6), but there are several ways to express this fundamental relationship explicitly by approximation of the VBSCD curve. Equation (8) is a barrier expression derived[66] from the VBSCD, and shows the explicit dependence on the two promotion gaps, on the thermodynamic driving force of the reaction, on the resonance energy of the transition state, and on the two f factors of the individual curves. These f factors determine the fraction of the promotion gap which enters under the crossing point in a reference thermoneutral situation. By simplification,[62, 67] we obtain a more lucid expression in Equation (9), which can be related to Equation (6) through Equation (10). Here it becomes apparent

$$\Delta E^{\ddagger} = [(f_r + f_p)G_r + (1 - f_r - f_p)\Delta E_{rp}]\frac{(G_p + \Delta E_{rp})}{(G_r + G_p)} - B \quad (8)$$

$$\Delta E^{\ddagger} = f_{av}G_r + (0.5 - f_{av})\Delta E_{rp} - B;\ f_{av} = 0.5(f_r + f_p) \quad (9)$$

$$f = f_{av} + \frac{\Delta E_{rp}}{G_r}(0.5 - f_{av}) \quad (10)$$

that the f used in Equation (6) is an effective parameter that sums up the various effects which determine the fraction of the promotion energy that enters under the crossing point of the VBSCD in Figure 21b.

Equations (8) and (9) have been tested and found to provide reasonable quantitative estimates of barriers.[4a, 62, 67, 68] The detailed comparison of these and other possible barrier

expressions will be waived since all the VBSCD expressions hold the same qualitative structure – reactivity patterns which are summarized in Figure 33.

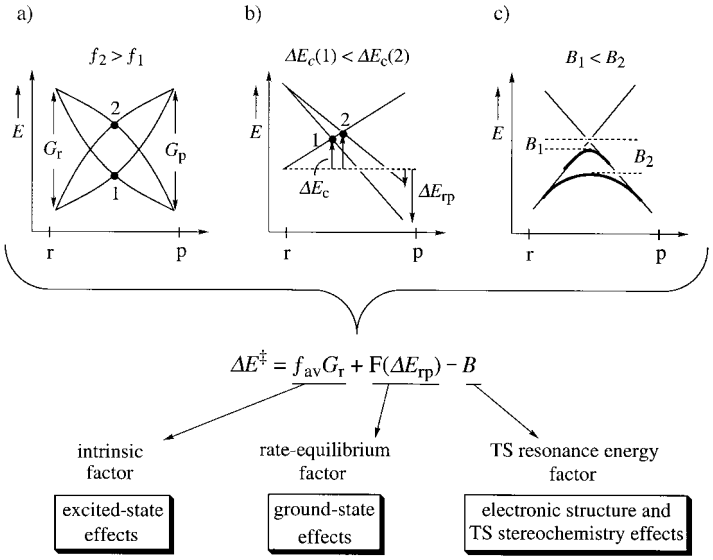

Figure 33. General reactivity patterns predicted by the VBSCD model. a) The effect of f on the height of the crossing point. The fG term brings in excited-state effects on reactivity; f is an intrinsic selectivity factor. b) The effect of the reaction energy driving force (ΔE_{rp}) on the height of the crossing point. $F(\Delta E_{rp})$ signifies some function of the ΔE_{rp} variable. The ΔE_{rp} term is responsible for rate – equilibrium relationships. c) The effect of the resonance energy B of the transition state; B is the electronic and structural code of the transition state.

The first barrier factor is an intrinsic quantity which reflects the electronic reorganization required in order to break old bonds and make new ones by the resonance mixing mechanism (avoided crossing) in the VBSCD. This term is determined by the promotion energy scaled by the average index f_{av}. Figure 33a shows that the effect of f_{av} is manifested by varying the height of the crossing point through the curvature of the intersecting curves (compare 1 with 2). Thus, f_{av} is a response and a selectivity factor which determines the dependence of the barrier on the promotion energy. In turn, variations of f_{av} size the height of the crossing points, and thereby the extent of bond deformations in the transition states of the series.

The second barrier factor brings in the effect of the thermodynamic driving force. As shown in Figure 33b, changes in the driving force factor modulate the height of the crossing point (compare 1 with 2), and thereby scale the barrier up or down. This dependence is the origin of the widespread rate – equilibrium relationships

Finally, the resonance energy of the transition state B lowers the energy of the transition state below the crossing point to an extent that reflects the electronic structure of the transition state itself and its stereochemical characteristics (Figure 33c). It is here in this factor that orbital symmetry and nodal properties are encoded.[7]

Thus, the VBSCD incorporates the role of traditional physical-organic factors with novel ones associated with the promotion energy and effects of excited states. The model predicts that reactivity patterns will form a collage which reflects an interplay of the effects in Figure 33. The straightforward patterns will correlate with a single organizing quantity, which is often the promotion energy and occasionally the reaction thermodynamic driving force. These uniparameter correlations may arise either because the other factors vary in the same direction as the organizing quantity, or are "quasi-constants". Complex patterns will arise whenever a few reactivity factors vary in an opposing manner, which will generate interesting patterns such as reactivity zigzags.[4a, 69]

8.1. Qualitative Applications of the Barrier Factors in the VBSCD Model

We proceed now with a few applications of the barrier factors in order to project qualitative insight and provide guidelines. Since the effect of the reaction driving force is well known, in the following we will deal mainly with the factors f and B, and their interplay with other factors (G and ΔE_{rp}). More detailed applications of the barrier equations can be found elsewhere.[4a, b, 62]

8.1.1. The Intrinsic Selectivity Factor: Chemical Aspects of f

To avoid excessive notations we simply use f for the average and individual indexes. As already pointed out, f determines the response of the barrier to changes in the promotion energy, and as such f is an intrinsic selectivity measure of a reaction series.[70] We may therefore start with the mechanistic significance of f in rule 3.

***Rule 3**: The f factor is an intrinsic selectivity measure of a reaction series: the larger the value of f, the more selective the reaction.*

According to Figure 33a, f is determined by the descent of the promoted states as well as by the ascent of the ground states toward the crossing point; shallow descent and steep ascent increase the f value. It is clear therefore that f is a collective index of many interactions along the reaction coordinate, for example, interactions due to bond ionicity and delocalization – localization of active electrons. These effects will be manifested in the structure of the transition state as deformations (relative to the reactants) which increase as f increases at a constant value of the promotion energy.

8.1.1.1. Relationship of f to the Electronic Structure of the Promoted States

A key factor which determines the ascent of the promoted states is the delocalization of the electrons which must be paired to form the new bonds. Turning back to Figure 28, which shows correlations between barrier and ionization energy for nucleophilic reactivity toward esters, one sees that the nucleophiles fall into two groups, localized ones like hydroxide and delocalized ones like acetate. The promoted states are the charge transfer states, and are depicted in Scheme 10 for the two types of nucleophiles using hydroxide (**23**) and acetate ions (**24**) as specific cases. It is apparent that in the case of hydroxide, the unpaired electron is localized on

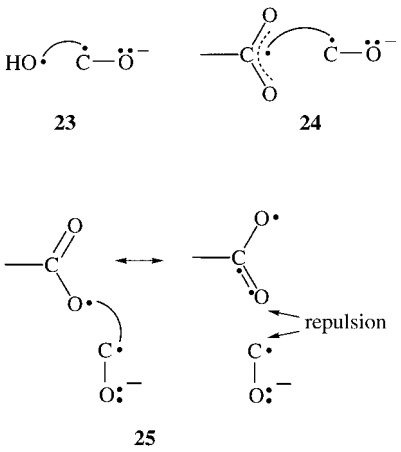

23 24 25

Scheme 10. VB structures to explain the different structure–reactivity slopes in the correlations in Figure 28.

the oxygen center and the coupling with the carbonyl radical anion can develop into a new O–C bond without additional electron reorganization. In contrast, in the case of the acetate radical, the unpaired electron is delocalized over the two oxygen centers. Thus, as shown in **25** for the left-hand resonance structure, the O–C bond making will be weakened by the delocalization, and will be further counteracted by exchange repulsion due to the nonbonding interaction in the right-hand resonance structure. These adverse interactions will impair the descent of the charge transfer state for acetate and will lead to a higher *f* value. It follows, therefore, that the different line slopes in Figure 28 derive from the delocalization properties of the charge transfer species,[48] such that a delocalized nucleophile produces a more deformed transition state structure in comparison with a localized nucelophile having the same vertical ionization energy.

To illustrate this effect further, the ratio of *f* values computed by the VB method for two S_N2 reactions[5b, c] is shown in Scheme 11. The charge transfer promoted state for the F^- exchange which is depicted in **26** has a charge that is virtually localized and is therefore prepared for the new bond making; this situation leads to a small *f* value. In contrast, for

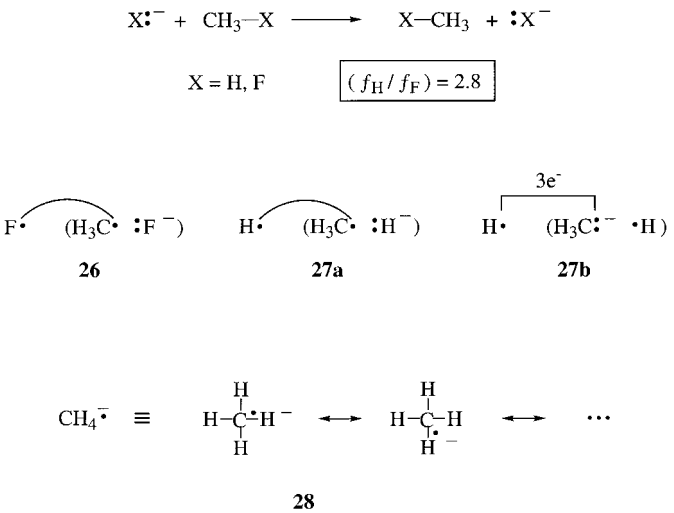

26 27a 27b

28

Scheme 11. Influence of the electronic structure of the excited state on *f* for the example of nucleophilic substitution.

the H^- exchange, the charge in the promoted state is delocalized in two manners, depicted in **27** and **28**. In **27a** and **27b** we show the electron of the radical anion in a single C–H linkage. Since H and C have very similar electronegativities, the electron of the radical anion is delocalized over the two centers, and two VB forms are required to describe the system; **27a** is the form that couples the new H–C bond, while **27b** is typified by three-electron overlap repulsion that counteracts the bond coupling. In addition, **28** shows that since CH_4 has four identical linkages, the electron of the radical anion is delocalized over all of them . This extensive delocalization is expected to lead to a large *f* value. The impact of delocalization is stated as rule 4.

***Rule 4**: Electronic delocalization in the promoted states of the VBSCD will be associated with larger f values and a higher intrinsic selectivity.*

8.1.1.2. Relationship of f to the Electronic Structure of the Ground States

An important electronic factor that affects the ascent of the VBSCD curves is the bond ionicity. Scheme 12 uses the S_N2 reaction to illustrate the effect. Here the C–X bond of the

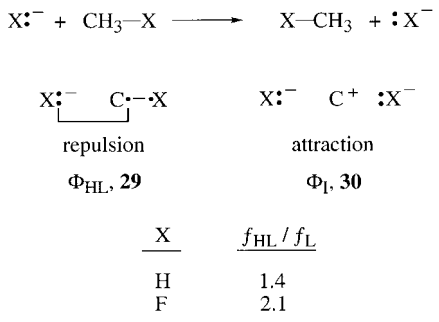

X	f_{HL}/f_L
H	1.4
F	2.1

Scheme 12. Influence of the electronic structure of the ground state on *f* for the example of nucleophilic substitution.

ground sate is a mixture of the HL structure **29** and the ionic structure **30**. It is apparent that the HL structure suffers from a repulsive interaction between the nonbonding $X:^-$ and the HL bond, while the ionic structure maintains an attractive electrostatic interaction. Accordingly increased bond ionicity should lower the *f* value. This was examined by Sini et al.[5b, c, 71] using ab initio VB computations of the HL and Lewis (L) curves for several systems. The result for the reactions with X = H and X = F is shown in Scheme 12. The HL curves have larger *f* values, and the ratio f_{HL}/f_L increases with the electronegativity of X. This trend can be summarized in rule 5.

***Rule 5:** Increased bond ionicity in the ground states of the VBSCD will be associated with smaller f values and lower intrinsic selectivity.*

8.1.1.3. Variation of f in the Main Group Element Block

The third important factor of *f* is manifested as the positions of the atoms in the periodic table change either down a column of the main group elements, or from a nonmetal to a metal. Thus, (for a given bond ionicity) the ascent of the ground state depends on the overlap repulsion of the non-

bonding electrons on the reacting atoms. In turn, the strength of bond coupling of the unpaired electrons in the promoted states affects the descent of these states toward the crossing point. As such, the atom contribution to the *f* factor will be determined by the ratio of the triplet repulsion to the singlet pairing energy. This ratio is large for strong binders and small for weak binders but especially so for metallic atoms. These trends in *f* are summarized in rule 6.

Rule 6: *Changing the reacting atoms to higher homologues down a column in the periodic table or to metals will be associated with smaller f values and smaller intrinsic selectivity.*

Experience with VB computations of the VBSCDs vindicates this rule. For example, exchange reactions of a monovalent atom with the diatomic molecule, studied by Maitre et al.,[5a] show a threefold decrease in the *f* values upon changing the atom from H to Li.

8.1.2. Interplay of f and G: Effects on the Barrier Height and Reactivity Reversals

When both the promotion energy and *f* vary in opposition in a reaction series, relative reactivity may be condensed or exhibit zigzag behavior.[69] A few examples illustrate these patterns.

8.1.2.1. Why Are Some Gas-Phase S_N2 Barriers Constants?

Recently, Wladkowski et al.[72] have studied the gas-phase reactivity of identity S_N2 reactions in Equation (11)—R = CH_3, $NCCH_2$, $ArCH_2$—and found an approximately constant

$$Cl{:}^- + R{-}Cl \rightarrow Cl{-}R + {:}Cl^- \qquad (11)$$

central barrier of 12 – 14 kcal mol^{-1}, irrespective of the substituents on the central carbon atom. This was further supported by AM1 calculations[72a] which revealed the invariance of the central barrier for a variety of Ar substituents.

This experimental trend had been anticipated in 1983[69b] by considering the VBSCD in Figure 34. The carbon substituents in Equation (11) are all good electron acceptors relative to H.

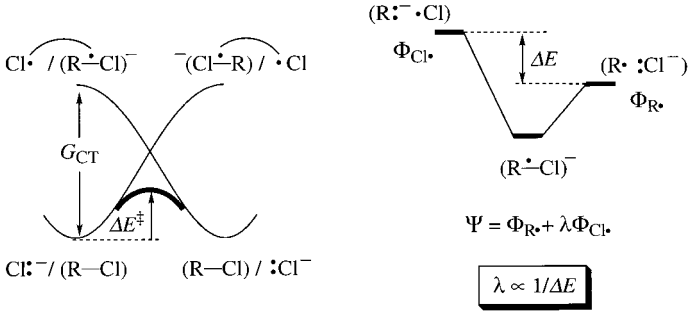

Figure 34. Left: VBSCD (based on Figure 20b) for gas-phase S_N2 reactions of the chloride ion with substituted alkyl chlorides. Right: VB interaction diagram for the formation of the radical ion promoted state from its VB constituents, and the dependence of its extent of delocalization (sized by the mixing coefficient λ) on the substituent on the central carbon atom. The *f* factor will increase as the radical anion becomes more delocalized (λ increases).

Therefore, they will render their corresponding R—Cl substrates better electron acceptors. As such, the charge transfer promotion energy will be lowered upon substitution of the methyl group with Ar or CN groups. At the same time, as shown in the VB interaction diagram on the right hand side of Figure 34, the substituent affects also the extent of delocalization of the radical anion in the charge transfer state. Thus, the radical anion species is a VB mixture of a form which places the unpaired electron on the R group ($\Phi_{R\cdot}$) and a form which places the electron on the Cl atom ($\Phi_{Cl\cdot}$). The extent of mixing of the latter form increases as the R group becomes a better electron acceptor, and this will increase electronic delocalization and, in turn, raise the value of the *f* factor according to rule 4. Clearly then, the electron-withdrawing carbon substituents in Equation (11) will, on the one hand, lower the promotion energy but, on the other hand, increase the *f* factor. Based on Equations (6) or (9), this opposition of the reactivity factors will narrow the range of barrier variation. The observation of this effect by Wladkowski and Brauman[72] along with similar experimental trends[4a, 69] indicate the predictive power of the VBSCD model.

8.1.2.2. Polyhalogenated Alkanes: Why Do They Undergo Sluggish S_N2 and Halide-Abstraction Reactions?

A long time ago, Hine et al.[73] demonstrated that polyhalogenated alkanes undergo very sluggish S_N2 reactions, so much so that reactions of, for example, simple alkyl halides can be carried out in dichloromethane. To understand this trend, consider S_N2 reactivity in the series Cl^-/CH_3Cl, Cl^-/CH_2Cl_2, $Cl^-/CHCl_3$, Cl^-/CCl_4. Here, successive chlorination of the substrate is known to improve modestly its acceptor ability.[69b] However, this improvement is attended by delocalization of the radical anion state over an increasing number of linkages according to the effect illustrated above for the hydride exchange reaction in **28** (Scheme 11). Evidently, the increase of the *f* factor overrides the modest reduction of the promotion energy and leads to an increase of the barrier.[4a, 69]

A related trend has been observed by Cornhel et al.[28a] and Harvey et al.[28b] in the C—F activation by metal ions, where polyfluorinated substrates undergo sluggish bond activation, in comparison with CH_3F, even when the reactions are very exothermic as with the early lanthanide cations.[28b] Scheme 13

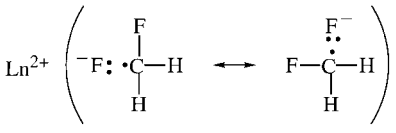

31

Scheme 13. Explanation of the sluggish C—F activation of polyfluorinated substrates by metal ions exemplified by the excited CT states **31** for difluoromethane.

exemplifies the effect using the promoted charge transfer state for difluoromethane in **31**. Here, the delocalization of the negative charge away from the F species that undergoes abstraction reduces the ionic stabilization due to the interaction with the M^{2+} ion. The expected increase of *f* will raise the barrier, and will contribute to the sluggish reactivity of polyfluorinated substrates.[28b]

8.1.2.3. What Is the Origin of Reactivity Crossovers in Reactions between Electrophiles and Nucleophiles?

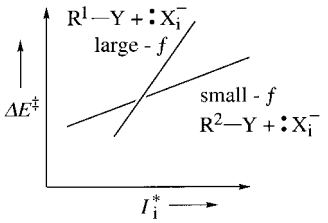

Figure 35. The phenomenon of reactivity reversal due to the opposite trends of *f* and *G* factors in the two series. The reversal is illustrated for two S_N2 series formed by substrates with different intrinsic selectivities (*f* factors).

Reactivity crossovers and zigzags are predicted as manifestations of the $f-G$ opposition.[4a, 69] Figure 35 is a schematic illustration of the situation for nucleophilic substitution series formed by two substrates with the same group of nucleophiles $:X_i^-$. The first substrate R^1—Y is a better electron acceptor than R^2—Y, but the radical ions formed from it are also more delocalized. Consequently, the first reaction series will be typified by smaller *G* values and larger *f* factors in comparison with the second series. Following rule 3, *f* is a selectivity factor which measures the slope of $\Delta E^{\ddagger} - G$ correlation, and hence the substrate with the larger *f* will be more selective. Consequently the relative reactivity of the two substrates may undergo reversal, as the vertical ionization energy of the nucleophile changes along the series. A situation like that in Figure 35 can be drawn for other reactions between electrophiles and nucleophiles because generally electronic delocalization in the electrophile or nucleophile will enhance their intrinsic selectivity, and may bring thereby reactivity crossover in two reaction series.

Reactivity crossovers which appear to follow the dictum of $f-G$ opposition have been reported for $NO_2C_6H_4CH_2Br$/$C_6H_5CH_2Br$,[74a] $PhCOCH_2Br/CH_3I$,[74b] and Me_3SiCH_2Cl/$CH_3CH_2CH_2Cl$[74c] in S_N2 reactions with a series of nucleophiles.[4a] Mayr et al.[22, 75] have observed reactivity reversals in the reactions of carbocations with olefins. Thus, olefins which are better electron donors and form more delocalized radical cation states seem to show higher selectivity toward carbocation addition, in comparison with olefins which are poorer donors but form more localized radical cation states. This situation fits the dictum of $f-G$ opposition, and the observed reversals may well reflect the predictions of the VBSCD.

The situation of $f-G$ opposition may be ubiquitous and occur in a variety of reactions. The foregoing discussion should provide a basis for anticipations of reactivity reversals, and trends in reactivity–selectivity relationships.

8.1.2.4. Regioselectivity Zigzags in Radical Addition to Olefins

The interplay of *f* with other reactivity factors may lead also to reactivity zigzags, as manifested in radical attacks on substituted olefins. The reaction normally proceeds with preference on the less substituted site, even though this is not necessarily the thermodynamically favorable path.[25] Certain substitution modes of the olefin disrupt the normal pattern, leading to preferred attack on the more substituted sites. Variation of the radical restores the normal regioselectivity, and the overall picture is one of regioselectivity zigzags.[76, 77]

This problem has been treated by Shaik and Canadell,[76] who employed a Morokuma analysis to obtain the VBSCD quantities. Scheme 14 shows in **32a** and **32b** the VBSCD

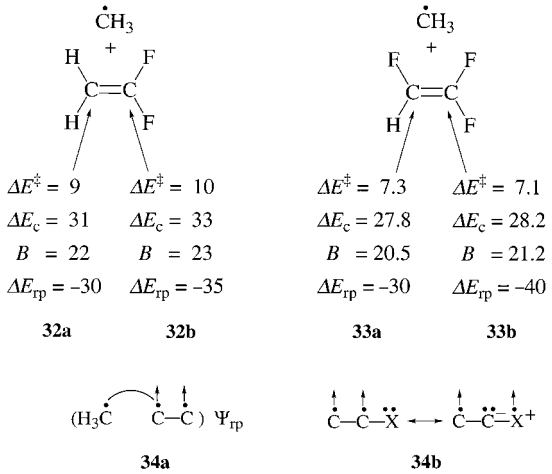

Scheme 14. Explanation for the zigzag behavior of regioselectivity in radical additions to alkenes.

quantities (in kcal mol^{-1}) for the two possible reactions of 1,1-difluoroethylene with methyl radical. The attack on the more substituted site is typified by a higher crossing point (ΔE_c), which dominates the trends in the barrier and overcomes the opposite preference of the thermodynamic driving force. Since the promotion energy is common for both regiochemical pathways, it follows that the attack on the substituted site (**32b**) must possess a larger *f* factor. The reason for this is projected in **34b**, which depicts the triplet olefin moiety in the promoted state, itself shown in **34a**. It is seen that the substituent X induces electronic delocalization in the triplet olefin, and depletes thereby the density of the unpaired electron on the substituted site. Consequently the bond coupling of the substituted site with the radical (in **34a**) will be weaker and will possess a larger *f* factor.

In the case of 1,1-difluoroethylene, the *f* factor overcomes the opposite directive preference of the thermodynamic driving force. However, in the case of trifluoroethylene, **33**, where the two sites are substituted, the directive preference of the reaction driving force gets larger while the *f* directivity decreases. Consequently, the regioselectivity shifts in favor of the more substituted site, but will reverse upone use of other radicals such as H and CF_3, for which the thermodynamic driving force becomes more balanced.[76] Thus, the regioselectivity zigzag may be understood as a manifestation of the opposition between the intrinsic selectivity factor *f* and the thermodynamic driving force.

8.1.3. The Resonance Energy of the Transition State: Chemical Aspects of B

Having elaborated the impact of the factors *f*, *G*, and ΔE_{rp} and their interplay, we turn to the remaining VBSCD quantity *B*. The crossing point in the VBSCD (Figure 21a) is the location where the two bonding motifs of reactants and products have equal energy, while *B* is the resonance energy due to their VB mixing (Figure 21b).[10] The VB mixing

generates the transition state and its twin-excited state as depicted again in Figure 36, which shows the relationship of the resonance energy and the excitation energy between the two states.[7a, c, 10, 78] The simplest approximation for this excitation energy is the orbital excitation energy of the

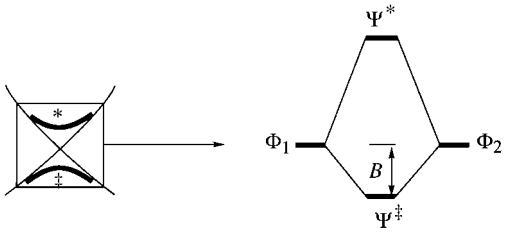

$$B = \frac{(1-S_{12})}{2}\,\Delta E\,(\Psi^{\ddagger} \rightarrow \Psi^{*})$$

Figure 36. Left: Schematic VBSCD. Right: The resonance mixing which generates the transition state and its twin excited state magnified using the VB interaction diagram which shows the relationship of the transition state's resonance energy to the gap between the states and to the overlap between the VB configurations at the crossing point.

transition state. In many cases these would be the HOMO (ho) and LUMO (lu) of the transition state, as expressed in Equation (12), where S_{12} is the overlap between the VB configurations at the crossing point.

$$B = [0.5(1 - S_{12})]\Delta E_{\mathrm{ho}\rightarrow\mathrm{lu}} \qquad (12)$$

The dependence on the orbital excitation energy projects that the quantity B is a code of the structure and stereochemical preference of the transition state. A lucid example for this aspect is given in Scheme 15, which shows the two

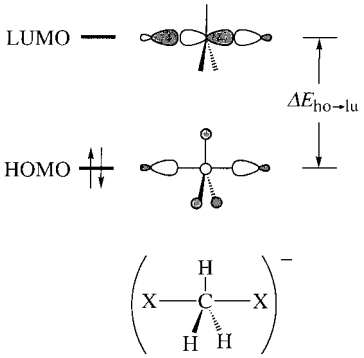

Scheme 15. HOMO and LUMO of the transition state of an identity S_N2 reaction.

orbitals for an identity S_N2 transition state. Since the orbital gap is maximum when the XCX axis is linear, the S_N2 transition state will prefer a trigonal-bipyramidal structure which maximizes the resonance energy. As soon as the angle of the XCX axis deviates from 180°, the LUMO energy decreases sharply, the orbital gap is minimized, and the resonance energy decreases.[10] At a certain limiting angle of bending, the two orbitals will collapse and the resonance energy of the transition state will drop to zero.

The other important term in Equation (12) is the overlap integral S_{12}. Neglecting all overlap terms between different VB structures, the S_{12} quantity is nonzero only if the bonding motifs at the crossing point contain some common VB structures. We note that electron delocalization and resonance stabilization only occur by mixing of different VB structures, while common structures make no such contribution. Thus, whenever the bonding motifs contain common structures, the resonance energy will be reduced in proportion to the contribution of the common structures, sized by the overlap integral S_{12}. At the limit of $S_{12} = 1$, the transition state is described by a single VB structure and hence will be devoid of resonance energy.

Let us follow therefore with a few illustrative applications which show that B holds the symmetry code and electronic structure characteristics of the transition state.

8.1.3.1. Estimates of Transition State Resonance Energies

Valence bond arguments[7a, c, 10, 78] show that B is related to the bond strengths or the singlet – triplet excitation energies of the active bonds in the transition state, for example" the C–X bonds in the S_N2 transition state in Scheme 15. Using this relationship to calibrate an extended Hückel orbital scheme renders Equation (12) very useful.

A good example is the transition state of the identity S_N2 reaction, which can be constructed from two Lewis structures, each of which corresponds to a mixture of one of two HL structures (**35a**, **b**) and the ionic structure (**35c**) in Scheme 16. The

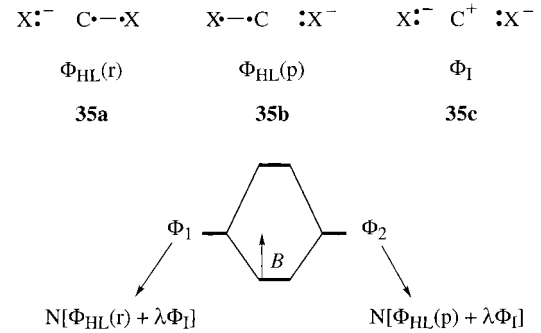

Scheme 16. Lewis structures, VB structures, and resonance energy for the transition state of an identity S_N2 reaction.

overlap between the bonding motifs of reactants and products is then proportional to the mixing coefficient λ of the ionic structure, which in turn determines the positive charge Q_R on the central alkyl group. With this relationship, and appropriate simplifications, Equation (12) becomes Equation (13),

$$B(\mathrm{S_N2}) \approx [(1 - Q_R)/(2 - Q_R)]\Delta E_{\mathrm{ho}\rightarrow\mathrm{lu}} \qquad (13)$$

which relates the resonance energy of the transition state to its HOMO – LUMO splitting and its charge distribution. Thus, an increase of the charge in the transition state will lower the resonance energy, which will drop to zero at a charge of unity, where a limiting transition state wavefunction would be described completely by the ionic structure. Equation (13) links the entire gamut of electronic structure, from purely covalent S_N2 transition states to completely ionic ones.

Using Equation (13) enables an approximation of B for a variety of transition states. With reasonable charges for the halide-exchange transition states (X = F, Cl, Br, I in Scheme 16), the corresponding B values are found to be proportional to the C–X bond energies D_{CX} of the parent molecules.[78] The range of B values is expressed in Equation (14a). Using them and charge transfer promotion energies from the literature,[4a, b] we estimated central barriers for the halide-exchange reaction based on Equation (14b). These barriers are displayed in Scheme 17 and compare quite well

$$B(XCH_3X^-) = m D_{CX};\ m = 0.25,\ 0.30;\ X = \text{halogen} \quad (14a)$$

$$\Delta E^{+} = f(I^{*}_{X^-} - A^{*}_{RX}) - B \quad (14b)$$

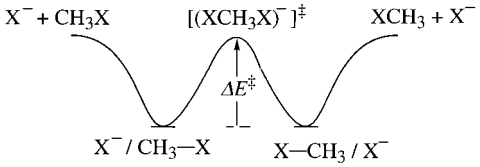

X	$\Delta E^{\ddagger}$ [kcal mol^{-1}] (m=0.25)	$\Delta E^{\ddagger}$ [kcal mol^{-1}] (m=0.30)	$\Delta E^{\ddagger}$ [kcal mol^{-1}] (ab initio)
F	12.4	12.4	12.4
Cl	12.0	12.6	12.8
Br	11.1	10.9	10.8
I	9.6	10.4	9.8

Scheme 17. Barriers of halide exchange reactions from Equations (14a) and (14b) and according to Glukhovtsev et al.[79]

with the recent ab initio results of Glukhovtsev et al.[79] obtained at the sophisticated G2 level.

Similar application of Equation (12) to the transition state for hydride exchange between alkyl or silyl groups $(R\cdots H\cdots R)^+$ led to B values which range between 20–30 kcal mol^{-1}.[56b] This study shows that the resonance energy increases as the R-H-R angle deviates from linearity, due to widening of the HOMO–LUMO gap. In addition, as the contribution of the hydrido configuration $[R^+H^-R^+]$ to the transition state increases, the B value decreases. The hydrido configuration is common to the two bonding motifs, and its contribution is expected to reduce resonance energy through the S_{12} term.

The value of B for three-electron species varies in proportion to the bond strength. Thus, B values range from 6 kcal mol^{-1} for $Li\cdots Li\cdots Li$ to 40–43 kcal mol^{-1} for $H\cdots H\cdots H$ and $F\cdots H\cdots F$.[5a, f, 10] Unlike the cases in the preceding paragraph, for three-electron transition states the bonding motifs do not share common structures. Therefore, ionicity of the three-electron transition state will lead to resonating VB structures and an increase in the resonance energy.[7c] This emphasizes the impact of bond ionicity in atom abstraction reactions.

Resonance energies were quantified also for a variety of six-electron/six-center and four-electron/four-center transition states.[41, 64, 80] In the six-electron case the resonance energies are significantly larger, as may be understood by invoking Equation (12). Thus, in the "forbidden" geometry of the four-electron cases, the HOMO and LUMO of the transition state are degenerate, and the resonance energy is 15–25 kcal mol^{-1} due to electron correlation which reduces electron repulsion.[81] On the other hand, in the "allowed" geometry of the six-electron cases, the HOMO–LUMO gap is very large and therefore the resonance energy is also large (40–60 kcal mol^{-1}). Thus, it is generally expected that "allowed" transition states will possess larger resonance energies in comparison with their "forbidden" analogues. This trend was discovered decades ago by Evans et al.[82] based on empirical VB calculations. Recent sophisticated computations by Bernardi, Robb et al.[83] arrived at the same conclusion.

It is apparent, therefore, that orbital-symmetry classification of pericyclic reactivity is based solely on the resonance energy of the transition state.[7a, c] This means that orbital-symmetry predictions of reaction rates will fail whenever other barrier factors vary in an adverse manner. This conclusion is a lead to the following section.

8.1.3.2. Why Do Some "Allowed" Reactions Have High Barriers, while Some "Forbidden" Reactions Have Small Barriers?

This comparison has been implicit in the discussion of the barrier data in Schemes 6 and 7, which show huge barriers for some "allowed" reactions and tiny barriers for some "forbidden" reactions. Since the resonance energy of the transition state is one of the barrier factors, a formally allowed reaction like the trimerization of ethylene can have a high barrier due to the large promotion gap.[37] In the same logic, a formally forbidden reaction like the dimerization of disylene can have a tiny barrier, even when the resonance energy is small, because the promotion gap is very small. It is the interplay of the promotion energy and the resonance energy that must be considered for understanding the broader trends of reactivity in these families.

8.1.3.3. Allowed Reactions and Synchronicity of Bond Rearrangement

A related aspect of orbital-symmetry effects is the concertedness or nonsynchronous nature of "allowed" reactions. This has been a hot issue[84] that was flared recently by the femtosecond dynamics study of Zewail et al., who showed that the retro-Diels–Alder reaction of norbornene proceeds by competing concerted and stepwise pathways.[85] Their study showed that stereochemistry would be conserved even in the stepwise process, because the diradical intermediate lives on the timescale of bond stretching but not long enough for internal rotation to occur.

The competition between the mechanisms can be discussed by considering the factors which affect transition state's resonance energy. Equation (12) shows that a wide orbital gap in the transition state would lead to a large resonance energy. The transition state's orbitals gap is determined, in turn, by the orbital mixing of the separate reactants. As shown with **36a** in Scheme 18, the distance

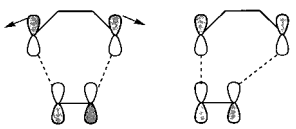

36a **36b**

Scheme 18. Transition state for the concerted symmetric and nonsynchronous [4+2] cycloaddition.

between the diene terminals is significantly longer than the dienophile's C=C bond length, and hence the orbitals are not aligned for a good atomic orbital overlap. Thus, while the synchronous transition state enjoys an orbital-symmetry match, the overlap of the atomic orbitals is impaired by the "loose bite" of the diene. An improvement of the AO overlap may be achieved by rotation of the diene terminals or by decrease of its C-C-C angles, but the extent of these structural changes is limited since they would have to occur with an increase in distortion energy. An alternative nonsynchronous transition state which lines up one pair of orbitals, as shown in **36b**, will compromise the orbital symmetry match-up but will possess a perfect AO alignment in one of the linkages. The net effect of this balance between the symmetry and AO overlap requirements may render the synchronous transition state very susceptible to a distortion to a nonsynchronous structure. This in turn implies that a transition state for the stepwise process may not be too much higher than the synchronous transition state. Computations show that the barrier for the stepwise process is indeed higher by only about 7–12 kcal mol^{-1} than that for the concerted mechanism.[84] Thus, given sufficient excess energy, as in the Zewail experiment, the diradical intermediate may become accessible thermally. It is emphasized though that, since the VB state correlation is determined by the nature of reactants and products, both the synchronous as well as the stepwise processes will involve the same type of avoided crossing in the VBSCD (see Figure 44), albeit along different reaction coordinates distinguished by the timing of the two bond formation steps.

8.1.4. Orbital Selection Rules for Reactivity

Trends in the resonance energy of the transition state can be deduced also by direct consideration of the VB mixing between the ground and the promoted states at the crossing point of the VBSCD. In this manner, it becomes possible to derive orbital selection rules[4a, 7] and make a priore predictions of the preferred stereochemical pathway and transition state structure for a reaction. The stereoselection rules specify the bonding requirements of the transition state in terms of the overlap conditions which must be met to produce an optimal resonance energy.

The principles of VB configuration mixing have been analyzed in detail elsewhere.[7a, c] The salient features of strong overlap mixing are condensed into rules 7 and 8, which are schematized in Figure 37 for generic situations.

Rule 7: *Two VB configurations which differ in a single electron shift between two orbitals will mix in proportion to the overlap of the two orbitals.*

Rule 8: *Two configurations which differ in a shift of two electrons will mix in proportion to the product of overlaps of the orbitals which partake in the electron shifting.*

To employ the rules correctly, electrons must be shifted without changing their spins. Figure 37a shows a case which subscribes to rule 7, where the resonance energy is proportional to the overlap of ϕ_1 and ϕ_2 which partake in the single electron shift. This situation is most common for reactions between electrophiles and nucleophiles or acceptors and donors, where the promoted state is a charge transfer state generated from the ground state by a single electron shift. Figure 37b describes two single electron shifts from ϕ_1 to ϕ_3, and from ϕ_2 to ϕ_1. Following rule 8, the resultant resonance energy is proportional to the product of the overlaps $\phi_1-\phi_3$ and $\phi_1-\phi_2$. This resonance energy will be typical in radical-exchange reactions where the promoted state involves a triplet unpairing of the bond undergoing cleavage during the reaction.

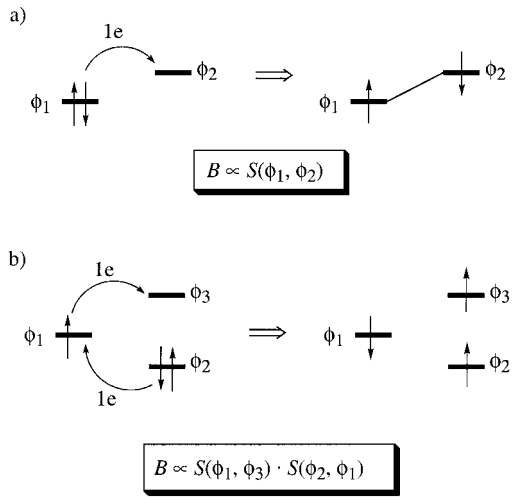

Figure 37. Pictorial representations of the VB mixing rules 7 (a) and 8 (b). Note that electrons are shifted with conservation of their individual spins. The rule is indicated as dependence of the resonance energy B on the specific orbital overlap S.

A straightforward way of analyzing the resonance interactions uses fragment orbitals in the VB configurations. These types of configurations have been used by Mulliken[86] in his theory of charge transfer complexes, and latter by Epiotis[87] and Shaik.[1, 4a, 7] Since the fragment orbitals possess information on local symmetry, the resulting orbital selection rules lead to lucid stereochemical predictions. A few derivations of selection rules follow for reactions which involve an odd number of electrons, where the usual MO arguments cannot be applied in a clear manner.

8.1.4.1. Stereoselection Rules for Nucleophilic Cleavage of σ-Radical Cations and for the Competing Electron Transfer Pathway

Shaik and Dinnocenzo[88] investigated the system of a nucleophile and a cyclopropane radical cation which can participate in a substitution reaction (SUB) and in an electron transfer (ET) reaction (Scheme 19). In both mechanisms, the nucleophile can approach the radical cation from the backside (bs) or frontside (fs) of the one-electron bond. In the case of substitution, the stereochemistry of the transition state is encoded into the products, while in the ET mechanisms the stereochemistry may be probed by kinetic isotope effect measurements.[62] As shall be seen, the VBSCD model leads to distinct orbital section rules for the two mechanisms.

The ground state for the reactant and promoted states for the two mechanisms are shown in Figure 38, and the orbital selection rules are specified on the arrows leading from the reactant to the promoted states. In both cases the promoted

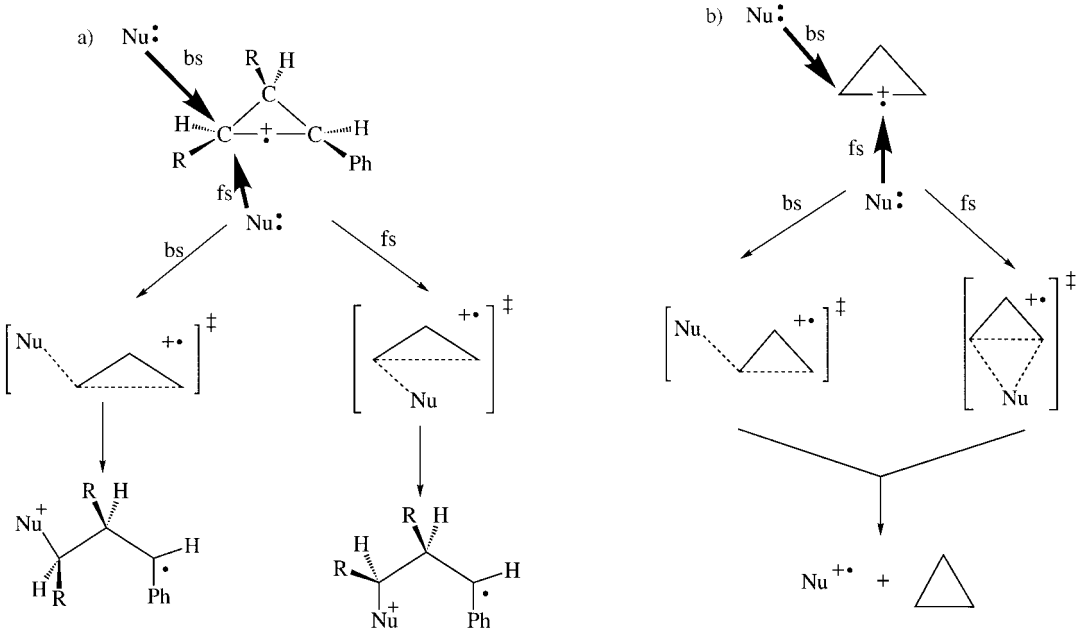

Scheme 19. Pathways for nucleophilic cleavage of a σ-radical cation (a) and for the competing ET path (b).

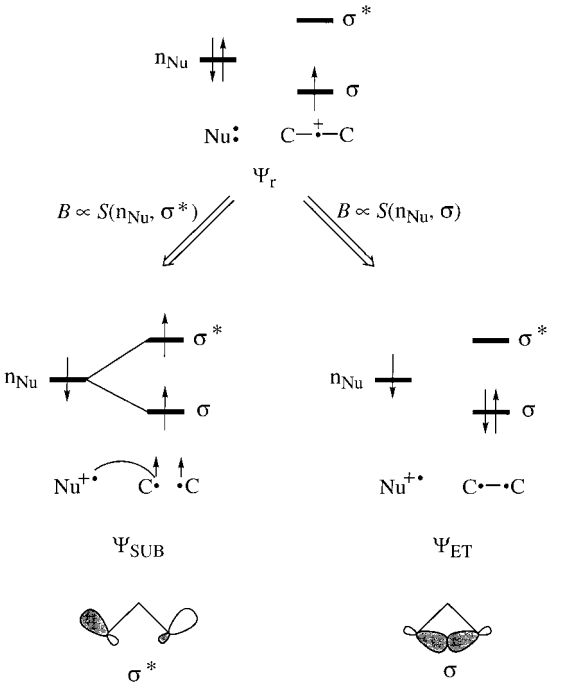

Figure 38. Orbital selection rules for nucleophilic cleavage and ET reactions between a cyclopropane σ-cation radical and a nucleophile. See text for further details.

states are generated by single electron shifts from the reactant state; in the substitution reaction the single electron shifts into the σ* orbital, while in the competing ET mechanism into the σ orbital.[62, 88] It is predicted, therefore, that the stereochemical course of the nucleophilic cleavage will be determined by the σ* orbital of the radical cation moiety, while the course of the ET reaction will be decided by the σ orbital. These orbitals, which are depicted underneath the configurations in Figure 38, illustrate vividly that the substitution reaction will involve a backside attack and lead to stereoinversion, whereas the ET process will partake in a frontside approach. Recent regiochemical studies by Eberson et al.[67, 89] provide further support for the orbital selection rules.

Experimental studies by Dinnocenzo et al.[90] have shown that the substitution reaction proceeds with virtually 100% stereoinversion. These results were followed by an extensive computational study by Shaik et al.,[62] which has demonstrated that the transition state for substitution by a backside attack by the nucleophile is 10–20 kcal mol^{-1} more stable than the transition state for frontside attack, which leads to stereoretention.

There are no matching results for the prediction about the ET mechanisms. Preliminary computational study of an ET reaction between NH_3 and cyclopropane cation radical shows that the transition state should be of the frontside variety.[91] This stereochemical dichotomy of the two mechanisms is worthy of pursuit.

8.1.4.2. Stereoselection Rules for Nucleophilic and Electron Transfer Reactivity of Ketyl Anion Radicals Toward Alkyl Halides

Eberson and Shaik[54] have derived orbital selection rules for reactions of radical anions with alkyl halides, based on rule 7. Sastry and Shaik[92] have used these rules to analyze the competing SUB and ET mechanisms in reactions of ketyl radical anions with alkyl halides. Scheme 20 summarizes the computational assignments obtained for the 1-formyl-ω-chloroalkane anion radicals,[92b] which are simple analogues of the 1-benzoyl-ω-haloalkane systems studied experimentally by Kimura et al.[93] Thus, the ET reaction, which is predicted[92b] to optimize the $\pi^*_{CO} - \sigma^*_{CCl}$ overlap, proceeds via a transition state which involves a C-C-Cl bonding in the plane perpendicular to that of the formyl group. In contrast, the SUB mechanism, which is predicted by the selection rule to optimize the overlap of the oxygen's lone pair orbital (n_O) with σ^*_{CCl}, proceeds via a transition state which involves O-C-

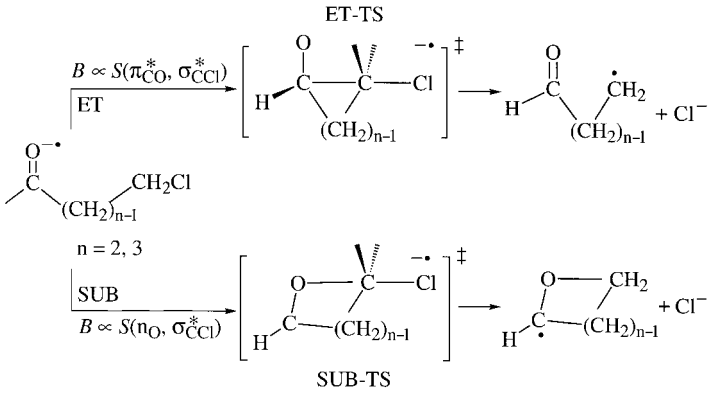

Scheme 20. Stereoselectivity in the reaction of ketyl radical anions with alkyl halides.

Cl bonding in the plane of the formyl group. The computational studies show that these rules are obeyed even when adverse stereochemical constraints exist, such as for $n = 3$, where the ET transition state has a strained four-membered ring structure. Thus, the negative charge of the ketyl anion radical is localized mostly on the carbonyl's oxygen atom, and the electron transfer could have occurred via an alternative O-C-Cl structure in a strain-free five-membered ring transition state. Nonetheless the ET reaction proceeds via the strained transition state structure which maintains the C-C-Cl bonding. It follows therefore that the orbital selection rules specify the bonding mode which a transition state of a given reaction must assume.

Scheme 21 shows two systems which may be appropriate probes for testing the selection rules. In **37** the axial chain is

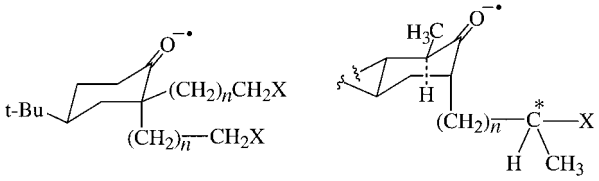

37 **38**

Scheme 21. Two compounds with which the validity of the prediction of stereoselectivity for the reaction of ketyl radical anions with alkyl halides can be tested.

constrained to optimize the $\pi^*_{CO} - \sigma^*_{CX}$ overlap in a C-C-X-type transition state and will undergo therefore only ET, while the equatorial chain is prone to optimize the $n_O - \sigma^*_{CX}$ overlap in a O-C-X-type transition state and will react by the substitution (O-alkylation) mechanism.[94] System **38** is prone to react via the C-C-X transition structure and will give rise to ET reactivity. Since now the carbon atom of the C–X moiety is chiral, the ET transition state will have two diasteriomers, one of which will be lower in energy and will lead to a faster depletion of one of the diasteriomers of **38**.[95] These predictions await their test.

8.1.4.3. Stereoselection Rules for Radical Cleavage of σ Bonds

Consider the reaction of a radical with an alkane, as in Scheme 22. Would this reaction proceed by stereoinversion (a) or stereoretention (b)? Or perhaps the two pathways should compete and lead to stereorandomization? The configurations which participate in VB mixing to generate the transition state are shown in Figure 39, and it is apparent that they subscribe to the situation depicted in Figure 37b and stated in rule 8. It follows that the resonance energy of the transition state will depend on the overlap product $(\phi_R - \sigma_{CC})(\phi_R - \sigma^*_{CC})$. Since the σ* orbital has a node, the overlap product vanishes (becomes zero) in a frontside attack and the transition state formed by backside attack leading to stereoinversion will be preferred. The existing experimental data is

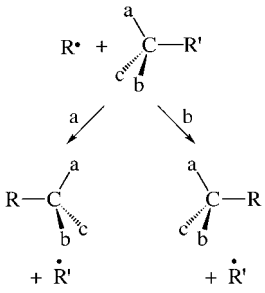

Scheme 22. Attack of a radical on an alkane with inversion (a) or retention of configuration (b).

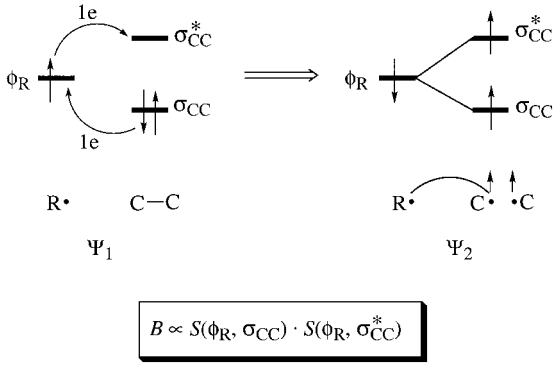

Figure 39. Orbital selection rules for σ-bond cleavage by a radical R•. The selection rule is indicated as the dependence of the resonance energy B on specific orbital overlaps.

in accord with this prediction.[96] To the best of our knowledge, no other qualitative approach is capable of deriving stereoselection rules for radical cleavage in an unequivocal manner as the VBSCD model.[97a]

There are a number of other predictions which can be made by application of rules 7 and 8. An example is the expected lack of synchronicity of bond making in transition states of cycloadditions involving cation radicals.[97b]

8.2. The Collage of Reactivity Patterns: Summary and Mini-Guide for Using the VBSCD Model

The foregoing sections outline a scheme for the applicability of the VBSCD. The model views reactivity as a collage of trends set by a small number of reactivity factors underlying the VB diagram of two interacting states in Figures 21b and 33. An effective way to apply the model to a new reaction begins with construction of the VBSCD, based on the principal configurations of reactants and products and following rules 1 and 2. Once the VBSCD is constructed and the promotion energy of the reaction is characterized, there already exist means to define the origins of the barrier and assess its gross variation in a reaction series. What follows depends ultimately on the type of questions one wishes to tackle.

Stereoselection questions are the least complex because they allow one to focus on the resonance energy B of the transition state. For polar covalent bonds the VB mixing rules (rules 7 and 8) provide means to predict stereoselectivity. Regioselection questions come next in the hierarchy of complexity because often an interplay of two reactivity factors will determine the regioselectivity.[67, 76] These may be ΔE_{rp} and f, as discussed in Section 8.1.2.2 for radical additions to olefins,[76] or B and f, as shown recently[67] for nucleophilic addition to odd-nonalternant-hydrocarbon cation radicals. Rules 3–6 outline the dependence of f values on fundamental properties of the ground states and the promoted states as well as on their atomic constitution. These rules along with the examples analyzed in Section 8.1 should constitute a reasonable basis for further application.

For situations of high ionicity, as described in Section 7.1.8, both stereo- and regioselectivities will be dominated by the electrostatic interactions, while the resonance energy of the transition state (albeit no longer as a selection rule) will still be determined by the VB mixing of the secondary covalent structures,[28b] and may be deduced from rules 7 and 8.

Questions of relative reactivity in a reaction series are inherently the most complex, because all the reactivity factors may in principle change simultaneously. A logical hierarchy of application begins with the search for a general correlation of the barriers with the characteristic promotion energy of the reaction, followed by an upgraded complexity of factor consideration. Deviations from the promotion energy trend will be encountered when one or more of the other factors change in a dominant fashion in the series (e.g., changes in f due to bond ionicity effects). A useful way to follow in such an event is to seek reactivity patterns which are set by the interplay of two factors (see Section 8.1.2). More complex situations, due to changes of all reactivity factors, will generally require a quantitative consideration.[4a, b, 10, 20, 37, 62] There exist by now quantum chemical ways to obtain G and B as well as the height of the crossing point.[5, 7a, c, 10, 37, 56b, 76, 98]

Yet another compact approach to pattern a set of kinetic data makes use of the various barrier expressions [Eqs. (6), (8), and (9)] as means for assessing the mechanism of activation.[4a, 7a, 10, 17, 48] For example, a plot of $\Delta E^{\ddagger}$ versus G according to Equation (6) will generate a fingerprint pattern found in reaction series (e.g., Figure 28) with correlation lines possessing different slopes, as illustrated generally in Figure 40. Whenever these plots are physically meaningful, then each line would correspond to a reaction "family" with member transition states which share common f and B values.[10] For these families, the slope of the line will correspond to f and its intercept to B. Since B is the difference between the heights of the crossing point and the barrier at a definitive structure of the transition state, it can be uniquely defined,[7c, 78] and the quantities extracted from experiment may serve as useful means to deduce the structure of the transition state in the reaction "family".[10]

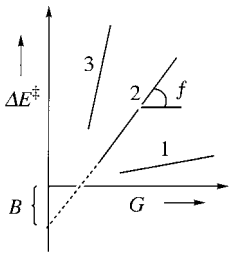

Figure 40. Finger-print reactivity patterns showing three "reaction families" (1–3), predicted by application of Equation (6). A reaction family is typified by a line with a slope equal to f and an intercept equal to B.

9. Valence Bond Configuration Mixing Diagrams (VBCMDs): Intermediate States and Their Role in Reactivity

The VBCMD is an alternative and a complementary diagram to the VBSCD,[4a, b, d, e–g, 7] typified by more than two curves which may either be individual VB structures or state curves. Any two-state VBSCD can be transformed into a VBCMD, where the HL and ionic VB structures are plotted explicitly as independent curves instead of being combined into state curves.[4d, 7, 5b, d, 62] Another type of VBCMD will be obtained whenever the description of a reaction mechanism requires, in addition to the two principal state curves which describe the net transformation from reactants to products, a third state curve which accounts for an intermediate situation. The following sections discuss the generation of VBCMDs and application to chemical problems.

9.1. Features of the VBCMD

Figure 41 shows the generic VBCMD, which features two fundamental curves Φ_r and Φ_p and an intermediate curve Φ_{int}. Figure 41a corresponds to a situation where the intermediate

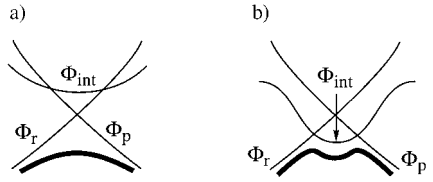

Figure 41. Generic VBCMDs with two fundamental curves of reactants and products (Φ_r and Φ_p) crossed horizontally by an intermediate curve (Φ_{int}). Case (a) is prone to generate a single step reaction, while case (b) a stepwise reaction.

curve lies higher than the crossing point of the fundamental curves, a situation prone to generate a single transition state that has a mixed character of the fundamental and intermediate VB structures. Figure 41b describes a situation where the intermediate curve is more stable than the crossing point of the fundamentals, which is prone, though not always,[5b] to generate an intermediate state in a stepwise mechanism. Thus, the intermediate structure provides a low-energy pathway that mediates the process, which itself is defined by the fundamental states transformation $\Phi_r \rightarrow \Phi_p$.

Scheme 23 classifies intermediate VB situations which are common in VBCMDs. In case (a) the fundamental curves are the principal HL structures of the active bonds which interchange along the reaction coordinate. The corresponding intermediate curve will then generally correlate to the ionic structure. Examples are **39**, which is a triple-ionic structure in, for example, a proton transfer process, or **40**, which is the corresponding ionic structure in an atom-abstraction reaction.[31, 99] As a rule, for polar covalent bonds the ionic

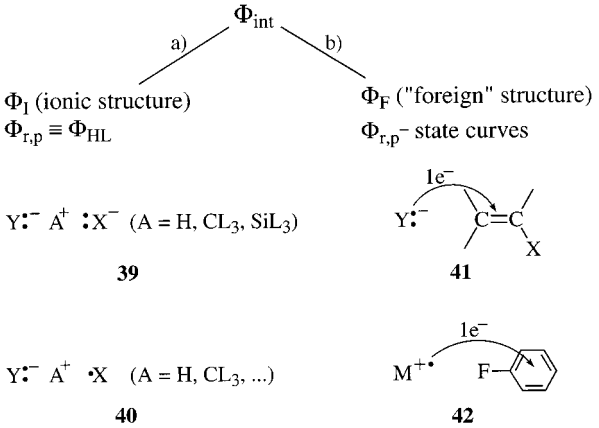

Scheme 23. Classification of typical VB intermediate situations; ionic VB structures in (a), foreign states in (b).

structures are higher in energy than the HL structures at the reactant and product geometries. Thus, while the HL curves will interchange along the reaction coordinate, the curve of the ionic VB structure will correlate horizontally and cross thereby those of the two HL structures either above or below their crossing point, as depicted schematically in Figures 41 a and 41 b. In case (b) of Scheme 23, the fundamental curves are the state curves which describe the rearrangements of the active bonds. As such, the intermediate curve is a "foreign" state which involves excitation of bonds and orbitals not associated with the net chemical reaction. For example, **41** is the π-charge transfer state shown[63] to be the origin of the carbanion intermediate in the S_NV mechanism which involves net nucleophilic exchange of the C–X bond by a Y–C bond. Similarly, **42** is a π-charge transfer state in the activation of the F–C σ bond by a metal cation.[28b] This state has recently been invoked[28b] to account for the very efficient reaction of aryl fluorides with lanthanide cations and Ca^{2+}, as opposed to the sluggish reactivity of simple alkyl fluorides.[28]

If we allow to stretch the definition of a "foreign" state we may include in case (b) situations where the intermediate curve constitutes a different spin situation in comparison with the fundamental curves. Such a mechanism has been described recently as two-state reactivity for the C–H bond activation by metal oxide cations like FeO^+, as well as by the active form of the P-450 enzyme.[46, 100] Here, the fundamental curves (see Figure 41 b) correspond to the high-spin situation while the intermediate curve to a low-spin situation which crosses the fundamental curves and provides a low-energy path for the bond activation. Without the intermediate curve the C–H bond activation would not be possible.[100]

Owing to the ubiquitous significance of intermediate VB structures in most, if not all, chemical reactions, any VBCMD treatment is bound to barely scratch the tip of the iceberg. Therefore, we have limited ourselves to a carefully selected choice of problems, with the intention to project some novel applications related to the role of intermediate VB structures on reaction rates and reaction mechanisms.

9.2. VBCMDs with Ionic Intermediate Curves

Ionic structures which are the secondary VB configurations of polar covalent bonds can become the dominant configurations in hypercoordinated geometries due to accumulated electrostatic interactions. Alternatively these VB structures can descend in energy below the covalent structures by means of solvent-assisted crossing as well as by metal-ion catalysis (Sections 2.1.3 and 2.1.4). The following examples serve to illustrate the impact of ionic VB structures on the reactivity of covalent bonds.

9.2.1. Proton Transfer Processes and the Intermediary of Low-Barrier Hydrogen Bonds

Since H^+ has no electrons, its ionic radius is small and is determined only by nuclear repulsion with the counterion. This enables very tight ion-pair geometries with large electrostatic energies. Consequently, the triple ionic structure $X:^- H^+ :X^-$ in a proton transfer process will usually possess a deep energy minimum and in some instances may become the dominant VB structure of the reaction and give rise to "low-barrier hydrogen bonds". Since this topic has recently been flared by debates on the role, or lack thereof, of low-barrier hydrogen bonding in enzyme catalysis,[101] we would like to analyze the case of the $(FHF)^-$ anion, which has a stable symmetric hydrogen bond, and elucidate its bonding features, especially its ionic–covalent resonance energy. It should be emphasized that most other hydrogen-bonded $(XHX)^-$ anions (X = Cl, Br, I) are nearly symmetric and feature double-well minima separated by a tiny barrier for the proton transfer.[102] An added dimension of the problem is the behavior of the corresponding neutral species, for example $(FHF)^•$, which are all quite high energy transition states for the hydrogen-abstraction reaction.[5f]

Figure 42a depicts the HL and ionic structures for a proton transfer process between bases $X:^-$ which have moderate or low stability as anions (e.g., carbanions with significant pK_a).

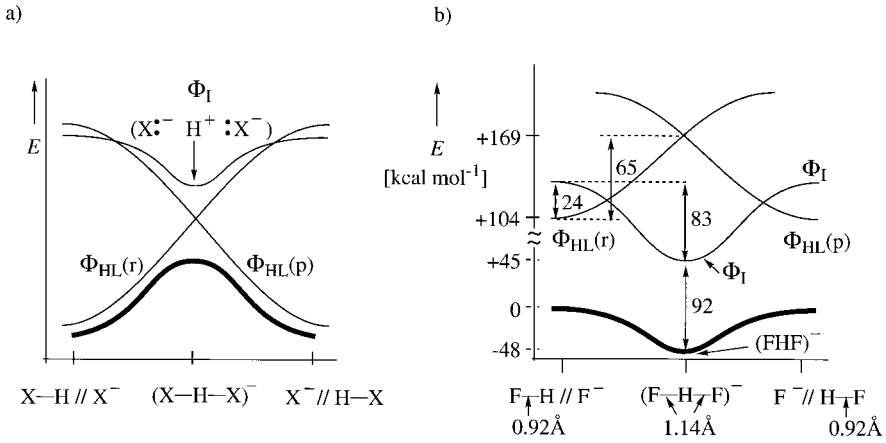

Figure 42. VBCMDs for proton transfer to and from X^- bases. a) The base has a moderate to low stability. b) The VB-computed situation for $X^- = F^-$, a stable base.

In such a case, the ionic structure lies above the HL structures in energy, and the avoided crossing leads to a single transition state separating the hydrogen-bonded clusters. Nevertheless, the ionic structure is seen to have a deep minimum near the crossing point of the HL curves, and as such the transition state will be expected to possess a significant triple-ion character.

As the anion $X:^-$ gets increasingly more stable, the ionic structure will descend more and more in energy and may dominate the region near the transition state. This is seen in Figure 42b, which depicts the calculated[71, 103] VB configurations for the F^- exchange along the reaction coordinate. On the side of the reactants, the ionic structure lies above the HL structure by a moderate energy gap of only about 24 kcal mol^{-1}. However, at the symmetric geometry, the lowest VB curve is the ionic structure which undergoes 83 kcal mol^{-1} of stabilization relative to its onset at the reactant geometry. The origins of this remarkable stability of the ionic structure is, as already noted, the small size of H^+, which leads to short F^-—H^+ distances at the cluster geometry of $(FHF)^-$ and thereby to very large electrostatic stabilization. This electrostatic stability along with its energetically low onset make the ionic structure the dominant configuration at the cluster geometry.

The short H—F distance is associated also with the inception of a very large resonance energy due to the mixing of the resonating HL state (which by itself is stabilized by resonance) with the ionic structure. This ionic–covalent resonance energy is seen in Figure 42b to be about 90 kcal mol^{-1}, which makes a significant contribution to the bonding in $(FHF)^-$. Thus, the symmetric hydrogen-bonded species is neither fully ionic nor fully covalent; it is virtually a resonating mixture of the two structures.[104]

The question of whether or not the symmetric $(FHF)^-$ species will be a minimum on the adiabatic (bold) curve is a question of balance between the difference in electrostatic stabilization and ionic–covalent resonance energies at the cluster geometry relative to the reactant and product geometries. It is seen from Figure 42b that the ionic–covalent resonance energy is largest at the reactant and product geometries. It follows, therefore, that the crucial factor responsible for the stability of the symmetric $(FHF)^-$ species is the electrostatic stabilization, which lowers the curve of the ionic structure well below onset of the curves of the HL structures. It is this difference that causes the final state profile (Figure 42b, in bold) to retain the shape of the ionic curve, and to exhibit a minimum. The relatively small size of the F^- anion is also important for the electrostatic stabilization, and we may expect that, as the anion increases in size (e.g., I^-) or becomes delocalized (e.g., benzoate), the intrinsic stabilization of the ionic structure at the cluster geometry will decrease, and the symmetric geometry may cease to be a minimum of the energy profile.[102]

Finally, the impact of the ionic structure is vividly appreciated by comparison of $(FHF)^-$ with the radical $(FHF)^{\bullet}$. Thus, with one electron less in $(FHF)^{\bullet}$, the triple-ionic structure disappears and is replaced by the $F^-H^+{}^{\bullet}F$ structures, which loose half of the electrostatic stabilization, and therefore their curve will remain above the HL curves. This loss has a tremendous impact on the reaction profile, and the greater than 40 kcal mol^{-1} deep energy well of $(FHF)^-$ becomes an $(FHF)^{\bullet}$ transition state that is about 18 kcal mol^{-1} above the reactants.[5f] For the same reason, it is expected therefore that any $(XHX)^{\bullet}$ species will generally be a transition state[30, 31] for the hydrogen-abstraction process, with a barrier significantly larger than for the corresponding proton transfer process via the $(XHX)^-$ species.

9.2.2. Nucleophilic Substitution on Silicon—Stable Hypercoordinated Species Exist because Silicenium Ions Are Analogues of H^+

Another demonstration of the role of ionic structure is the nucleophilic substitution on Si which proceeds via pentacoordinated intermediates,[39b, 105] in contrast to the situation in carbon where the pentacoordinated species is a transition state. Recently, Lauvergnat et al.[14a] and Sini et al.[14b] performed VB calculations for C—X and Si—X bonds (X = H, F, Cl) and made the interesting observation that the minimum of the ionic curve for Si^+X^- is significantly shorter than the corresponding minimum for C^+X^-. In contrast, the minima of the HL curves for Si—X were found to be at longer distances than for C—X. Since X is common for the two bonds, these differences mean that while the covalent radius of Si is longer than that of C; the opposite is true for the ionic radii. Thus, the ionic radii of CH_3^+ was determined as 0.64 Å, in comparison with only 0.35 Å for SiH_3^+.[14a] It was concluded that the origins of these effective ionic sizes is the charge distribution of the corresponding ions. In CH_3^+ and generally in CL_3^+ (L = ligand) the charge is distributed over the ligands, and the central carbon possesses therefore a relatively small positive charge. Consequently, the minimum distance of approach of an anion X^- toward CL_3^+ will be relatively long, and the electrostatic energy will be small. In contrast, in SiL_3^+ the charge is localized on Si, and consequently the minimum distance of approach of an X^- anion will be relatively short, and the electrostatic stabilization large. Indeed, the depth of the ionic curve $H_3Si^+X^-$ was found to exceed the depth of $H_3C^+X^-$ by more than 50 kcal mol^{-1}. In conclusion, therefore, the silicenium ion SiL_3^+ is expected to behave more like the small proton, while the corresponding carbocation CL_3^+ will be bulky.

Based on these differences, it is possible to represent the VBCMDs for typical nucleophilic substitution reactions on Si versus C as shown in Figure 43. The ionic curve for Si (Figure 43a) is seen to be very stable in the pentacoordinated geometry due to the electrostatic energy of the triple ion, much like the case of the $(FHF)^-$ species discussed before. Consequently, the pentacoordinated species will become an intermediate for the reaction. By the same analogy, to the $(FHF)^-$ species, the pentacoordinated silicon intermediate will be neither ionic nor covalent, but rather a resonating mixture of the two structures with bonding augmented by the ionic–covalent resonance.

Figure 43b shows the typical situation for the carbon analogue where the ionic structure is of relatively high energy and the VB mixing leads to a single-step reaction with a pentacoordinated transition state. Intermediate pentacoordinated carbon may be envisioned if the reaction is conducted in

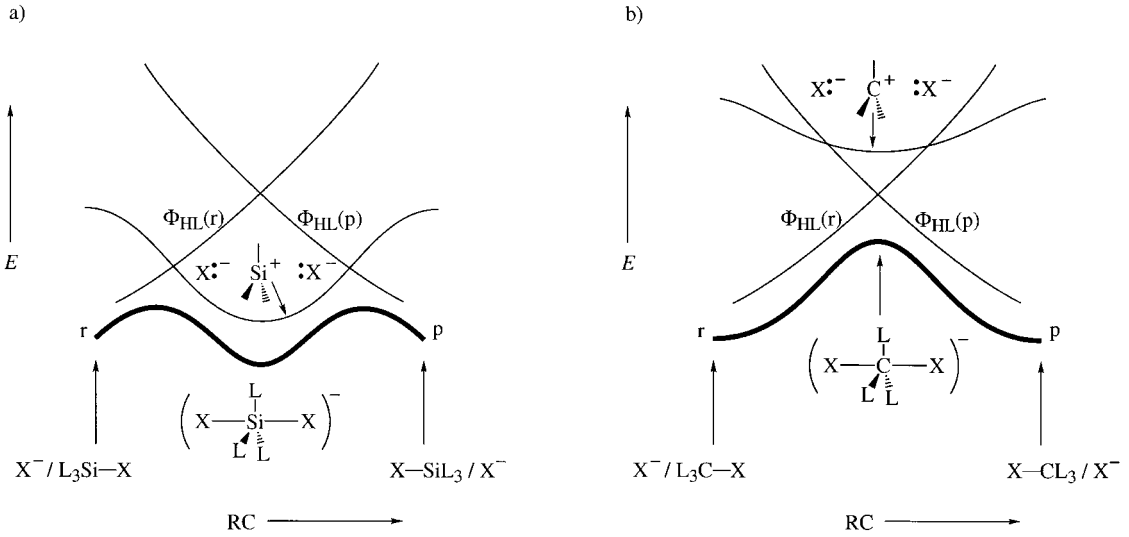

Figure 43. VBCMDs for nucleophilic displacements on a) silicon and b) carbon. Shown are the HL curves of reactants and products as well as the ionic curve.

the presence of external positive ions or immobilized charge centers (see Section 2.1.4) which will stabilize the ionic structure ($X^- CL_3^+ X^-$) well below the crossing point of the HL curves. However, even in such an event the pentacoordinated species of carbon will be different than the corresponding silicon species. Thus, due to the small size of SiL_3^+ the covalent–ionic resonance energy will always make an important contribution to the bonding of the species. In contrast, the large size of the CL_3^+ species enables a smaller ionic–covalent resonance energy,[14a] which will further decrease in the presence of external charges due to the widening energy gap between the ionic ($X^- CL_3^+ X^-$) and the HL structures. Consequently, should a pentacoordinated intermediate of carbon become stable, it will generally be highly ionic. A recent study of ion-pair S_N2 reactions by Harder et al.[106] shows that the presence of a single Li^+ cation or of an XLi_2^+ moiety makes the transition states virtually ionic. One wonders if more accurate calculations or modification of the external ions will not result in a stable pentacoordinated carbon possessing high ionicity.

9.2.3. Concerted, Nucleophilic, and Electron Transfer Pathways in Polar Cycloadditions

Ionic VB structures play a cardinal role in polar cycloaddition, which has been a subject of intense research by the groups of Huisgen and Sauer,[107] who were concerned with the orbital symmetry rules and their apparent violations. Let us consider for example, the Diels–Alder reactions of diene–dienophile pairs with varying donor–acceptor properties, a system investigated by Sustmann et al.[108] Figure 44a shows the VBCMD, based on Figure 17, with the addition of the charge transfer (CT) state Φ_{CT}. For a pair of diene and dienophile with weak to moderate donor–acceptor capabil-

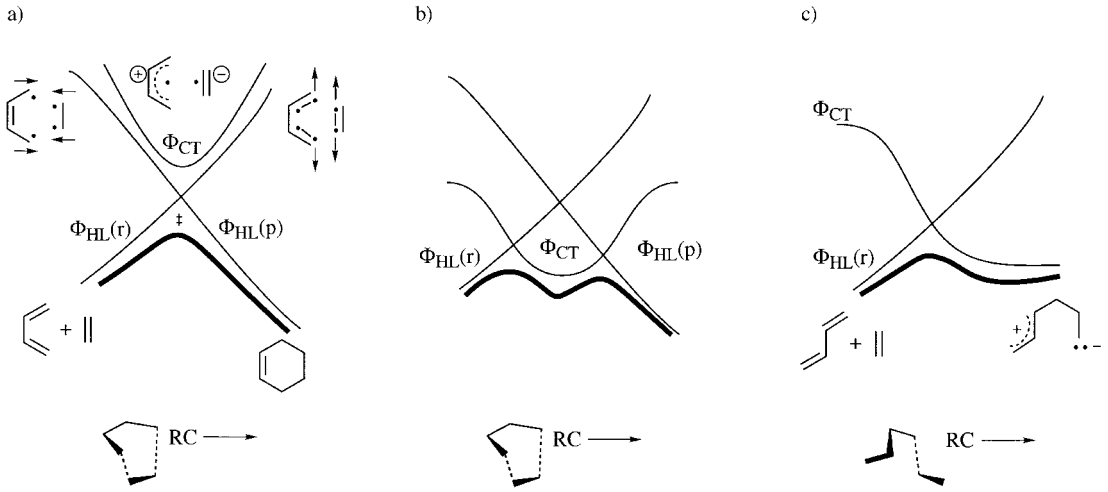

Figure 44. VBCMDs for Diels–Alder reactions. a) A nonpolar situation with a high-lying charge transfer state Φ_{CT}. b) A polar case, where solvent-assisted crossing brings the Φ_{CT} configuration below the crossing point of the HL curves. The cycloaddition proceeds in a synchronous fashion via a pericyclic polar intermediate. c) Nucleophilic attack of the diene on the dienophile along a one-bond coordinate. The $\Phi_r - \Phi_{CT}$ avoided crossing leads initially to the open form of the zwitterion intermediate. In the case of (a) and (b), the reaction coordinate RC describes the changes in two bonds, and in the case of (c) that of only one bond.

ities, the CT state is significantly higher than the HL curves. Since the mixing of the CT state with the resonating HL state is allowed (see rule 7), this occurs and a polar transition state is formed. The electronic VB structure of the CT state is depicted in the resonance mixture of **43a** and **43b** in Scheme 24, which illustrates that the ion pair possesses pericyclic bonding as long as the structure retains synchronous bonding or approximately so.

Scheme 24. VB structures whose resonance mixing provides the pericyclic charge transfer state of a cycloaddition of the type shown in Figures 44a and 44b.

Figure 44b shows the situation when the diene is a very good donor and the dienophile is a very good acceptor. In this case, the CT state is low in energy at the onset of the VBCMD, and solvation will cause it to descend further, below the HL structures. The CT configuration forms a pericyclic intermediate state which facilitates the cycloaddition by providing a low-energy path in comparison with the less polar cycloaddition in Figure 44a.

Once the CT state is lowered, the intermediate can take up different structures and lead thereby to different mechanisms. Figure 44c shows the VBCMD along a reaction coordinate which involves a one-bond attack of the diene on the dienophile. Since the CT state is lower than the promoted state for the synchronous reaction, the initial step will involve only avoided crossing of the reactant's HL configuration with the charge transfer state, much like a nucleophilic attack of the diene on the dienophile. This avoided crossing will lead to the zwitterion intermediate, which may subsequently close the second bond by an additional avoided crossing, involving Φ_{CT} with the HL configuration of the products. Alternatively, the intermediate may be trapped by the solvent or undergo side reactions (such as oligomerizations) typical of the dipolar nature. By analogy to nucleophile–electrophile reactivity (see Figure 30), here too the formation of the dipolar intermediate will compete with the corresponding electron transfer process[108c, e] if the avoided crossing in Figure 44c takes place along a coordinate which is either outer sphere or a recoil inner sphere in character, as in Figure 30. Clearly, the accessibility of the ionic structure endows polar cycloadditions with a rich mechanistic scheme of competing concerted and nonconcerted pathways, which is very different from the classical Diels–Alder reaction.[108]

9.3. VBCMD with "Foreign" States as Intermediate Curves

Every reaction system possesses, in addition to the promoted states which are localized in the active bonds, numerous "foreign" excited states which involve electronic excitations in orbitals and bonds which do not belong to the active bonds. Some of these foreign states are high in energy, while some which are of low energy can become accessible along the reaction coordinate. As already stated, mixing of foreign states is the means by which complex molecules find low-energy pathways for otherwise difficult transformations. To elucidate this mechanistic feature of the foreign states, we have chosen three mechanisms in which the foreign state plays a cardinal role.

9.3.1. Nucleophilic Cleavage of Esters

Figure 45 shows the reaction in which a nucleophile X^- cleaves the C–OR bond of an ester via a tetrahedral intermediate[48–50] (see Section 7.1.7). Structures **44** and **45**

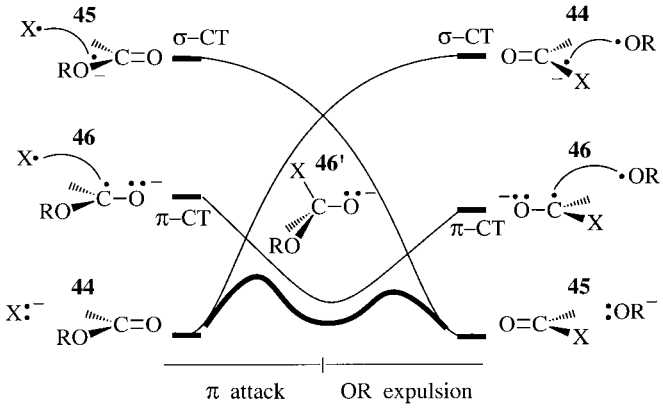

Figure 45. VBCMD showing the cleavage mechanism of an ester by a nucleophile X^- via the tetrahedral intermediate **46′**. See text for details.

depict the ground state and σ-CT state which form the fundamental curves that describe the net reaction, while **46** is the π-CT state which correlates to the tetrahedral intermediate. It is seen that the ground and σ-CT states generate a high-energy crossing point, due to the large promotion gap. In contrast, the low lying π-CT state can cross the ground state at a lower energy to define a transition state for the formation of the tetrahedral intermediate. The latter then undergoes conformational changes and expels in a subsequent step the RO^- leaving group. Thus, the π-CT state facilitates the exchange of the σ bonds by providing a low-energy path.

Clearly, a single-step reaction which involves a direct backside attack on the C–OR bond will have a significantly higher barrier, due inter alia to the loss of the electronic advantage of mixing of the π-CT state. One may anticipate that in the case of acyl halides (e.g., Br and I), where the σ-CT state is not so high, the π-CT and σ-CT states will be close in energy, so that the avoided crossing will generate a single transition state and the process will become synchronous.[63] In such an event, a competition between π attack and a backside σ attack similar to that in a S_N2 reaction may ensue. Similar conclusions have been derived for the S_NV mechanism.[63, 109a]

A dominant backside σ attack on the ester or acyl halide will become likely when the π-CT state rises well above the corresponding σ-CT state. This will require, however, at least an acyl iodide or the use of a catalyst which can activate specifically the bond to the leaving group without affecting the π-CT state of the carbonyl group much. Reagents which form hypercoordinated iodide may serve as such catalysts. A case of this sort has been recently observed experimentally in an S_NV reaction of styryl iodonium salts.[109b]

9.3.2. The $S_{RN}2$ and $S_{RN}2^c$ Mechanisms

Intermediate states are also capable of changing a reaction mechanism. A case in point is the recent proposition of new nucleophilic substitution mechanisms, termed $S_{RN}2$ and $S_{RN}2^c$, by Zipse as part of his "methylenology" strategy to speed up rates of classical reactions by the presence of a radical center adjacent to the reaction centers.[9] Scheme 25 shows these

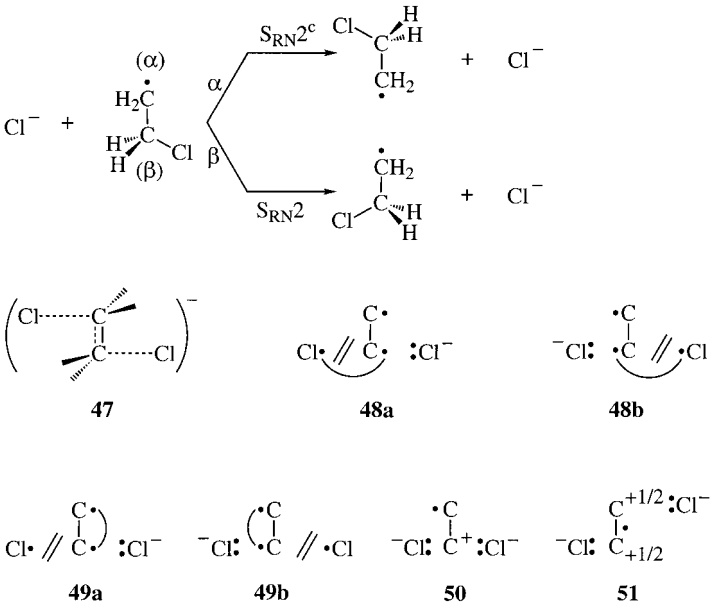

47 **48a** **48b**

49a **49b** **50** **51**

Scheme 25. The indentity reaction between Cl^- and the β-chloroethyl radical as well as structures important for an understanding of the mechanisms.

mechanisms for the identity reactions of the β-chloroethyl radical, where Cl^- exchange can occur by attack on the β or α position. It was found by Zipse[9] that the $S_{RN}2$ mechanism is a single-step reaction with a transition state which is very similar to that of the corresponding S_N2 reaction between Cl^- and ethyl chloride. At the same time, the $S_{RN}2$ barrier was shown to be about 11 kcal mol^{-1} lower than the S_N2 barrier. Even more intriguing are the most recent findings by Zipse,[110] triggered by application of the VBCMD model, revealing that the $S_{RN}2^c$ mechanism proceeds in a stepwise manner via a C_{2h}-symmetric intermediate **47**, which is lower by about 3 kcal mol^{-1} relative to the transition state of the $S_{RN}2$ mechanism. Thus, the adjacent radical center on the one hand lowers considerably the barriers for the Cl^- exchange, and on the other hand leads to a novel intermediate species.

The effect of the radical center can be appreciated by inspecting the VB structures **48** and **49**, which correspond to promoted states for the process. Thus, **48a** and **48b** are the standard charge transfer states which arise by electron transfer from the attacking Cl^- into the C–Cl linkage, while pairing the spins across the Cl···C intermolecular linkage. There is, however, an alternative way of coupling the spins and generating thereby states with a much lower promotion energy. This alternative is shown in **49a** and **49b**, where the spins are paired across the intramolecular C_α–C_β linkage. The resulting states are lower in energy relative to the standard promoted state in **48**. As such, the resonating combination of **49a** and **49b** will give rise to a low-lying intermediate curve cutting across the fundamental curves.

Figure 46 shows the VBCMD for the two mechanisms. Thus, in both cases there exist two fundamental curves identical to those of the classical S_N2 reaction, and a low-lying intermediate curve. According to the calculations of Zipse[110] the vertical gap to the intermediate curve is less than half of the promotion energy of the fundamental curve. It is the mixing of this intermediate structure into the fundamental curves that accounts for the much lower energetics of the $S_{RN}2$, and $S_{RN}2^c$ mechanisms in comparison with S_N2.

The difference between the $S_{RN}2$ and $S_{RN}2^c$ mechanisms is seen to be the relationship between the intermediate structure and the fundamental curves. Our placement of the intermediate curve in Figure 46 is based on the spin and charge-density analysis of Zipse.[9, 110] The crossing point of the fundamental curves is lower for the $S_{RN}2$ mechanism, because the triple-ion structure shown as **50** in Scheme 25 can optimize better the electrostatic interactions in comparison with the

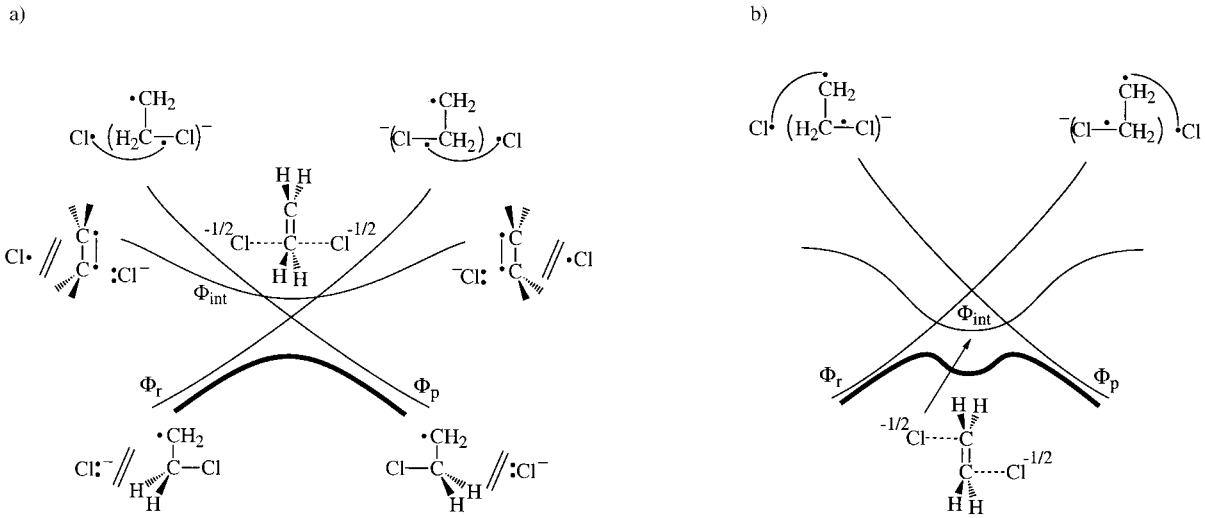

Figure 46. VBCMDs for $S_{RN}2$ (a) and $S_{RN}2^c$ mechanisms (b) for reaction of the chloride ion with the chloroethyl radical. Φ_r, Φ_p = curves of reactant and product, Φ_{int} = intermediate curve.

corresponding structure **51** of the $S_{RN}2^c$ mechanism. This effect would be enhanced by the somewhat preferred intrinsic stability of the intermediate structure in the $S_{RN}2^c$ case. Consequently, the crossing point of the fundamental curves for the $S_{RN}2$ mechanism may well be lower than the intermediate curve, as shown in Figure 46a, while the opposite would be true for the $S_{RN}2^c$ mechanism, as shown in Figure 46b. Indeed, the computed[110] C_α–C_β distances, charge development on the C_2H_4 moiety, and the spin density on the chlorine moieties demonstrate that the intermediate state character is more dominant in the $S_{RN}2^c$ mechanism. Thus, $S_{RN}2^c$ is a stepwise mechanism mediated by a low-energy state due to strong electronic coupling with the adjacent radical center.

Clearly, the intermediate VB state **49** (Scheme 25) emerges as the key feature which affects the intrinsic barriers for Cl^- exchange in the $S_{RN}2$ and $S_{RN}2^c$ mechanisms. A radical center adjacent to the reaction center is a novel strategy to generate low-energy pathways via intermediate states.[9, 111] Furthermore, different substitution patterns may create a whole mechanistic manifold, including intermediates of cation radical states, for example via **50** and **51** (Scheme 25), which feature in Giese's mechanism for radical-induced DNA strand cleavage.[112]

9.3.3. Mechanistic Crossovers and Entangled Mechanisms

An interesting effect of intermediate configurations can be observed when two mechanisms share a common set of VB structures which mix along the trajectories that lead to the two mechanisms. The competing mechanisms will be entangled, and a series of reactants, with appropriate substituents, will exhibit a mechanistic crossover while the corresponding transition state is undergoing a smooth geometric variation.

This phenomenon has been discovered recently[92c, 113] for the reactivity of ketyl radical anions and alkyl halides. As shown in Scheme 26, the reactants may undergo both C-alkylation (SUB(C)) as well as dissociative electron trans fer (ET(C)) via isostructural transition states (**52**). The key VB structures are **53**–**55**, the reactant Φ_r, the ET(C) Φ_{ET}, and SUB(C) Φ_{SUB} configurations. The mixing of Φ_r and Φ_{ET} is determined by the $\pi^*_{CO}-\sigma^*_{CX}$ overlap (see Scheme 20), which is optimal in a C-C-X structure. However, in this structure the Φ_{SUB} configuration mixes both with Φ_r and Φ_{ET}. As such, the three configurations blend along the C-C-X trajectory. The resulting species will possess in principle a gamut of electronic structures, with two extremes and probably a grey area in between.

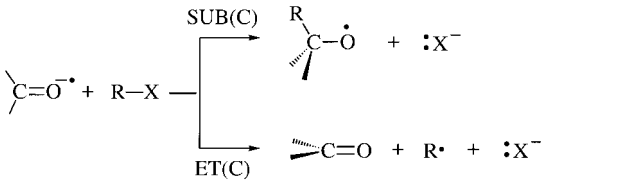

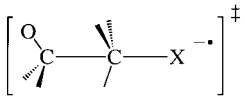

52

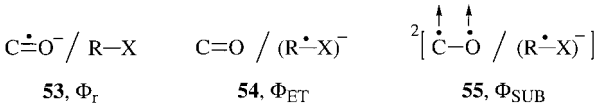

53, Φ_r **54**, Φ_{ET} **55**, Φ_{SUB}

Scheme 26. Two mechanistic alternatives occuring via isostructural transition states for the reaction of ketyl radical anions with alkyl halides and important VB structures.

The extremes are shown in Figure 47 and arise from the pairwise avoided crossing of Φ_r with either Φ_{ET} or Φ_{SUB}. Figure 47a shows the $\Phi_r-\Phi_{ET}$ avoided crossing, which leads to

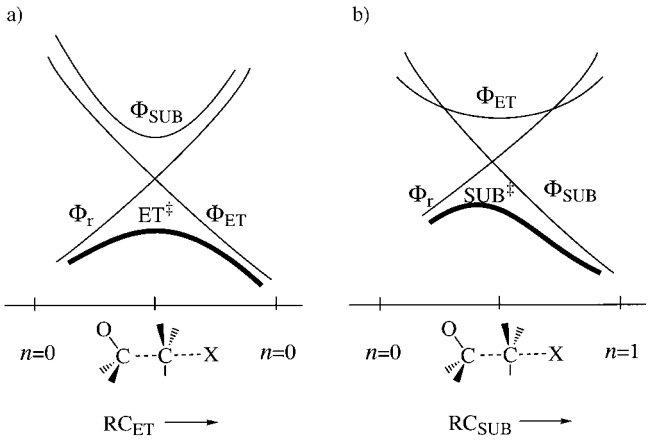

Figure 47. The distinct mechanisms for a reaction between ketyl anion radicals with methyl halides. a) An ET mechanism due to $\Phi_r-\Phi_{ET}$ avoided crossing. b) A C-alkylation mechanism, SUB(C), by $\Phi_r-\Phi_{SUB}$ avoided crossing. In each case, the third configuration mixes into the transition state and creates entangled mechanisms. n = C–C bond order.

the ET transition state having the C-C-X structure (required by the $\pi^*_{CO}-\sigma^*_{CX}$ selection rule in Scheme 20). The Φ_{SUB} configuration serves as an intermediate state which mixes into the ET transition state ($ET^{\ddagger}$) and endows it with some substitution character. Past the transition state, the C–C bond recoils, leading to dissociated ET products. In the other extreme (Figure 47b) there is a $\Phi_r-\Phi_{SUB}$ pairwise avoided crossing which leads to a SUB(C) transition state ($SUB^{\ddagger}$). Now, Φ_{ET} is the intermediate curve that mixes into the SUB(C) transition state and endows it with an ET character. Thus, the constituent VB configurations of the two extreme mechanisms are mixed in the C-C-X structure, and the mechanisms are therefore entangled borrowing characters from each other.

The consequences of this entangled nature are vividly represented in Figure 48, taken from a recent computational study by Sastry et al.,[113a] as a mechanistic crossover with a sharp boundary zone. In the figure the C–C distance in the C-C-X transition state is shown as a function of the parameter α defined by Equation (15) in terms of the ET promotion gap

$$\alpha = \frac{G_{ET}}{2(G_{ET} - \Delta E_{ET})} \qquad (15)$$

and reaction energy driving force. Thus, for good donor–acceptor pairs which lead to very exothermic ET, the Φ_{ET} configuration lies well below Φ_{SUB} curve, and the

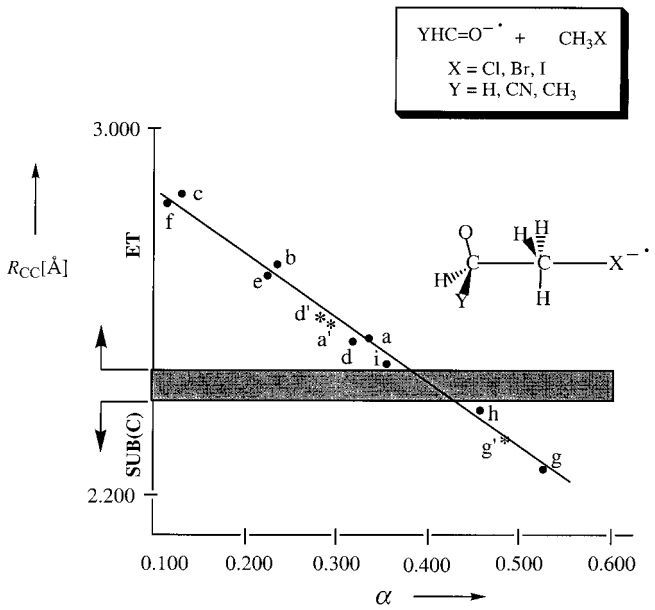

Figure 48. Plot of the C–C distance against the "earliness" parameter α [Eq. (15)] for transition states of the C-C-X type, obtained from the ketyl radical anions and alkyl halides shown in the box (adapted from ref. [113a]). A mechanistic crossover is indicated by the shaded zone. Transition states in the vicinity of the crossover zone may give mixtures of ET and SUB(C) products by surface bifurcation.

$\Phi_r - \Phi_{ET}$ avoided crossing occurs at a longish C–C distance (small α), leading to an ET transition state. As the donor–acceptor relationship becomes poorer, and the ET process less exothermic, the Φ_{SUB} configuration takes over and crosses Φ_r at a shorter C–C distance (larger α) and the corresponding avoided crossing results in a SUB(C) transition state. It is seen that the C–C distance at the C-C-X transition state decreases smoothly, while the mechanism changes abruptly from the ET to the SUB(C) variety within a narrow changeover zone.

The region around the changeover zone is likely to exhibit a borderline in which the three VB configurations are strongly mixed and lead to entangled behavior. Our more recent study of the reaction of H_2CO^- with CH_3Cl (point a in Figure 48)[113b] shows that the ET transition state is separated from the SUB(C) valley by a shallow energy ridge which will be crossed whenever sufficient kinetic energy becomes available to the system. In this case, the ET transition state will most likely have a leakage channel to the SUB(C) pathway. We expect that ultimately at some limiting situation, the entangled nature of the mechanisms will be strong enough, the ridge which separates the mechanisms will altogether disappear, and a surface bifurcation[114] will result. In such a limiting situation, the transition state structure will serve as a common species which leads to generation of C-alkylated as well as dissociated ET products. Such behavior must be found near the changeover zone of Figure 48, for example, for the reaction of the cyanoformaldehyde radical anion with CH_3I[113a] or with a secondary alkyl chloride.[113c] Stereochemical studies near the changeover zone may contribute to a better articulation of the entangled-mechanism paradigm. We are looking forward to a molecular dynamics study which will test the notion that a single transition state can serve two different mechanisms.

9.4. The VBCMD: A Primary Model for Chemical Reactivity

The notion that an intermediate VB state or configuration can mediate a transformation by a low-energy path is quite evident by now, and its importance can hardly be overemphasized. This is very likely the situation in many chemical reactions of large molecules, where many intermediate states are sufficiently low in energy to affect almost any transformation. Applications to organometallic reactivity is an obvious direction because organometallic molecules have plenty of low lying excited states which can mediate low-energy processes.[100] Creative approaches such as Zipse's[9, 110, 111] "methylenology" strategy can be exploited to effectuate other reactions and to generate for them novel intermediates.

From another general viewpoint, not elaborated in this review, the VBCMD model leads to a systematic conceptualization of reaction mechanisms in terms of the constituent building block VB configurations. The elementary processes for a given reactant pair are defined by the pairwise avoided crossings within the VB set, which constitute the mechanistic manifold available for the reactants.[115] The remaining VB configurations for each pairwise avoided crossing will serve as intermediate curves which can mix in and endow the particular transition states with their characters. In certain cases where the reaction manifold share similar trajectories, there will result "entangled" mechanisms as discussed above, which may exhibit surface bifurcations where a single transition state structure becomes a common critical species for two mechanisms. In other cases, where the trajectories are very distinct, the mechanisms will simply borrow electronic characters from each other through the mixing of the intermediate VB structure, as has recently been shown for nucleophilic cleavages, proton transfers, and electron transfers of cation radicals.[62, 115]

Thus, as sufficient proficiency in VB theory builds up, it is our feeling that ultimately VBCMD could become a central paradigm for mechanistic chemical reactivity.

10. Summary and Outlook

At this point, the fundamental principles of VB diagrams have been illustrated and applied to a wide range of chemical reactivity problems. The central idea that the curves of VB configurations, which describe the electronic reorganization inherent in the process, cross along the reaction coordinate, generating by resonance mixing barriers and intermediate states, is both chemically lucid as well as resting on solid quantum-chemical principles.[5] Two generic diagrams, the VBSCD in Figure 21 and the VBCMD in Figure 41, provide a consistent frame of thought for making predictions on barrier heights, transition state structures, selection of reaction mechanisms, the nature of reaction intermediates, and the low-energy pathways available to a chemical process.[4, 7] The formulation of eight rules along with a presentation of a variety of applications and a few new predictions should provide the reader with a basis and hopefully a drive to extend

the ideas to new chemical problems which certainly overstep the knowledge and imagination of the authors.

There are also limitations in the model as well as challenges which need to be met in the future. A thorny problem of the VB diagram approach is its implicit quantitative aspect. Thus, while quantitative expressions for the barrier [e.g., Eqs. (8)–(10)] exist and have been applied successfully to estimate barrier heights, such as in S_N2 reactivity,[4a–c] it is not a straightforward matter to quantify the f and B factors routinely for other reactions. It would have been desirable to formulate the barrier equations with explicit expression of the reactivity factors in a manner that enables a routine estimate of the barrier. While this is certainly a worthy challenge, it may not be met easily, if at all, on a general basis.

A major challenge of any reactivity model is its "dialogue" with experiment in a manner which may generate some meaningful physical information from the data, beyond just correlations. A simple idea which is being explored rests on the concept of reaction "family", discussed above in reference to Figure 40 (Section 8.2), where a family is a series of closely related reactions for which the quantities f and B are constants. Once these parameters are derived from the experimental data, they may be used to model the transition states of the family and lead thereby to a crude resolution of transition state structure under real conditions. Criteria for identifying true reaction families are still being sought (perhaps Hammett series), and while the means for modeling are in principle known,[10] the task is still difficult.

The role of intermediate states as the means of providing low-energy pathways for difficult reactions has been focused on in the context of organic reactivity. But it is clear that the vast potential for this rests in organometallic reactivity.[8, 46, 100] This is where future efforts might be fruitful.

The notion of entangled mechanisms (Section 9.3.3) with mechanistic crossovers (see Figure 48) and a borderline transition state which serves several mechanisms has novel aspects which are largely unexplored. We expect that quite a few mechanistic manifolds will exhibit this behavior, for example, substitution and ET mechanisms of ion radicals (Figure 48) or $S_{RN}2/S_{RN}2^c$ reactions[9, 110] and their isoelectronic mechanistic manifold[112] with radical-cation intermediate states. In all of these cases a single transition state may serve a few mechanisms (by surface bifurcation). Microscopic reversibility will certainly have to be questioned then as a necessary rule of nature.

Photochemistry is an important field of potential application. Use of VB notions highlights[116] the role of conical intersections as decay channels[117] in the chemistry of organic molecules in excited states. A recent application[78] of VB diagrams to the photochemistry of S_N2 systems[118a] illustrates a simple mechanism for formation of conical intersections. This mechanism is based on the notion that the twin states Ψ^{+} and Ψ^{*} in the avoided-crossing region of the VBSCD (Figure 36) are related by resonance mixing of degenerate VB configurations. Therefore, there should exist a specific distortion mode which would convert the avoided crossing region into a conical intersection where the twin states Ψ^{+} and Ψ^{*} become degenerate, thereby enabling the excited reaction complex to decay into the ground-state surface. The photoproducts would therefore be characteristic of the distortion mode which is required to convert the avoided crossing region into a conical intersection. This concept works successfully[78] for the charge transfer photochemistry of S_N2 systems,[118a] but its potential is extendable to other reactions and may be far reaching. We are currently investigating the photosolvolytic mechanism[118b] in an attempt to explore the correlation between product distribution and the nature of the distortion modes which convert the avoided crossing states in Figure 5b into a conical intersection.

The notion of twin states has some exciting implications on the characterization of transition states. Thus, since the twin states Ψ^{+} and Ψ^{*} are related electronically, they may also be geometrically coincident or nearly so. Since the excited state Ψ^{*} is in principle bound, it can be accessed by experimental means and serve thereby as a source of spectral information on the transition state Ψ^{+} of the thermal process. Candidates where the geometric coincidence of the states can be manifested are rigid systems. The semibullvalene system in a recent study of Quast et al.[118c] appears to be a good choice for such explorations.

With all the foregoing features taken together, the VB diagram approach is an art of piecing together reaction profiles from their building blocks, and as such the method has a potential to become a central paradigm for the science of chemical reactivity.

Enduring collaborations with A. Pross and P. C. Hiberty and instructive seminal discussions with H. Köppel and L. S. Cederbaum on avoided crossing are acknowledged. The work has been supported in part by a grant from the Israel Science Foundation (ISF), The Lise Meitner-Minerva Center, and the Volkswagenstiftung. Allocation of computer time by the IUCC is acknowledged. The authors are indebted to H. Zipse for taking on the colossal work of translating this review into German, and for very helpful suggestions throughout the work. The idea of writing this review was conceived during the visit of S. Shaik to the Technische Universität Berlin as an Alexander von Humboldt Awardee. The hospitality and support of H. Schwarz is acknowledged.

Received: July 28, 1997 [Z A247 IE]
German version: *Angew. Chem.* **1999**, *111*, 616–657

[1] S. S. Shaik, *J. Am. Chem. Soc.* **1981**, *103*, 3692.
[2] R. B. Woodward, R. Hoffmann, *Angew. Chem.* **1969**, *81*, 797; *Angew. Chem. Int. Ed. Engl.* **1969**, *8*, 781.
[3] For example, a) M. G. Evans, M. Polanyi, *Trans. Faraday Soc.* **1938**, *34*, 11; b) A. Warshel, R. M. Weiss, *J. Am. Chem. Soc.* **1980**, *102*, 6218; c) W. T. A. M. van der Lugt, L. J. Osterhoff, *J. Am. Chem. Soc.* **1969**, *91*, 6042; d) J. Michl, *Top. Curr. Chem.* **1974**, *46*, 1; e) "Unified Valence Bond Theory of Electronic Structure. Applications": N. D. Epiotis, *Lect. Notes Chem.* **1983**, *34*, 1; f) L. Salem, *Science* **1976**, *191*, 822.
[4] a) S. S. Shaik, *Prog. Phys. Org. Chem.* **1985**, *15*, 197; b) S. S. Shaik, H. B. Schlegel, S. Wolfe, *Theoretical Aspects of Physical Organic Chemistry*, Wiley-Interscience, New York, **1992**; c) S. S. Shaik, *Acta Chem. Scand.* **1990**, *44*, 205; d) S. S. Shaik, P. C. Hiberty in *Theoretical Models for Chemical Bonding*, *Vol. 4* (Ed.: Z. B. Maksic), Springer, Heidelberg, **1991**, p. 269; e) A. Pross, S. S. Shaik, *Acc. Chem. Res.* **1983**, *16*, 363; f) A. Pross, *Adv. Phys. Org. Chem.* **1985**, *21*, 99; g) A. Pross, *Theoretical and Physical Principles of Organic Reactivity*, Wiley-

Interscience, New York, **1995**; h) A. Pross, *Acc. Chem. Res.* **1985**, *18*, 212; i) A. Pross, D. M. Chipman, *Free Radicals Biol. Med.* **1987**, *3*, 55.
[5] a) P. Maitre, P. C. Hiberty, G. Ohanessian, S. S. Shaik, *J. Phys. Chem.* **1990**, *94*, 4089; b) G. Sini, S. Shaik, P. C. Hiberty, *J. Chem. Soc. Perkin Trans. 2* **1992**, 1019; c) G. Sini, S. S. Shaik, J.-M. Lefour, G. Ohanessian, P. C. Hiberty, *J. Phys. Chem.* **1989**, *93*, 5661, d) G. Sini, G. Ohanessian, P. C. Hiberty, S. S. Shaik, *J. Am. Chem. Soc.* **1990**, *112*, 1407; G. Sini, P. C. Hiberty, S. S. Shaik, *J. Chem. Soc. Chem. Commun.* **1989**, 772, e) P. Maitre, F. Volatron, P. C. Hiberty, S. S. Shaik, *Inorg. Chem.* **1990**, *29*, 3047; f) P. R. Benneyworth, G. G. Balint-Kurti, M. J. Davis, I. H. Williams, *J. Phys. Chem.* **1992**, *96*, 4346.
[6] For recent methods of good accuracy, see for example a) P. C. Hiberty, J. P. Flament, E. Noizet, *Chem. Phys. Lett.* **1992**, *189*, 259; P. C. Hiberty, S. Humbel, C. P. Byrman, J. H. van Lenthe, *J. Chem. Phys.* **1994**, *101*, 5969; b) W. A. Goddard III, L. B. Harding, *Annu. Rev. Phys. Chem.* **1978**, *29*, 363; A. F. Voter, W. A. Goddard III, *J. Chem. Phys.* **1981**, *75*, 3638; c) J. Verbeek, J. H. Langenberg, C. P. Byrman, J. H. van Lenthe, *TURTLE--an Ab Initio VB/VBSCF/VBCI Program*, Theoretical Chemistry Group, Debye Institute, University of Utrecht, **1993**; J. Verbeek, J. H. van Lenthe, *Int. J. Quantum Chem.* **1991**, *XL*, 201; d) D. L. Cooper, J. Gerratt, M. Raimondi, *Adv. Chem. Phys.* **1987**, *69*, 319; D. L. Cooper, J. Gerratt, M. Raimondi, *Chem. Rev.* **1991**, *91*, 929; e) Y. Mo, Q. Zhang, *J. Phys. Chem.* **1995**, *99*, 8535; Y. Mo, Z. Lin, W. Wu, Q. Zhang, *J. Phys. Chem.* **1996**, *100*, 6469; f) W. Wu, R. McWeeny, *J. Chem. Phys.* **1994**, *101*, 4826.
[7] a) S. S. Shaik in *New Theoretical Concepts for Understanding Organic Reactions*, *Vol. C267* (Eds.: J. Bertrán, I. G. Csizmadia), Kluwer, Dordrecht, **1989**, p. 165; b) S. Shaik, *J. Mol. Liq.* **1994**, *61*, 49; c) S. Shaik, P. C. Hiberty, *Adv. Quantum Chem.* **1995**, *26*, 99.
[8] D. Schröder, H. Schwarz, *Angew. Chem.* **1995**, *107*, 2126; *Angew. Chem. Int. Ed. Engl.* **1995,** *34*, 1973.
[9] H. Zipse, *Angew. Chem.* **1994,** *106*, 2019; *Angew. Chem. Int. Ed. Engl.* **1994,** *33*, 1985; b) H. Zipse, *J. Am. Chem. Soc.* **1994,** *116*, 10773.
[10] S. S. Shaik, E. Duzy, A. Bartuv, *J. Phys. Chem.* **1990**, *94*, 6574.
[11] R. McWeeny, *Methods of Molecular Quantum Mechanics*, 2nd ed., Academic Press, London, **1992**, chapters 4 and 7.
[12] W. Heitler, F. London, *Z. Phys.* **1927**, *44*, 455.
[13] S. Shaik, P. Maitre, G. Sini, P. C. Hiberty, *J. Am. Chem. Soc.* **1992**, *114*, 7861.
[14] a) D. Lauvergnat, P. C. Hiberty, D. Danovich, S. Shaik, *J. Phys. Chem.* **1996**, *100*, 5715; b) G. Sini, P. Maitre, P. C. Hiberty, S. S. Shaik, *J. Mol. Struct. (THEOCHEM)* **1991**, *229*, 163; c) H. Basch, P. Aped, S. Hoz, *Mol. Phys.* **1996**, *89*, 331.
[15] T. F. O'Malley, *Adv. Atom. Mol. Phys.* **1971**, *7*, 223.
[16] R. A. Ogg, Jr., M. Polanyi, *Trans. Faraday Soc.* **1935**, *31*, 604.
[17] S. S. Shaik, *J. Org. Chem.* **1987**, *52*, 1563.
[18] H. J. Kim, J. T. Hynes, *J. Am. Chem. Soc.* **1992**, *114*, 10508, 10528.
[19] a) P. Delahay, *Acc. Chem. Res.* **1982**, *15*, 40; b) M. J. Blandamer, M. F. Fox, *Chem. Rev.* **1970**, *70*, 59.
[20] S. S. Shaik, *J. Am. Chem. Soc.* **1984**, *106*, 1227.
[21] C. D. Ritchie, *J. Am. Chem. Soc.* **1983**, *105*, 7313.
[22] H. Mayr, M. Patz, *Angew. Chem.* **1994**, *106*, 990; *Angew. Chem. Int. Ed. Engl.* **1994**, *33*, 938.
[23] a) H. Feinberg, H. M. Greenblatt, G. Shoham, *J. Chem. Inf. Comput. Sci.* **1993**, *33*, 501; b) H. Feinberg, H. M. Greenblatt, V. Behar, C. Gilon, S. Cohen, A. Bino, G. Shoham, *Acta Crystallogr. Sect. D* **1995**, *51*, 428.
[24] a) A. Warshel, *Acc. Chem. Res.* **1981**, *14*, 284; b) A. Warshel, *Proc. Natl. Acad. Sci. USA* **1978**, *75*, 5250.
[25] a) J. M. Tedder, J. C. Walton, *Adv. Phys. Org. Chem.* **1978**, *16*, 51; b) B. Giese, X. Beyrich-Graf, J. Burger, C. Kesselheim, M. Senn, T. Schäfer, *Angew. Chem.* **1993**, *105*, 1850; *Angew. Chem. Int. Ed. Engl.* **1993**, *32*, 1742.
[26] Z. Rappoport, *Acc. Chem. Res.* **1981**, *14*, 7.
[27] A. Sevin, P. C. Hiberty, J.-M. Lefour, *J. Am. Chem. Soc.* **1987**, *109*, 1845.
[28] a) H. H. Cornehl, G. Hornung, H. Schwarz, *J. Am. Chem. Soc.* **1996**, *118*, 9960; b) J. N. Harvey, D. Schröder, W. Koch, D. Danovich, S. Shaik, H. Schwarz, *Chem. Phys. Lett.* **1997**, *278*, 391.
[29] R. Hoffmann, *Angew. Chem.* **1982**, *94*, 725; *Angew. Chem. Int. Ed. Engl.* **1982**, *21*, 711.
[30] H. Yamataka, S. Nagase, *J. Org. Chem.* **1988**, *53*, 3232.
[31] a) A. Pross, H. Yamataka, S. Nagase, *J. Phys. Org. Chem.* **1991**, *4*, 135; b) M. W. Wong, A. Pross, L. Radom, *Isr. J. Chem.* **1993**, *33*, 415.
[32] D. J. Bellville, D. D. Wirth, N. L. Bauld, *J. Am. Chem. Soc.* **1981**, *103*, 718; D. J. Bellville, N. L. Bauld, *J. Am. Chem. Soc.* **1982**, *104*, 2665; R. A. Pabon, D. J. Bellville, N. L. Bauld, *J. Am. Chem. Soc.* **1983**, *105*, 5158.
[33] F. Bernardi, A. Bottoni, M. Olivucci, A. Venturini, M. A. Robb, *J. Chem. Soc. Faraday Trans.* **1994**, *90*, 1617.
[34] P. Jungwirth, T. Bally, *J. Am. Chem. Soc.* **1993**, *115*, 5783.
[35] The fairly small localization energy of the cation is neglected for simplicity; see also F. M. Bickelhaupt, R. Hoffmann, R. D. Levine, *J. Phys. Chem. A* **1997**, *101*, 8255.
[36] a) T. P. Begley, *Acc. Chem. Res.* **1994**, *27*, 394; b) H.-W. Park, S.-T. Kim, A. Sancar, J. Deisenhofer, *Science* **1995**, *268*, 1866.
[37] A. Ioffe, S. Shaik, *J. Chem. Soc. Perkin Trans. 2* **1992**, 2101.
[38] a) E. T. Seidl, R. S. Grev, H. F. Schaefer III, *J. Am. Chem. Soc.* **1992**, *114*, 3643; b) F. Bernardi, A. Bottoni, M. Olivucci, M. A. Robb, A. Venturini, *J. Am. Chem. Soc.* **1993**, *115*, 3322.
[39] a) R. West, *Angew. Chem.* **1987**, *99*, 1231; *Angew. Chem. Int. Ed. Engl.* **1987**, *26*, 1201; b) Y. Apeloig in *The Chemistry of Organic Silicon Compounds* (Eds.: S. Patai, Z. Rappoport), Wiley, Chichester, **1989**, chapter 2.
[40] S. Shaik, A. Ioffe, unpublished results.
[41] S. S. Shaik, P. C. Hiberty, G. Ohanessian, J.-M. Lefour, *J. Phys. Chem.* **1988**, *92*, 5086.
[42] M. J. S. Dewar, *J. Am. Chem. Soc.* **1984**, *106*, 209.
[43] D. L. King, D. R. Herschbach, *Faraday Discuss. Chem. Soc.* **1973**, *55*, 331.
[44] a) G. K. Cook, J. M. Mayer, *J. Am. Chem. Soc.* **1994**, *116*, 1855; b) G. K. Cook, J. M. Mayer, *J. Am. Chem. Soc.* **1995**, *117*, 7139; c) K. A. Gardner, J. M. Mayer, *Science* **1995**, *269*, 1849.
[45] A. K. Rappé, W. A. Goddard III, *J. Am. Chem. Soc.* **1982**, *104*, 3287.
[46] a) A. Fiedler, D. Schröder, S. Shaik, H. Schwarz, *J. Am. Chem. Soc.* **1994**, *116*, 10734; b) M. F. Ryan, A. Fiedler, D. Schröder, H. Schwarz, *J. Am. Chem. Soc.* **1995**, *117*, 2033; c) Y.-M. Chen, D. E. Clemmer, P. B. Armentrout, *J. Am. Chem. Soc.* **1994**, *116*, 7815; d) D. E. Clemmer, Y.-M. Chen, F. A. Khan, P. B. Armentrout, *J. Phys. Chem.* **1994**, *98*, 6522; e) S. Shaik, D. Danovich, A. Fiedler, D. Schröder, H. Schwarz, *Helv. Chim. Acta* **1995**, *78*, 1393, f) S. Shaik, M. Filatov, *J. Phys. Chem. A* **1998**, *102*, 3835.
[47] a) C. L. Lasko, R. M. Miller, D. S. Tinti, *Chem. Phys. Lett.* **1986**, *130*, 359; b) R. M. Miller, D. S. Tinti, D. A. Case, *Inorg. Chem.* **1989**, *28*, 2738.
[48] E. Buncel, S. S. Shaik, I.-H. Um, S. Wolfe, *J. Am. Chem. Soc.* **1988**, *110*, 1275.
[49] I. M. Kovach, J. P. Elrod, R. L. Schowen, *J. Am. Chem. Soc.* **1980**, *102*, 7530.
[50] D. G. Oakenfull, T. Riley, V. Gold, *J. Chem. Soc. Chem. Commun.* **1966**, 385; V. Gold, D. G. Oakenfull, T. Riley, *J. Chem. Soc. B* **1968**, 515.
[51] J. K. Kochi, *Angew. Chem.* **1988**, *100*, 1331; *Angew. Chem. Int. Ed. Engl.* **1988**, *27*, 1227.
[52] S. Fukuzumi, S. Koumitsu, K. Hironaka, T. Tanaka, *J. Am. Chem. Soc.* **1987**, *109*, 305; M. Ishikawa, S. Fukuzumi, *J. Chem. Soc. Faraday Trans.* **1990**, *86*, 3531.
[53] E. Baciocchi, L. Mandolini, *Tetrahedron* **1987**, *43*, 4035.
[54] For a discussion of ET mechanisms of ion radicals, see: L. Eberson, S. S. Shaik, *J. Am. Chem. Soc.* **1990**, *112*, 4484. Note the different VB situation in comparison with ET between closed-shell reactants as depicted in Figure 30
[55] L. Eberson, *Electron Transfer Reactions in Organic Chemistry*, Springer, Berlin, **1987**.
[56] a) J. W. Verhoeven, W. van Gerresheim, F. M. Martens, S. M. van der Kerk, *Tetrahedron* **1986**, *42*, 975; b) Y. Apeloig, O. Merin-Aharoni, D. Danovich, A. Ioffe, S. Shaik, *Isr. J. Chem.* **1993**, *33*, 387.
[57] M. Patz, H. Mayr, J. Maruta, S. Fukuzumi, *Angew. Chem.* **1995**, *107*, 1351; *Angew. Chem. Int. Ed. Engl.* **1995**, *34*, 1225.
[58] H. H. Cornehl, C. Heinemann, D. Schröder, H. Schwarz, *Organometallics* **1995**, *14*, 992.
[59] M.-D. Su, *Inorg. Chem.* **1995**, *34*, 3829.
[60] A. Pross, R. A. Moss, *Tetrahedron Lett.* **1990**, *31*, 4553.

[61] S. Goldstein, G. Czapski, H. Cohen, D. Meyerstein, S. Shaik, *J. Chem. Soc. Faraday Trans.* **1993**, *89*, 4045.

[62] S. Shaik, A. C. Reddy, A. Ioffe, J. P. Dinnocenzo, D. Danovich, J. K. Cho, *J. Am. Chem. Soc.* **1995**, *117*, 3205.

[63] D. Cohen, R. Bar, S. S. Shaik, *J. Am. Chem. Soc.* **1986**, *108*, 231.

[64] S. S. Shaik, P. C. Hiberty, J.-M. Lefour, G. Ohanessian, *J. Am. Chem. Soc.* **1987**, *109*, 363.

[65] A. Demolliens, O. Eisenstein, P. C. Hiberty, J. M. Lefour, G. Ohanessian, S. S. Shaik, F. Volatron, *J. Am. Chem. Soc.* **1989**, *111*, 5623.

[66] See the appendix to chapter 3 in ref. [4b], pp. 128 – 131.

[67] L. Eberson, R. González-Luque, M. Merchán, F. Radner, B. O. Roos, S. Shaik, *J. Chem. Soc. Perkin Trans. 2* **1997**, 463.

[68] An expression which conserves microscopic reversibility and can be derived from Equation (8), but is quite complex itself, is the following:

$$\Delta E^{\neq} = \frac{(f_r + f_p)G_rG_p}{(G_r + G_p)} + 0.5\,\Delta E_{rp} + x\Delta E_{rp}^2 - B$$

$$x = \frac{(1 - f_r - f_p)}{(G_r + G_p)}$$

Using mean values for both f and G, one obtains:

$$\Delta E^{\neq} = f_{av}G_{av} + 0.5\,\Delta E_{rp} + (0.5 - f_{av})\frac{\Delta E_{rp}^2}{G_{av}} - B$$

[69] a) S. S. Shaik, *Nouv. J. Chim.* **1983**, *7*, 201; b) S. S. Shaik, *J. Am. Chem. Soc.* **1983**, *105*, 4359.

[70] a) S. S. Shaik, *Can. J. Chem.* **1986**, *64*, 96; b) S. S. Shaik, *Isr. J. Chem.* **1985**, *26*, 367.

[71] G. Sini, Dissertation, Université de Paris-Sud, Orsay, France, **1991**.

[72] a) B. D. Wladkowski, J. L. Wilbur, J. I. Brauman, *J. Am. Chem. Soc.* **1994**, *116*, 2471; b) B. D. Wladkowski, K. F. Lim, W. D. Allen, J. I. Brauman, *J. Am. Chem. Soc.* **1992**, *114*, 9136.

[73] a) J. Hine, *J. Am. Chem. Soc.* **1950**, *72*, 2438; b) J. Hine, A. M. Dowell, Jr., *J. Am. Chem. Soc.* **1954**, *76*, 2688; c) J. Hine, C. H. Thomas, S. J. Ehrenson, *J. Am. Chem. Soc.* **1955**, *77*, 3886; d) J. Hine, S. J. Ehrenson, W. H. Brader, Jr., *J. Am. Chem. Soc.* **1956**, *78*, 2282.

[74] a) R. F. Hudson, G. Klopman, *J. Chem. Soc.* **1962**, 1062; V. P. Vitullo, J. Grabowski, S. Sridharan, *J. Am. Chem. Soc.* **1980**, *102*, 6463; F. P. Ballistreri, E. Maccarone, A. Mamo, *J. Org. Chem.* **1976**, *41*, 3364; b) S. D. Ross, M. Finkelstein, R. C. Petersen, *J. Am. Chem. Soc.* **1968**, *90*, 6411; A. Halvorsen, J. Songstad, *J. Chem. Soc. Chem. Commun.* **1978**, 327; c) C. Eaborn, J. C. Jeffrey, *J. Chem. Soc.* **1954**, 4266; M. A. Cook, C. Eaborn, D. R. M. Walton, *J. Organomet. Chem.* **1971**, *29*, 389.

[75] H. Mayr in *Cationic Polymerizations* (Ed.: K. Matyjaszewski), Marcel Dekker, New York, **1996**, chapter 2, p. 51.

[76] S. S. Shaik, E. Canadell, *J. Am. Chem. Soc.* **1990**, *112*, 1446.

[77] E. Canadell, O. Eisenstein, G. Ohanessian, J. M. Poblet, *J. Phys. Chem.* **1985**, *89*, 4856.

[78] S. Shaik, A. C. Reddy, *J. Chem. Soc. Faraday Trans.* **1994**, *90*, 1631.

[79] M. N. Glukhovtsev, A. Pross, L. Radom, *J. Am. Chem. Soc.* **1995**, *117*, 2024. The barrier datum for X = F is used to obtain the f value, which is carried over to all other reactions.

[80] G. Ohanessian, P. C. Hiberty, J.-M. Lefour, J.-P. Flament, S. S. Shaik, *Inorg. Chem.* **1988**, *27*, 2219.

[81] Here $B = K_{ab}$ of the degenerate orbitals $\langle a|$ and $|b\rangle$, and the quantity $\Delta E(\Psi^{\neq} \rightarrow \Psi^*)$ in Figure 36 would be $2K_{ab}$.

[82] M. G. Evans, E. Warhurst, *Trans. Faraday Soc.* **1938**, *34*, 614; M. G. Evans, *Trans. Faraday Soc.* **1939**, *35*, 824.

[83] M. A. Robb, F. Bernardi in *New Theoretical Concepts for Understanding Organic Reactions*, *Vol. C267* (Eds.: J. Bertrán, I. G. Csizmadia), Kluwer, Dordrecht, **1989**, pp. 101; F. Bernardi, M. Olivucci, M. A. Robb in *New Theoretical Concepts for Understanding Organic Reactions*, *Vol. C267* (Eds.: J. Bertrán, I. G. Csizmadia), Kluwer, Dordrecht, **1989**, p. 147.

[84] a) K. N. Houk, Y. Li, J. D. Evanseck, *Angew. Chem.* **1992**, *104*, 711; *Angew. Chem. Int. Ed. Engl.* **1992**, *31*, 682; b) K. N. Houk, J. González, Y. Li, *Acc. Chem. Res.* **1995** *28*, 81; c) B. R. Beno, S. Wisley, K. N. Houk, *J. Am. Chem. Soc.*, in press. Note that the diradical in the Zewail experiment may originate in the excited state (K. N. Houk, private communication).

[85] B. A. Horn, J. L. Herek, A. H. Zewail, *J. Am. Chem. Soc.* **1996**, *118*, 8755.

[86] R. S. Mulliken, *J. Am. Chem. Soc.* **1952**, *74*, 811; R. S. Mulliken, *J. Phys. Chem.* **1952**, *56*, 801.

[87] N. D. Epiotis, *Angew. Chem.* **1974**, *86*, 825; *Angew. Chem. Int. Ed. Engl.* **1974**, *13*, 751; N. D. Epiotis, *Theory of Organic Reactions*, Springer, Berlin, **1978**.

[88] S. S. Shaik, J. P. Dinnocenzo, *J. Org. Chem.* **1990**, *55*, 3434.

[89] L. Eberson, M. P. Hartshorn, F. Radner, M. Merchán, B. O. Roos, *Acta Chem. Scand.* **1993**, *47*, 176; L. Eberson, F. Radner, *Acta Chem. Scand.* **1992**, *46*, 312, 802.

[90] J. P. Dinnocenzo, W. P. Todd, T. R. Simpson, I. R. Gould, *J. Am. Chem. Soc.* **1990**, *112*, 2462.

[91] S. Shaik, A. C. Reddy, unpublished results.

[92] a) G. N. Sastry, S. Shaik, *J. Am. Chem. Soc.* **1995**, *117*, 3290; b) G. N. Sastry, A. C. Reddy, S. Shaik, *Angew. Chem.* **1995**, *107*, 1619; *Angew. Chem. Int. Ed. Engl.* **1995**, *34*, 1495; c) G. N. Sastry, S. Shaik, *J. Phys. Chem.* **1996**, *100*, 12241.

[93] N. Kimura, S. Takamuku, *J. Am. Chem. Soc.* **1994**, *116*, 4087; N. Kimura, S. Takamuku, *Bull. Chem. Soc. Jpn.* **1991**, *64*, 2433.

[94] This system (see ref. [92c]) was suggested by J. P. Dinnocenzo during the sojourn of one of the authors (S.S.) on a sabbatical leave in the university of Rochester.

[95] This system was suggested by M. Schmittel to one of the authors (S.S.) after his talk at the International Symposium of the Volkswagenstiftung on Intra- and Intermolecular Electron Transfer in Berlin, **1996**.

[96] a) J. H. Incremona, C. J. Upton, *J. Am. Chem. Soc.* **1972**, *94*, 301; C. J. Upton, J. H. Incremona, *J. Org. Chem.* **1976**, *41*, 523; b) B. B. Jarvis, *J. Org. Chem.* **1970**, *35*, 924; c) G. G. Maynes, D. E. Applequist, *J. Am. Chem. Soc.* **1973**, *95*, 856; d) K. J. Shea, P. S. Skell, *J. Am. Chem. Soc.* **1973**, *95*, 6728; e) M. L. Poutsma, *J. Am. Chem. Soc.* **1965**, *87*, 4293.

[97] a) The VBSCD selection rule is a product of the two interactions $(\phi_R - \sigma_{CC})$ and $(\phi_R - \sigma_{CC}^*)$, and hence makes an unequivocal prediction. Frontier MO theory predicts that the sum of these interactions determines the regioselectivity. The sum behaves undecidedly for qualitative reasoning. If one of the interactions is more important than the other, it is not easy to decide which one would that be (see ref. [90]). b) M. Schmittel, C. Wöhrle, I. Bonn, *Chem. Eur. J.* **1996**, *2*, 1031.

[98] S. Shaik in *Encyclopedia of Computational Chemistry, Vol. 5* (Eds.: P. von R. Schleyer, N. L. Allinger, T. Clark, J. Gasteiger, P. A. Kollman, H. F. Schaefer III), Wiley, Chichester,pp. 3143 – 3159.

[99] G. L. Fox, H. B. Schlegel, *J. Phys. Chem.* **1992**, *96*, 298.

[100] a) D. Danovich, S. Shaik, *J. Am. Chem. Soc.* **1997**, *119*, 1773; b) S. Shaik, M. Filatov, D. Schröder, H. Schwarz, *Chem. Eur. J.* **1998**, *4*, 193.

[101] A. Warshel, A. Papazyan, P. A. Kollman, *Science* **1995**, *269*, 102; W. W. Cleland, M. M. Kreevoy, *Science* **1995**, *269*, 104; P. A. Frey, *Science* **1995**, *269*, 104.

[102] B. S. Ault, *Acc. Chem. Res.* **1992**, *15*, 103. The matrix-isolated hydrogen dihalide anions XHX^- (X = Cl, Br, I) are centrosymmetric or nearly so. The effect of the counterion is not clear though. Our computational results (QCISD/6-311++G(3p,3d)) for $ClHCl^-$ suggest a very small barrier.

[103] Essentially similar results have been recalculated by us using the BOVB theory described in references [6a,b].

[104] This resonance energy is different than the B value for the corresponding VBSCD, which is evaluated as 32 kcal mol^{-1} with respect to a Lewis reference structure.[71, 78]

[105] a) R. J. P. Corriu, M. Henner, *J. Organomet. Chem.* **1974**, *74*, 1; b) A. E. Reed, P. von R. Schleyer, *J. Am. Chem. Soc.* **1990**, *112*, 1434.

[106] S. Harder, A. Streitwieser, J. T. Petty, P. von R. Schleyer, *J. Am. Chem. Soc.* **1995**, *117*, 3253.

[107] a) R. Huisgen, *Acc. Chem. Res.* **1977**, *10*, 117, 199; b) J. Sauer, R. Sustmann, *Angew. Chem.* **1980**, *92*, 773; *Angew. Chem. Int. Ed. Engl.* **1980**, *19*, 779.

[108] a) R. Sustmann, M. Rogge, U. Nüchter, H. Bandmann, *Chem. Ber.* **1992**, *125*, 1647; b) R. Sustmann, M. Rogge, U. Nüchter, J. Harvey, *Chem. Ber.* **1992**, *125*, 1665; c) M. Rese, M. Dern, K. Lücking, R. Sustmann, *Liebigs Ann.* **1995**, 1139; d) R. Sustmann, M. Rogge, U. Nüchter, H. Bandmann, *Chem. Ber.* **1992**, *125*, 1657; e) K. Lücking, M. Rese, R. Sustmann, *Liebigs Ann.* **1995**, 1129.

[109] a) M. N. Glukhovtsev, A. Pross, L. Radom, *J. Am. Chem. Soc.* **1994**, *116*, 5961. Note that the large barrier for π attack at the substituted

carbon atom was analyzed in ref. [63]. This larger π barrier tips the balance in favor of the S_N2-type attack; b) T. Okuyama, M. Ochiai, *J. Am. Chem. Soc.* **1997**, *119*, 4785.
[110] H. Zipse, *J. Chem. Soc. Perkin Trans. 2* **1997**, 2691.
[111] H. Zipse, *J. Am. Chem. Soc.* **1997**, *119*, 1087, 2889; H. Zipse, *J. Chem. Soc. Perkin Trans. 2* **1996,** 1797.
[112] B. Giese, X. Beyrich-Graf, J. Burger, C. Kesselheim, M. Senn, T. Schäfer, *Angew. Chem.* **1993**, *105*, 1850; *Angew. Chem. Int. Ed. Engl.* **1993**, *32*, 1742.
[113] a) G. N. Sastry, D. Danovich, S. Shaik, *Angew. Chem.* **1996**, *108*, 1208; *Angew. Chem. Int. Ed. Engl.* **1996**, *35*, 1098; b) S. Shaik, D. Danovich, G. N. Sastry, P. Y. Ayala, H. B. Schlegel, *J. Am. Chem. Soc.* **1997**, *119*, 9237; c) G. N. Sastry, S. Shaik, *J. Am. Chem. Soc.* **1998**, *120*, 2131.
[114] H. B. Schlegel, *J. Chem. Soc. Faraday Trans.* **1994**, *90*, 1569; P. Valtazanos, K. Ruedenberg, *Theor. Chim. Acta* **1986**, *69*, 281.
[115] A. C. Reddy, D. Danovich, A. Ioffe, S. Shaik, *J. Chem. Soc. Perkin Trans. 2* **1995**, 1525.
[116] F. Bernardi, M. Olivucci, M. Robb, *Isr. J. Chem.* **1993**, *33*, 265.
[117] U. Manthe, H. Köppel, *J. Chem. Phys.* **1990**, *93*, 1669.
[118] a) D. M. Cyr, G. A. Bishea, M. G. Scranton, M. A. Johnson, *J. Chem. Phys.* **1992**, *97*, 5911; b) M. Lipson, A. A. Deniz, K. S. Peters, *J. Am. Chem. Soc.* **1996**, *118*, 2992; c) H. Quast, K. Knoll, E.-M. Peters, K. Peters, H. G. von Schnering, *Chem. Ber.* **1993**, *126*, 1047.